



UNIVERSITÀ DEGLI STUDI DI PADOVA

Department of Civil, Environmental and Architectural Engineering

Master degree in Environmental Engineering

Master thesis

Modelling the role of compaction in the aggradation and progradation of the Mississippi Delta during the Holocene

Supervisor

Prof. Pietro Teatini

Co-supervisors

Ing. Claudia Zoccarato

Dr. Philip Minderhoud

Candidate

Giulio Carazzolo

1242472

Academic Year 2021/2022

22/04/2022

Contents

Contents	i
List of Figures	iii
List of Tables	xi
1 Introduction	1
2 The Mississippi river delta	3
2.1 Location and characteristics	3
2.2 Site evolution over the Holocene	5
2.3 The problem of land subsidence	6
3 The Myrtle Grove Superstation	11
4 NATSUB3D model	17
4.1 The governing equations	18
4.2 Structure of the model	22
4.3 Main parameters	24
5 Modeling the evolution at the Myrtle Grove Superstation	33

5.1	Model set-up	33
5.2	Preliminary analysis	36
5.3	Possible scenarios for the overbank deposition	38
5.4	Results	41
5.5	Model validation	49
5.6	Uncertainty quantification and sensitivity analysis	56
6	Predicting the effects of artificial nourishment	93
7	Conclusions	99
	References	103

List of Figures

2.1	A view of the three main subdeltas composing the Mississippi delta (after Chamberlain et al., 2018).	4
2.2	Simplified stratigraphy associated to bayhead delta progradation and aggradation	8
3.1	Location of Myrtle Grove Superstation in the Mississippi delta (from Google Maps visualization).	12
3.2	Location of CRMS sites in the Mississippi delta. The CMRS site 276 with corresponding coordinates is highlighted. The map is provided by the CRMS website (https://www.lacoast.gov/CRMS/).	12
3.3	Schematic representation of the three wells in Myrtle Grove (after Bridgeman, 2017).	14
3.4	Litho-stratigraphic section of the Mississippi delta passing through the Myrtle Grove Superstation (after (Bridgeman, 2017)).	15
4.1	A scheme of the functioning of NATSUB3D model (after Zoccarato and Teatini (2017)).	24
4.2	A scheme of soil components.	25
4.3	A cross section showing grain-to-grain and void-to-void contacts.	26
4.4	A qualitative example of void ratio vs effective stress behaviour.	27

5.1	Lithological classes composing the sedimentary column of the Myrtle Grove Superstation and their parameters as provided by Bridgeman (2017) and Keogh et al. (2021).	34
5.2	Myrtle Grove I representation of the grain size and dating of the lithology after Bridgeman (2017).	35
5.3	Case 1 - Temporal behaviour of the sedimentary column and the soil strain due to autocompaction for the case of a single soil class. Notice that the horizontal and vertical scale change from plot to plot, only colours are consistent for plot comparison.	37
5.4	Case 2 - Model outputs in terms of column thickness and strain for the various soil parameters considered in the preliminary analysis. The results refer to the simulation time $t=300$ yr. Notice that the horizontal and vertical scale change from plot to plot, only colours are consistent for plot comparison.	38
5.5	Case 3 - Temporal behaviour of the sedimentary column and strain in the case of two soil classes. Notice that the horizontal and vertical scale change from plot to plot, only colours are consistent for plot comparison.	39
5.6	Sedimentation rates [mm/yr] in the different scenarios for overbank deposition. Notice that the years are indicated in terms of simulation time, not as yr BP.	40
5.7	Variation over time of the elevation of the soil column computed by NATSUB3D for the three scenarios.	42
5.8	Variation over time of the elevation of the soil column computed by NATSUB3D for the three scenarios between 2500 yr BP and 0 yr BP.	42
5.9	Scenario A: sediment classes and overpressure [kPa] at simulation time $t=7401$ yr (i.e. 3599 yr BP).	43

5.10 Scenario A: sediment classes and overpressure [kPa] at simulation time $t=9702$ yr (i.e. 1298 yr BP).	44
5.11 Scenario B: sediment classes and overpressure [kPa] at simulation time $t=10778$ yr (i.e. 222 yr BP).	44
5.12 Scenario B: sediment classes and overpressure [kPa] at simulation time $t=10824$ yr (i.e. 176 yr BP).	45
5.13 Scenario B: sediment classes and overpressure [kPa] at simulation time $t=10921$ yr (i.e. 79 yr BP).	45
5.14 Effective stress behaviour versus depth for the three scenarios of overbank deposition.	46
5.15 Comparison between the effective stress behaviour versus depth provided by Bridgeman (2017) to the left and computed with NATSUB3D to the right.	47
5.16 Strain distribution computed along the sedimentary column at present (simulation time $t=11000$ yr, i.e. 0 yr BP) in the three scenarios of overbank deposition.	48
5.17 Integrated compaction [m] for the three scenarios of overbank deposition at present time (simulation time $t=11000$ yr, i.e. 0 yr BP).	48
5.18 RSL curve and present elevation of dated samples of Myrtle Grove station as provided by Bridgeman (2017).	50
5.19 Location of the 4 samples involved in the PDL validation phase within the Myrtle Grove sedimentary column.	51
5.20 Comparison between Bridgeman (2017) data and NATSUB3D outcome for scenario A and the four DS values. Notice that Myrtle Grove data are reported in terms of upper and lower bound. The range for humic clay 2 is so restricted that only one dot is apparently visible in the plot.	53

5.21	Comparison between Bridgeman (2017) data and NATSUB3D outcome for scenario B and the four values for DS. Notice that Myrtle Grove data are reported in terms of upper and lower bound. The range for humic clay 2 is so restricted that only one dot is apparently visible in the plot.	54
5.22	Comparison between Bridgeman (2017) data and NATSUB3D outcome for scenario C and the four values for DS. Notice that Myrtle Grove data are reported in terms of upper and lower bound. The range for humic clay 2 is so restricted that only one dot is apparently visible in the plot.	55
5.23	Surface Elevation Change (SEC) over the last 12 years at the CRMS 276. The regression line is provided.	57
5.24	Model results in terms of SEC for scenarios A, B and C over the last 12 years at the Myrtle Grove site.	57
5.25	Monte Carlo outcomes in terms of effective stress [kPa] with respect to depth considering all soil parameters as uncertain.	60
5.26	Monte Carlo outcomes in terms of strain [-] with respect to depth considering all soil parameters as uncertain.	60
5.27	Monte Carlo outcomes in terms of PDL [m] with respect to depth considering all soil parameters as uncertain.	61
5.28	Monte Carlo outcomes in terms of porosity [-] with respect to depth considering all soil parameters as uncertain.	61
5.29	Monte Carlo outcomes in terms of bulk density [g/cm ³] with respect to depth considering all soil parameters as uncertain.	62
5.30	Monte Carlo outcomes in terms of compressibility [kPa ⁻¹] with respect to depth considering all soil parameters as uncertain.	62

5.31	Monte Carlo outcomes in terms of integrated compaction [m] with respect to depth considering all soil parameters as uncertain.	63
5.32	Monte Carlo outcomes in terms of strain [-], porosity [-], bulk density [g/cm ³] and compressibility [kPa ⁻¹] with respect to depth considering all soil parameters as uncertain. These four pictures provide a focus on the upper overbank portion. . . .	64
5.33	Monte Carlo outcomes and related statistics in terms of effective stress [kPa] versus model layer number for the four analyses developed in the study assuming as uncertain (a) all the parameters and (b) the hydraulic, (c) the geomechanical, and (d) the density parameters only.	66
5.34	Monte Carlo outcomes in terms of effective stress [kPa] versus model layer number and depth/thickness [m] for the four analyses developed in the study assuming as uncertain (a) all the parameters and (b) the hydraulic, (c) the geomechanical, and (d) the density parameters only.	67
5.35	Monte Carlo outcomes and related statistics in terms of strain [-] versus model layer number for the four analyses developed in the study assuming as uncertain (a) all the parameters and (b) the hydraulic, (c) the geomechanical, and (d) the density parameters only.	69
5.36	Zoom of Figure 5.35 for the shallower overbank units (corresponding to the layer numbers between 400 and 518, i.e. approximately the upper 12 m of the soil column) where a high lithological variability is observed.	70
5.37	Monte Carlo outcomes in terms of strain [-] versus model layer number and depth/thickness [m] for the four analyses developed in the study assuming as uncertain (a) all the parameters and (b) the hydraulic, (c) the geomechanical, and (d) the density parameters only.	71

- 5.38 Monte Carlo outcomes and related statistics in terms of PDL [m] versus model layer number for the four analyses developed in the study assuming as uncertain (a) all the parameters and (b) the hydraulic, (c) the geomechanical, and (d) the density parameters only. 73
- 5.39 Monte Carlo outcomes in terms of PDL [m] versus model layer number and depth/thickness [m] for the four analyses developed in the study assuming as uncertain (a) all the parameters and (b) the hydraulic, (c) the geomechanical, and (d) the density parameters only. 74
- 5.40 Comparison of simulations $K_{z0,2}$ and $K_{z0,6}$ in terms of elevation [m] of the soil column. 75
- 5.41 Comparison of simulations $K_{z0,2}$ and $K_{z0,6}$ in terms of pressure [kPa] of the bottom of the soil column. 75
- 5.42 Monte Carlo outcomes and related statistics in terms of porosity [-] versus model layer number for the four analyses developed in the study assuming as uncertain (a) all the parameters and (b) the hydraulic, (c) the geomechanical, and (d) the density parameters only. 77
- 5.43 Zoom of Figure 5.42 for the shallower overbank units (corresponding to the layer numbers between 400 and 518, i.e. approximately the upper 12 m of the soil column) where a high lithological variability is observed. 78
- 5.44 Monte Carlo outcomes in terms of porosity [-] versus model layer number and depth/thickness [m] for the four analyses developed in the study assuming as uncertain (a) all the parameters and (b) the hydraulic, (c) the geomechanical, and (d) the density parameters only. 79

5.45	Monte Carlo outcomes and related statistics in terms of bulk density [g/cm^3] versus model layer number for the four analyses developed in the study assuming as uncertain (a) all the parameters and (b) the hydraulic, (c) the geomechanical, and (d) the density parameters only.	81
5.46	Zoom of Figure 5.45 for the shallower overbank units (corresponding to the layer numbers between 400 and 518, i.e. approximately the upper 12 m of the soil column) where a high lithological variability is observed.	82
5.47	Monte Carlo outcomes in terms of bulk density [g/cm^3] versus model layer number and depth/thickness [m] for the four analyses developed in the study assuming as uncertain (a) all the parameters and (b) the hydraulic, (c) the geomechanical, and (d) the density parameters only.	83
5.48	Monte Carlo outcomes and related statistics in terms of compressibility [kPa^{-1}] versus model layer number for the four analyses developed in the study assuming as uncertain (a) all the parameters and (b) the hydraulic, (c) the geomechanical, and (d) the density parameters only.	84
5.49	Zoom of Figure 5.48 for the shallower overbank units (corresponding to the layer numbers between 400 and 518, i.e. approximately the upper 12 m of the soil column) where a high lithological variability is observed.	85
5.50	Monte Carlo outcomes in terms of compressibility [kPa^{-1}] versus model layer number and depth/thickness [m] for the four analyses developed in the study assuming as uncertain (a) all the parameters and (b) the hydraulic, (c) the geomechanical, and (d) the density parameters only.	86

5.51	Monte Carlo outcomes and related statistics in terms of integrated compaction [m] versus model layer number for the four analyses developed in the study assuming as uncertain (a) all the parameters and (b) the hydraulic, (c) the geomechanical, and (d) the density parameters only.	88
5.52	Monte Carlo outcomes in terms of integrated compaction [m] versus model layer number and depth/thickness [m] for the four analyses developed in the study assuming as uncertain (a) all the parameters and (b) the hydraulic, (c) the geomechanical, and (d) the density parameters only.	89
5.53	Average compaction of the geologic unit used to represent the Myrtle Grove sedimentary sequence. Mean and standard deviation are computed from the Monte Carlo simulation with all parameters assumed uncertain.	90
5.54	Average compaction of the geologic unit used to represent the Myrtle Grove sedimentary sequence. Mean and standard deviation are computed from the Monte Carlo simulation with only K_{z0} assumed uncertain.	90
5.55	Average compaction of the geologic unit used to represent the Myrtle Grove sedimentary sequence. Mean and standard deviation are computed from the Monte Carlo simulation with only C_c , C_r and σ_p assumed uncertain.	91
5.56	Average compaction of the geologic unit used to represent the Myrtle Grove sedimentary sequence. Mean and standard deviation are computed from the Monte Carlo simulation with only e_0 and γ_s assumed uncertain.	91
6.1	Soil parameters data used in the simulations by Keogh et al. (2021).	95

6.2	Additional compaction [m] along the Myrtle Grove column after the additional 50 years of nourishment operations as computed by Keogh et al. (2021) for the three scenarios.	95
6.3	Additional compaction [m] along the Myrtle Grove column after the additional 50 years of nourishment operations as computed by NATSUB3D.	96

List of Tables

5.1	Elevation and displacement data of humic clay, sand and peat samples dated at Myrtle Grove Superstation. Notice that for the two humic clay samples some parameters report the lower bound only because they are identified as freshwater and therefore they only have minimum formation elevations of mean tide level. The "+" marks the absence of a value for the upper bound.	50
5.2	Average age and deep subsidence for the four dated samples at Myrtle Grove Superstation.	52
5.3	Computed PDL obtained with scenario A and PDL+DS for the four samples and the four DS values.	52
5.4	RSL and FCER obtained with scenario A and the four DS values.	53
5.5	Computed PDL in scenario B and PDL+DS for the four samples and the four DS values.	53
5.6	RSL and FCER obtained with scenario B and the four DS values.	54

5.7	Computed PDL in scenario c and PDL+DS for the four samples and the four DS values.	54
5.8	RSL and FCER obtained with scenario C and the four DS values.	55
5.9	Range of soil parameters for the Monte Carlo simulations (part1). The central column for each parameter provides the values used in the deterministic analysis. .	58
5.10	Range of soil parameters for the Monte Carlo simulations (part2). The central column for each parameter provides the values used in the deterministic analysis. .	58
5.11	Values of the hydraulic conductivity for the various lithological classes used in the reference simulation and the two simulations $K_{z0,2}$ and $K_{z0,6}$ providing the minimum and maximum PDL, respectively.	72
6.1	Characteristics of silty clay loam used for the additional 50-year nourishment operations.	94
6.2	Accretion data after silty clay loam nourishment with 10 mm/yr sedimentation rate.	97
6.3	Accretion data after silty clay loam nourishment with 10 mm/yr sedimentation rate.	97
6.4	Accretion data of silty clay loam nourishment by Keogh et al. (2021).	98
6.5	Comparison of stress and pressure at the bottom of the soil column before and after the nourishment operation.	98

Abstract

River deltas are undoubtedly one of the increasingly significant number of natural environment whose equilibrium is being altered by human interventions. The effects of hydraulic structures along the river course is visible through the insufficient sediment supply towards the shoreline and becomes even more alarming when dealing with a remarkable increase in sea-level rise as the one observed during the last century. The Mississippi River Delta is an example of coastal landforms experiencing such processes and it is fundamental to study its litology, morphology and evolution in order to be able to address the problem as effectively as possible and try to understand what the scenarios of the future could be in terms of interventions. This thesis work, which results from a collaboration between Padua and Tulane university, is aimed at reproducing the evolution of a site in the Mississippi River Delta called Myrtle Grove Site during the Holocene through an advanced sedimentation and compaction 1D numerical model and to analyse the impact that a future nourishment operation could have on the system. Many geological, geotechnical and hydraulic aspects are considered throughout the analysis, thus giving a complete portrait of the case study. The results obtained take advantage of a certain number of scientific papers developing the same theme and used as source for comparison.

Chapter 1

Introduction

Deltas are landforms occurring when a river mouth is welcomed by a sea, a lake or an ocean. They are involved in dynamic phenomena which make them important to be monitored. Indeed, they may undergo morphological transformations as a consequence of reduction in sediment supply, increase of the sea-level rise or subsidence rate. Most of these phenomena are enhanced by human activity, especially the construction of check dams and other hydraulic structures along the river course, which trap sediments and cause depletion in the deltaic area, but also the withdrawal of fluids from the underground, leading to land loss because of land subsidence. The dredging of navigation canals plays an important role and has to be included as well. It goes without saying that understanding these dynamics through monitoring stations of the deltaic area and the development of a model which studies these phenomena is essential to predict the future of deltas all over the world and plan the most suitable strategies to restore their morphological characteristics. The Mississippi delta is a quite relevant example of all these processes. It is exposed to land loss and the total rate referred only to the last century gives the dramatic value of $45 \text{ km}^2/\text{yr}$ (Chamberlain et al., 2018). It has been estimated, indeed, that dams have trapped nearly half of the historic sediment load of the Mississippi River (Kesel

et al., 1992). In addition to this, new pipelines and navigation channels have led to increasing erosion rates and accretion has lowered significantly due to the built-up of artificial levees which had a relevant impact on the overbank flow. Present-day sea-level rise, which is experiencing one of the highest values ever registered (12 ± 8 mm per yr), makes it necessary to understand if the gain in surface elevation is able to safely withstand relative sea-level rise (Jankowski et al., 2017). The aim of this thesis is to provide a portrait of the evolution of the Mississippi delta formation through the Holocene, which corresponds to the last 11000 years. The model takes advantage of a finite-element mesh which develops in time according to the deposit of new material and it accounts for subsidence and consolidation. Indeed, even though land subsidence can be enhanced by human activities, it must be pointed out that there is a natural component of this phenomenon given by sediment compaction which is a process inherently related to the delta evolution and progradation (Zoccarato et al., 2018). The different steps composing this thesis work are the following. First of all, a deep literature research was necessary to understand the context of the Mississippi River Delta system and to find out enough information related to its litology and the main changes in its morphology during the Holocene. Then, the Myrtle Grove Superstation site has been considered as case study and the NATSUB3D model has been properly set in order to reproduce the evolution of sediment deposition and compaction during the Holocene (Xotta et al., in press.). All steps required for the application of a model have been followed, i.e. calibration, validation, uncertainty quantification and prediction. In all such steps, several reference papers already discussing this case study have been considered as reliable source for comparison. For the prediction phase, a period of 50 additional years of nourishment with properly chosen material has been considered to understand how effective such operation could be in order to withstand sea-level rise.

Chapter 2

The Mississippi river delta

The Mississippi river delta covers an area of about 12 000 km² overall located in the southeastern portion of the United States, joining the Louisiana coastal plain and the Gulf of Mexico. Many research studies conducted here have given proof that it is a quite complex system because it includes a series of subdeltas which formed as a result of avulsions. This term indicates a phenomena consisting on the gradual shift of the depocenter within deltas which, in this case, brought to the formation of the Lafourche delta, the Plaquemines-Modern delta and the Atchafalaya delta (Figure 2.1). Before introducing the evolution of the Mississippi river delta it is necessary to briefly summarise the characteristics of these three subdeltas.

2.1 Location and characteristics

The subdelta which is still actively growing is the Atchafalaya, as a consequence of the activity of the Atchafalaya branch. Such lobe is characterized by an area of 2800 km² (Roberts, 1997) which started developing in the 16th century (Fisk, 1961). The creation of this new subdelta followed the abandonement of the Lafourche delta but discharge was never shared between

them. Indeed, the latter subdelta originates from a divergence of the modern Mississippi river and then splits into a number of small branches at around 55 river km downstream of the Modern Mississippi branch. The result of such polyfurcation is a shallow bay of about 6 000 – 8 000 km². The overall area hosting the sedimentation process is called subdelta: it covers around 10 000 km² and was active from about 1.6 to 0.6 ka ago when relative sea-level rise did not display significant variations (Chamberlain et al., 2018). Finally, the activity of the Plaquemines-Modern subdelta began around 1.0-1.4 ka and is still currently developing (Bridgeman, 2017). The process, though, is hampered by the construction of artificial levees, which caused a lowering in direct sediment and water supply. Consequently, part of the wetlands in this area display a lack of accretion. This aspect has to be kept in mind when the results of the analysis of the thesis will be discussed because the field site which is taken as reference for data comparison with our model is located in this area.

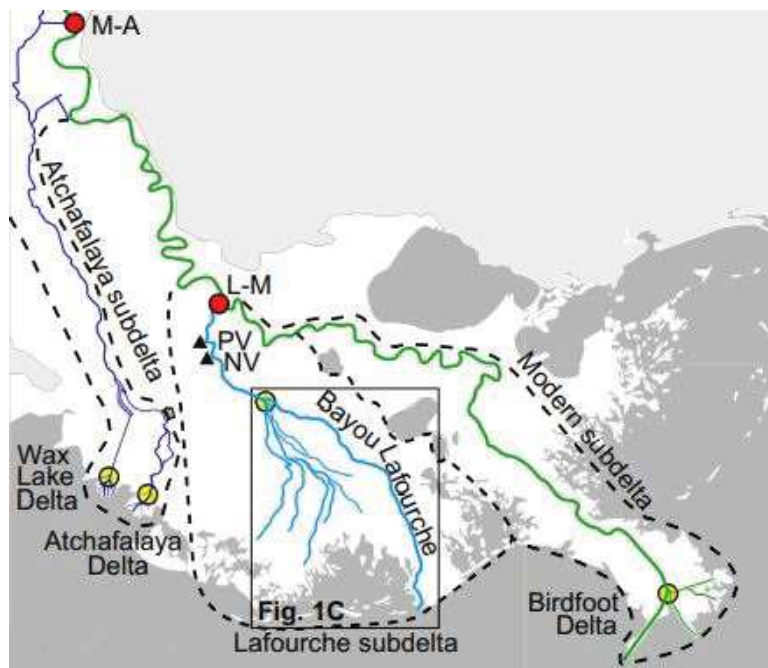


Figure 2.1: A view of the three main subdeltas composing the Mississippi delta (after Chamberlain et al., 2018).

2.2 Site evolution over the Holocene

The choice of studying the evolution of the Mississippi river over the Holocene derives from the fact that over this period, covering 11700 years, a series of events occurred, shaping the river floodplain to the configuration that we can notice nowadays. First of all, it must be stated that during this historical period the Mississippi River system was very dynamic because the stream was let free to meander across its region continuously modifying and reshaping its configuration. This is mainly due to the frequent flood events as a consequence of which the sediments were carried from the river bed to the nearby areas. Flood by flood new layers were created and deposited over the old ones which remained preserved in the underground. Their composition is mostly muddy but turns to sandy or pebbly as soon as we come closer to the river. When the river reaches the ocean, the area known as Mississippi River delta is formed. Its unique shape is due to its ability to overcome tidal and wave forces up to tens of kilometers far from the nearby Gulf of Mexico (Fisk, 1961). This action was carried out by its distributaries and estimates lead to the conclusion that over the Holocene about 100 m thickness of delta-sediment have been built as a consequence of a transport of 400 million tons of sediment per year (Roberts, 1997). In an equilibrated system, the natural subsidence consequent due to the increasing sediment weight would be compensated in terms of elevation by the new amount of material reaching the river mouth. This natural phenomenon, as previously mentioned, has been hampered by human interventions in terms of hydraulic structures in the river system. Another important natural phenomenon regarding the Mississippi River delta is lobe switching. This occurs when a more resistant path to the ocean is created and, therefore, the older stream is abandoned. It may happen as a consequence of a dramatic flood event taking place or during a wider time scale when many subsequent floods happen (Bentley et al., 2014; Roberts, 1997). Nowadays the river

delta growth rate has decreased due to human interventions, but before Anthropocene, when the river could carry a higher amount of sediments to the ocean, the delta in the Lafourche lobe progradated at a rate of $6 - 8 \text{ km}^2$ new land per year (Chamberlain et al., 2018). From a general point of view, although very old data cannot be considered as accurate as recent ones, it has been estimated that 460 million metric tons of sediment per year were carried by the river at the beginning of the Anthropocene. In the last 50 years this value has dramatically plummeted to 130 million tons per year (Bentley Sr et al., 2016), indeed the river path and its tributaries can count a total of more than 50000 dams impacting on sediment transport (Syvitski & Milliman, 2007).

2.3 The problem of land subsidence

No doubt can be raised when stating that land subsidence is a tangible issue in the Mississippi delta area. Indeed, a lot of effort has been recently put in order to monitor this phenomenon, which is being studied through a number of techniques such as remote sensing, tide-gauge records, measurement of marsh elevations, coring of sediment cores and analysis of radiocarbon dates. They allow to understand how the situation in a given system developed at geological and historical time scales. They have strongly confirmed the negative influence of uncontrolled extraction of hydrocarbons or sulfur mining. It has been estimated that in the Mississippi delta plain subsidence rates reached about 8-12 mm/yr between 1965 and 1993 whereas in the previous 5000 years they were limited to 1 or maximum 5 mm/yr as a consequence of natural processes (Morton et al., 2005). Of course this comparison is affected by time scale, as historical rates of geological processes occurring in a short time-scale prove to be significantly higher than those taking place in a longer time interval. However, this is not the only side from

which the phenomenon should be considered. Indeed, there is a relevant difference between the driving forces acting during such periods. Fault-slip and storm beach erosion events have always taken place in this area, but for sure not with the same frequency and impact of hydrocarbon extraction, which has occurred in relatively recent times. Some examples of land subsidence in this area can be outlined. First of all, Bay St. Elaine area is characterized by production of oil and gas field and a number of canals dredged for hydrocarbon and sulphur production. The evidence of subsidence here is provided by recent historical research. In this area gas production increased in the 1960s reaching a peak in 1970 and continued, together with oil production, at high performance also in the 1980s. Data collected in 2002 outline the following dramatic results: 177 million bbls of oil produced, then 942 Bcf of gas and 155 million bbls of water (Morton et al., 2005). Another example displaying more variability in land subsidence than the previous case is the Bully Camp study area, which is in the western part of Bayou Lafourche. The construction of much more wells took place here in order to perform dredge-and-fill activities associated with oil-and-gas development and sulfur extraction. As a result, subsidence rates reach 68 to 149 cm (Morton et al., 2005). Many more examples could be cited but such information already provide a dramatic portrait and give motivation for further research on this topic, as the evidence of its impact cannot be ignored anymore. This thesis is the result of a research work conducted by Padua and Tulane University, whose collaboration is still ongoing, on subsidence in the Mississippi river delta and its focus achieves a very specific target in the field of subsidence. Indeed, the aim is to point out the relevant contribution of natural subsidence occurring in the Holocene portion of a considered soil column. As developed in Jankowski et al. (2017) if the Holocene deposits of the Mississippi river delta, which are typically very thick (32.8 ± 22.5 m), are compared with those for example of the Chenier plain (SE Louisiana, displaying lower Holocenic thickness around 5.8 ± 3.5 m), the results

prove that the correspondent shallow subsidence occurring is extremely similar in the two sites (Jankowski et al., 2017). These observations confirm that a deep investigation of such portion of soil litology is fundamental in order not to exclude a significant contribution to the overall process. More in detail, a focus has to be made on the so-called "overbank" portion, which occupies the upper part of the stratigraphy as it can be seen in a simplified form in Figure 2.2 and is involved in the shallow component of subsidence. It has been found out that in coastal Louisiana more than 60% of subsidence is verified in the first 5 to 1 m below land surface (Jankowski et al., 2017), therefore it must not be ignored.

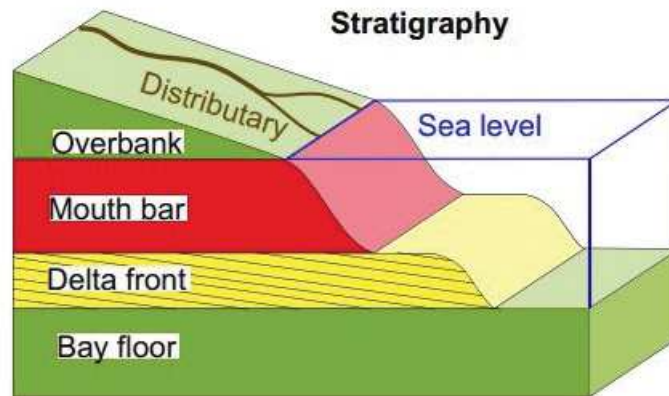


Figure 2.2: Simplified stratigraphy associated to bayhead delta progradation and aggradation

Overbank layers are typically fine-grained with a remarkable organic component at the base, which make them prone to subsidence. Scientific research on the stratigraphy of the overbank in this area has shown that, initially, elevation gain in the zone immediately close to the channel was mainly given by clayey deposits probably as a consequence of annual flooding. Then, silt deposits associated with crevasse channels prevailed (Jankowski et al., 2017). Organic-rich deposit, then, have to be seriously considered because they are well known to compact rapidly. Most compaction is observed to occur during the earliest stage after formation and burial (Törnqvist et al., 2008). A relevant role is played by peat material. Its abundance in the

Mississippi delta is evident as well as its contribution to relative sea-level rise and subsidence issues. Bayou Lafourche can be identified as the main source for widespread of wood peat and silty or clayey deposits in the overbank during the Holocene. The influence of secondary consolidation of peat in the overbank is proved by the 1:1 correspondence between overburden thickness and compaction rate found by Tornqvist et al., 2008. A remarkable influence is exerted also by strata underlying the peat, especially by the sand bodies which reduce the compaction rate significantly. This phenomenon has to be contextualized also along a specific time scale. Indeed, overbank aggradation is generally found to take place very rapidly and the peat layers are well known to undergo a very fast primary consolidation, with a rapid decreased in permeability, followed by a secondary consolidation mostly referred to as "creep". Therefore, their influence among the first 10-15 m below land surface must be considered, even though it is not the only layer undergoing natural subsidence. These first considerations lead to the conclusion that a focus on the complex overbank portion of the Mississippi delta site is needed, together with a deep investigation of the Holocene sequence of soil deposit, which is shown to host a relevant component of natural subsidence. This thesis will analyse all such aspects in the Myrtle Grove site, whose characteristics are reported in the next chapter.

Chapter 3

The Myrtle Grove Superstation

The thesis is focused on the Myrtle Grove Superstation (Figure 3.1) which is a monitoring site specifically devoted to understand shallow subsidence in the Mississippi Delta. Developed over the last few years, it is located about 2 km far from the Mid-Barataria sediment diversion and 60 km downstream of New Orleans (Keogh et al., 2021). It is not far also from one of the 390 Coastwide Reference Monitoring System (always referred to as CRMS) sites. This system was promoted by the U.S. Congress and began its active contribution to monitor the effectiveness of restoration actions at multiple spatial scales in response to Louisiana land loss crisis since 1990. Figure 3.2 shows some of the CRMS sites located throughout coastal Louisiana, specifically in the Birdfoot Delta lobe where the Myrtle Grove Superstation was established too. More specifically, CRMS site 276, which is highlighted with a red circle in Figure 3.2 provides insights about surface elevation change and vertical accretion in the nearby of the Superstation.

The Superstation is made up of three wells (Figure 3.3) equipped with a permanent GNSS station and a fiberoptic strainmeter having the following depths: 38.7 m (well1), 25 m (well2), 10 m (well3). The first well crosses the entire Holocene sequence, therefore it is the one to be

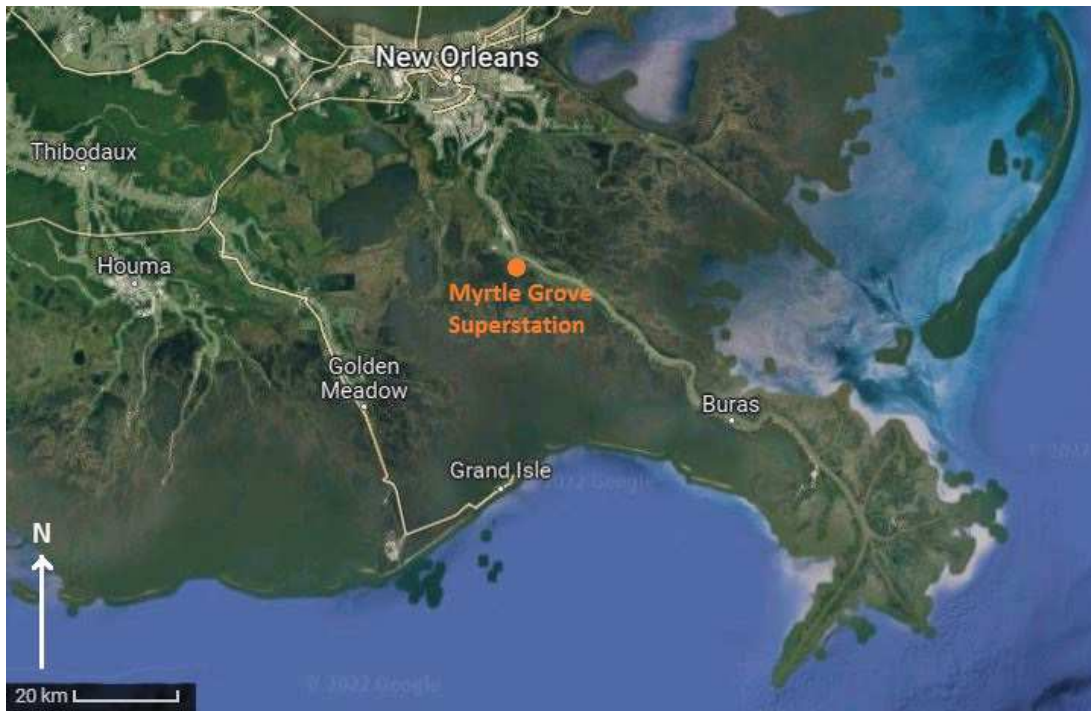


Figure 3.1: Location of Myrtle Grove Superstation in the Mississippi delta (from Google Maps visualization).



Figure 3.2: Location of CRMS sites in the Mississippi delta. The CMRS site 276 with corresponding coordinates is highlighted. The map is provided by the CRMS website (<https://www.lacoast.gov/CRMS/>).

considered for the analysis of the present thesis. It is important to highlight that the "very shallow" compaction, referred to the upper part of the soil column, cannot be identified by the wells because of some metal casings containing the instrumentation which occupy the first 3 m (Bridgeman, 2017). Myrtle Grove I core is 38.7 m long and it can be classified as a "piston core" because it takes advantage of the action of a piston which improves the ease to perform sample entry, reduces significantly the internal friction and prevents core shortening and plugging (Blomqvist, 1991; Mudroch & MacKnight, 1994; Wright Jr, 1993).

Three main soil units can be identified in the core (Bridgeman, 2017):

- the top 12 metres build up the so-called "overbank", which includes alternate layers of silty clay loam and silt loam with a top portion of modern marsh peat. All these layers are relatively fine-grained with low organic content and formed as a consequence of river floods. They are highly variable and may contain wood and herbaceous material. Typically, finer grains are located farther than coarser sediments, which do not spread away from the river banks;
- below, the central part of the soil column is made up of homogeneous sandy loam located among silt loam layers;
- finally, a sand body stands over a very thick silty clay layer marking the base of the Holocene stratification. This last sandy layer has to be considered as a mouth-bar deposit which accumulated within a matter of few years, therefore geologically instantaneously. It is classified as a thick and coarse-grained layer.

A representation of the stratigraphy is provided in Figure 3.4.

It is also important to summarize the landscape evolution around the Superstation to give a correct interpretation to the stratigraphy and also to understand the dynamics which lead to

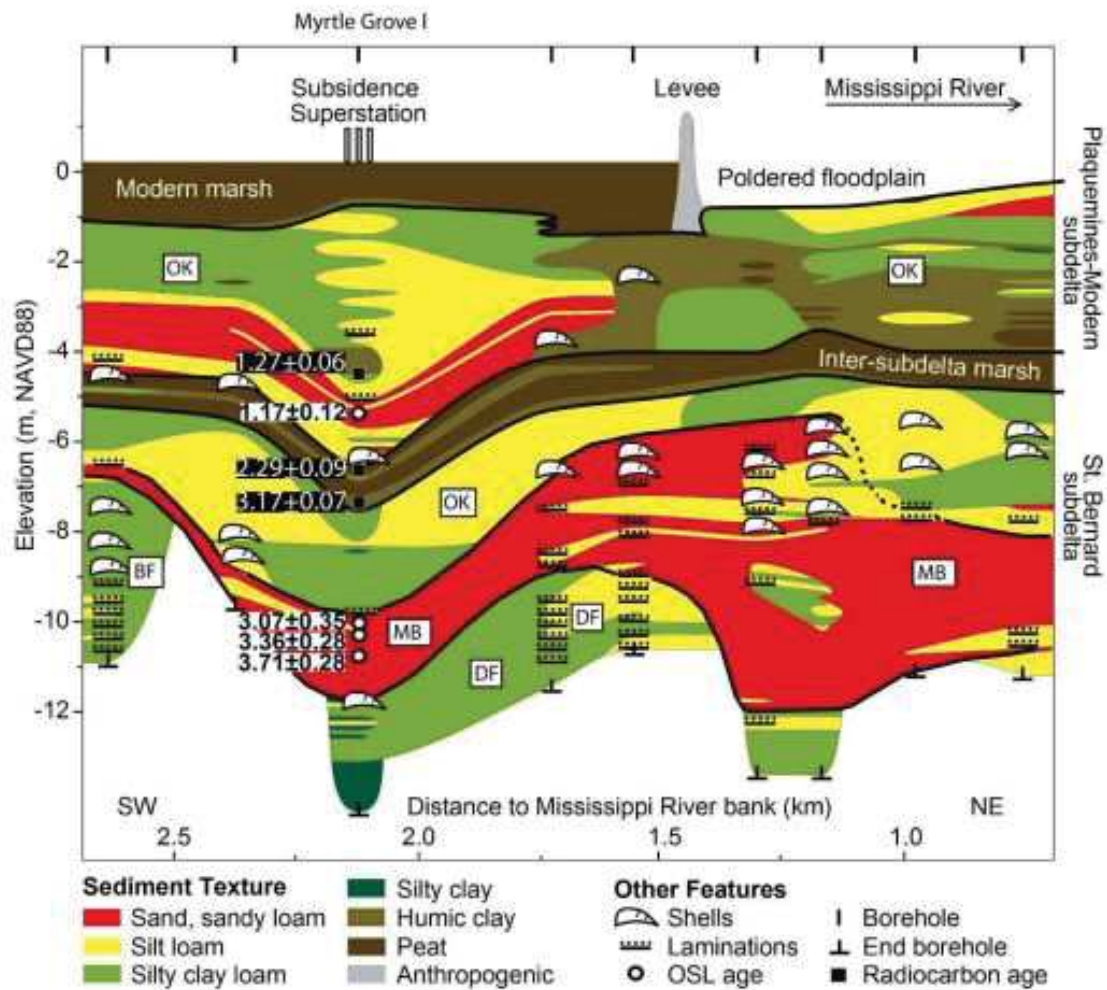


Figure 3.4: Litho-stratigraphic section of the Mississippi delta passing through the Myrtle Grove Superstation (after (Bridgeman, 2017)).

completing the mouth bar deposit around 3.4 ka BP. The site thus became subaerial up to a sudden decrease in sedimentation rate around 3.1 ka BP when marsh began to form and the St. Bernard lobe was soon abandoned. The presence of shells on top of the inter-subdelta marsh proves the subsequent transformation of the landscape into a bay. Then, at around 1.4 ka BP, the Plaquemines-Modern subdelta (Figure 2.1), started to form and most of the bay was eroded by a crevasse splay. A quick aggradation of the landscape occurred and overbank sedimentation continued up to the construction of the river levees which prevented sediment supply in a significant way.

The Superstation site does not provide only information about subsidence, but samples were collected for laboratory analysis which return bulk density, organic matter together with compressibility, permeability tests and geochronology. It is undoubtedly true that such characteristics help to give a more complete portrait of the dynamics of a given stratigraphic profile. For example, organic-rich sediments give a more significant contribution to subsidence respect to mineral matter dominated ones. Organic matter has to be considered, therefore, both a contributor to accretion and compaction. Moreover, sediment dry bulk density, expressed as g of dry material per cm^3 wet volume, increases with depth as a consequence of compaction. These last data are essential in the modelling phases, as will be explained in detail in the discussion of the results. The Myrtle Grove I core has to be considered, in conclusion, as a representative site of the Mississippi Delta.

Chapter 4

NATSUB3D model

The simulation of the evolution of the Mississippi river delta over the Holocene has been carried out by using the 3D numerical model NATSUB3D recently developed by Xotta et al., in press and based on the prior 1D and 2D formulation developed in Gambolati, 1973 and Zoccarato and Teatini, 2017. The results of the NATSUB3D application will allow to perform the prediction of elevation dynamics of the delta deposition environment based on reconstructed evolution of the Holocene formation. The model solves in a coupled way fashion the groundwater flow equation in a 3D setting and the consolidation equation based on the Terzaghi's principle. The model accounts for large soil deformations with geometric non-linearity and accounts for non-linear soil constitutive laws. The equations are solved by Finite Element (FE) discretization using a dynamic mesh changing over time (lagrangian approach). To follow the deposition and consolidation processes, the two main mechanisms are considered as follows:

- Depositional mechanism: the sedimentation rate is set as a condition imposed on the upper boundary of the domain and a specific threshold referred to the amount of sediment being deposited allows to understand if a new element is going to be added on the surface

or not;

- Consolidation mechanism: it accounts for soil compaction due to overpressure dissipation with the mesh node position updated at each time step to follow the deformation process.

Before discussing this procedure in detail it is important to provide an overview of the governing equations and the structure of the model.

4.1 The governing equations

The NATSUB3D model results from the coupling of a 1D geomechanical module based on the Terzaghi approach with a 3D groundwater flow module. A generalization of the formulation developed by Gambolati, 1973 leads to the equation describing the groundwater flow in a 3D porous system undergoing large deformations (Xotta et al., in press):

$$\nabla \cdot \left(\frac{K}{\gamma} \nabla p \right) = (c_b + \phi\beta) Dp - c_b(1 - \phi_0)(\gamma_s - \gamma)\omega \quad (4.1)$$

The main parameters of equation (4.1) are summarized below.

- $K = \begin{bmatrix} K_x(\sigma_z) & 0 & 0 \\ 0 & K_y(\sigma_z) & 0 \\ 0 & 0 & K_z(\sigma_z) \end{bmatrix}$

is the hydraulic conductivity tensor with $K_x(\sigma_z)$, $K_y(\sigma_z)$ and $K_z(\sigma_z)$ the horizontal and vertical components along the principal anisotropy directions;

- σ_z is the vertical effective stress;
- ϕ is the soil matrix porosity with ϕ_0 the value at the land surface where the vertical stress is negligible;

- γ is the specific weight of water;
- γ_s is the specific weight of soil grains;
- c_b is the soil oedometric compressibility;
- β is the volumetric water compressibility;
- D is the total (or Eulerian) derivative which can be treated as a partial time derivative $\partial/\partial t$ by using a Lagrangian approach with a dynamic mesh where the grid nodes follow the grains in their consolidation movements:

$$D = \frac{\partial}{\partial t} + \mathbf{v}_g \cdot \nabla \quad (4.2)$$

with $\mathbf{v}_g = [v_{gx} \ v_{gy} \ v_{gz}]^T$ is the grain velocity vector;

- p is the incremental pore pressure with reference to the hydrostatic condition (overpressure);
- ω is the sedimentation rate which expresses how much material is being deposited in a given time interval;
- x, y, z are horizontal, lateral and vertical spatial coordinates;
- t is time.

The parameters K_x, K_y, k_z, ϕ , and c_b may depend on the vertical effective stress.

The numerical solution of equation (4.1) is based on a Lagrangian approach in which the grid nodes of the dynamic mesh follow the consolidation process lead by grain movement, thus resulting in a deformation of the finite elements. The system of non-linear ordinary differential

equations which results from the finite element discretization approach used for equation (4.1) is solved through a back Euler method in time with a fixed-point iteration scheme.

At this point it is important to introduce the equations related to soil compaction and accumulation of sediments on the depositional surface as well as some fundamental constitutive relations. Indeed, quantification of the geostatic load and the consequent change in the length of the soil column are fundamental to give a correct description of the process but also the role of compressibility and void ratio has to be taken into account. The equations which are now going to be discussed will be recalled while explaining the structure of the model, therefore it is suggested to deeply understand them.

To start with, the increase of geostatic load resulting from the accumulation of a certain quantity of material with sedimentation rate ω in a time interval Δt is defined as:

$$\Delta\sigma_t = (1 - \phi_0)(\gamma_s - \gamma)\omega\Delta t \quad (4.3)$$

where $\Delta\sigma_t$ is the external factor causing the pore pressure to change compared to the equilibrated condition. The Terzaghi's principle links the increase of the geostatic load $\Delta\sigma_t$, the overpressure change p and the vertical effective stress $\Delta\sigma_z$ with the shortening Δh of a soil column with initial thickness H_0 that can be expressed as:

$$\Delta h = \alpha H_0 \Delta\sigma_z \quad (4.4)$$

In this equation α represents the classical soil compressibility and it can be linked to c_b through the following relation (Gambolati et al., 1998):

$$c_b = \frac{p \frac{d\alpha}{dp} + \alpha}{1 + \alpha p} \quad (4.5)$$

It is important to state that soil compressibility is proved to play a primary role among the parameters controlling soil compaction and it can be evaluated in laboratory through oe-

dometric tests. It is related to void ratio e and σ_z as expressed in the following formula:

$$c_b = -\frac{1}{1+e} \frac{de}{d\sigma_z} \quad (4.6)$$

It can be also expressed as function of the compression index C_c , which depends only on the type of sediment, as

$$c_b = \frac{1}{\ln 10} \frac{C_c}{(1+e)\sigma_z} \quad (4.7)$$

It is useful, then, to remind that for stress values lower than the pre-consolidation stress the recompression index C_r has to be considered instead of C_c . For $\sigma_z \leq \sigma_p$ with σ_p the pre-consolidation stress, the void ratio is equal to:

$$e = e_0 - C_r \log\left(\frac{\sigma_z}{\sigma_{z0}}\right) \quad (4.8)$$

Whereas if $\sigma_z \geq \sigma_p$, the void ratio is calculated as:

$$e = e_c - C_c \log\left(\frac{\sigma_z}{\sigma_p}\right) \quad (4.9)$$

Where:

- e_0 is the void ratio at very shallow depth;
- σ_{z0} is the effective stress at very shallow depth;
- e_c is the void index at pre-consolidation stress.

Finally, the mathematical expression of compaction of a soil column can be introduced Gambolati et al., 1998:

$$u(z, t) = - \int_0^z \frac{\alpha(\sigma_z)\sigma_z}{1 - \alpha(\sigma_z)\sigma_z} dz \quad (4.10)$$

The two extremes of the integral indicate a soil column extending from the basement to a generic elevation z .

4.2 Structure of the model

NATSUB3D is a simulator coded in fortran language. It is composed of a series of ascii files. Some of them play only a technical role because their purpose is only to read, create, open or close input and output files or define the characteristics of the materials and the grid data. Some others host significant steps for the development of the calculations, such as the computation of variables (stress, strain, pressure, post depositional lowering) and the construction of the 3D mesh by adding new soil layers with proper thickness. An important focus has to be made on the numerical implementation of the model. NATSUB3D is developed to solve equations (4.1) and (4.10) numerically through the FE method adopting a tetrahedral discretization. The steps of this procedure are summarized below:

- Computation of the sedimentation thickness ($dh_i = \omega(x, t) \cdot \Delta t_i$) in order to obtain the amount of soil deposited during time Δt_i . If dh_i exceeds a threshold value Δz_{max} consequently the model reduces Δt_i to $\Delta t_i = \frac{\Delta z_{max}}{\omega}$;
- Update of the total stress σ_t through the equation (4.3);
- Implementation of a Picard iterative scheme to compute the solution of the nonlinear ordinary differential system of equations obtained through the numerical discretization of equation (4.1);
- Effective stress $\sigma^{(k+1)}$ is computed through Terzaghi's relation ($\sigma^{(k+1)} = \sigma_t - p^{(k+1)}$) once $p^{(k+1)}$ is computed. k indicates the nonlinear iteration. No variation of σ_t is assumed as its value changes only in response to sediment accumulation on the landform surface;
- The constitutive relations previously mentioned allow to update the hydrogeomechanical parameters of each element at each time step, while the depth interval between two

adjacent nodes $\Delta z^{(k+1)}$ is updated following this equation: $\Delta z^{(k+1)} = \Delta z^0 + \Delta u^{(k+1)}$.

The depth interval at the previous time step is given by Δz^0 , whereas the compaction term is $\Delta u^{(k+1)}$ calculated with equation (4.10);

- Convergence is reached when the difference between the solutions of two subsequent iterations is no more exceeding the established tolerance;
- At this point a new time step starts and the first thing the model does is to check the need for mesh update by comparing the element thickness h_{i+1} above a generic node j with the threshold Δz_{max} . If $\Delta z_{max} \geq h_{i+1}$, a new element is added above node j and its characteristics are assigned according to the properties of the corresponding sediment type at shallower depth.

It is important to state that the mesh develops above a marsh basement assumed as incompressible. It could be associated to the upper part of the Pleistocene litology. In any case, it is assumed as impermeable or "no flux" boundary layer. As regards the boundary conditions for the other sides of the soil column, the model is set considering them as either no-flow or zero pressure surfaces. The first case refers to a Neumann boundary condition because it is imposed on the flux through the considered surface. The second case, on the other hand, imposes a Dirichlet boundary condition as the value of pressure is assigned. In order to summarise the steps discussed up to this point through a more complete and clear visualization, a scheme provided in the paper by Zoccarato and Teatini, 2017 is reported in Figure 4.1.

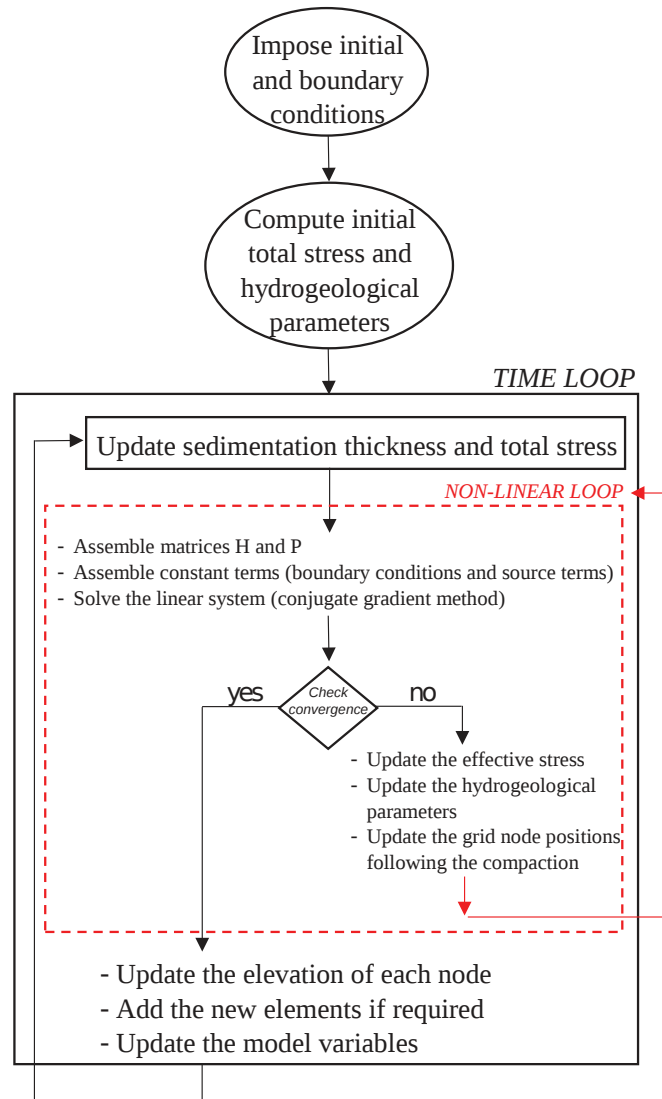


Figure 4.1: A scheme of the functioning of NATSUB3D model (after Zoccarato and Teatini (2017)).

4.3 Main parameters

The description of a soil from a geotechnical point of view includes the definition of the following parameters: void ratio (e_0), saturation degree (S), compressibility coefficient (C_c), pre-consolidation stress (σ_p) and hydraulic conductivity ($K_{z,0}$). The meaning of each of them is briefly explained in the next paragraphs.

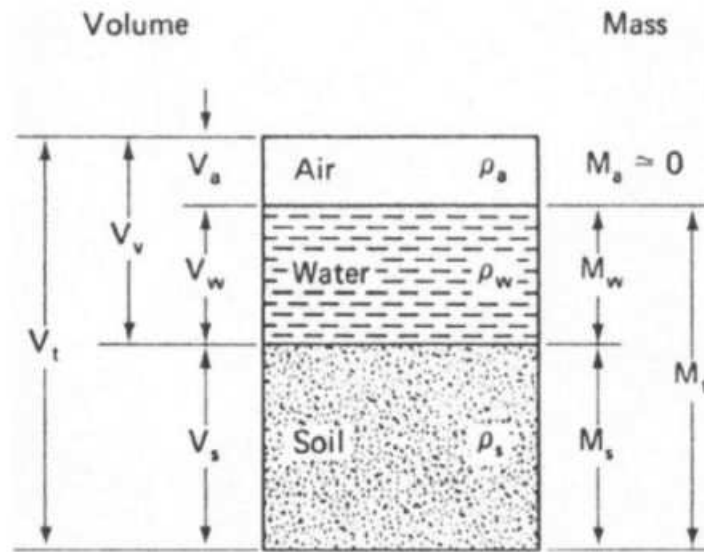


Figure 4.2: A scheme of soil components.

Void ratio. It is defined as the ratio between the volume of voids (V_v), filled by water and/or air, and the volume occupied by grain particles (V_s). It allows to describe how compaction behaves in the considered soil. Our model considers the initial void ratio e_0 as one of the input parameters for each soil, corresponding to the soil condition at the land surface with effective stress σ_z almost null.

$$e = \frac{V_v}{V_s} \quad (4.11)$$

Saturation degree. It is expressed in percentage of volume of water (V_w) with respect to the total volume (V_t)

$$S(\%) = \frac{V_w}{V_t} \times 100\% \quad (4.12)$$

In our model it is set equal to 1 because conditions of fully saturated soil are considered.

All parameters described so far refer to a soil scheme similar to the one shown in Figure 4.2.

Then, it is important to understand the meaning of some important geotechnical parameters which allow to give a complete and detailed description of the characteristics of a soil.

Stress, pressure and Terzaghi's principle. The stress at a point in a soil is a quite fictitious concept because since it is defined as the ratio between a force and a unit area, in this case the area contains both grain-to-grain and voids-to-voids contacts (Figure 4.3).

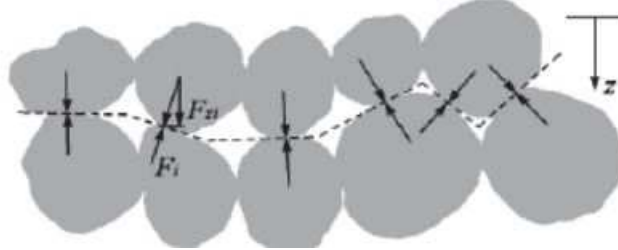


Figure 4.3: A cross section showing grain-to-grain and void-to-void contacts.

The effect of compaction is to reduce the pore space between grains, which are considered as incompressible. Such reduction of the pore space is a consequence of an increase of the effective intergranular stress, defined as the vertical component of the stress exchanged between a couple of considered grains:

$$\sigma_{zi} = \frac{F_{zi}}{A_i} \quad (4.13)$$

If the number of contact points is extended to n , the equation assumes the following form:

$$\sigma_z = \sum_{i=1}^n F_{zi} \quad (4.14)$$

By defining the total stress σ_c as the weight of a soil column with unit horizontal section at given depth, in conditions of full saturation it is balanced by the sum of the effective stress and the hydrostatic pressure p according to the relation (Terzaghi, 1926)

$$\sigma_c = \sigma_z + p \left(1 - \sum_{i=1}^n A_i \cos \alpha_i \right) \quad (4.15)$$

where A_i refers to the contact area between grains, n the number of contacts within the unit area and α_i the angle between the vertical direction and the normal to A_i . The contact area between grains is very small and it can be considered negligible, leading to a simplified form of

the previous equation which becomes

$$\sigma_c = \sigma_z + p \quad (4.16)$$

In our model it is important to understand the distribution of stress and pressure in order to identify periods over which, due to fast deposition of sediments (possibly characterised by a large specific weight γ_s and a small hydraulic conductivity), overpressure may occur. It is therefore important to understand, for example, how much time is needed to dissipate it.

Pre-consolidation stress. If the $e - \log \sigma_z$ curve is taken into account, the pre-consolidation stress σ_p corresponds to the maximum vertical stress which acted on the soil sample in the past. It marks the limit between the phase of reloading consolidation and the one of virgin loading (Figure 4.4).

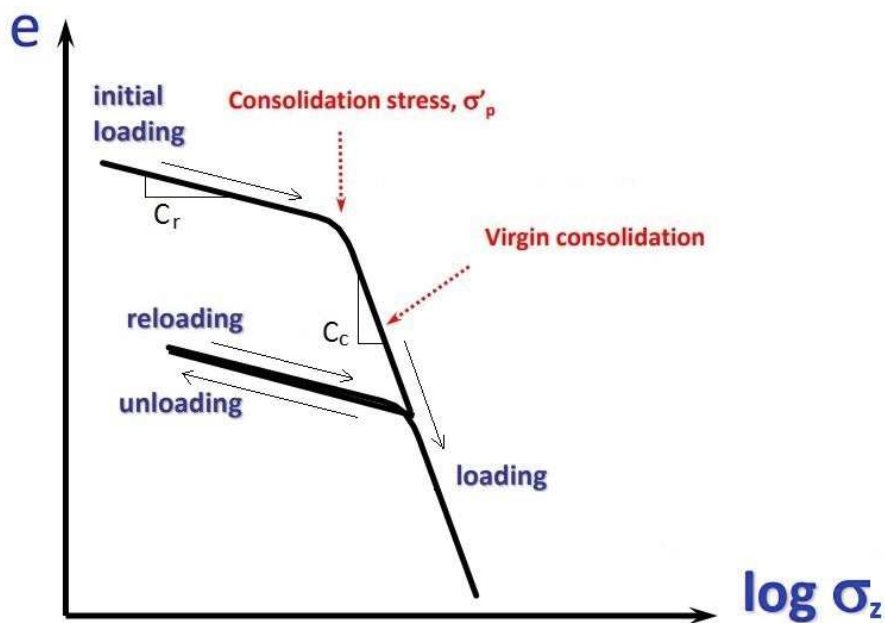


Figure 4.4: A qualitative example of void ratio vs effective stress behaviour.

Strain. It is a non-dimensional parameter describing the variation in height ΔH of a given soil layer respect to its original thickness H_0 . It returns how much deformation it has undergone

as a consequence of external loading.

$$\epsilon = \frac{\Delta H}{H_0} \quad (4.17)$$

In our model it helps identifying which layers in the final time step of the simulation have undergone more or less reduction of their original thickness, thus giving an idea of their compaction.

Compression index. Considering the $e - \log(\sigma_z)$ curve, it corresponds to the ratio between the void ratio change and the difference in $\log(\sigma_z)$ during the loading phase:

$$C_c = \frac{\Delta e}{\Delta \log \sigma_z} \quad (4.18)$$

C_c usually ranges between 0.1 and 10. For example, this index ranges from 0.20 to 0.50 in clays, whereas for silts it would be equal to 0.16 - 0.24. It is important to state that C_c differs from the soil uniaxial vertical compressibility c_b (already discussed in paragraph 4.1), which is on the other hand a geomechanical parameter controlling the amount of vertical soil deformation caused by pressure change.

Recompression index It is indicated as C_r and used to characterise the consolidation settlement for overconsolidated soils and the expansion behaviour during unloading. By recalling the $e - \log \sigma_z$ curve, it corresponds to the ratio between the void ratio change and the difference in $\log \sigma_z$ during the loading phase with $\sigma_z \leq \sigma_p$:

$$C_r = \frac{\Delta e}{\Delta \log \sigma_z} \quad (4.19)$$

It is possible to define that the softer the soil, the larger the ratio C_c/C_r . As stated in Teatini et al., 2011, then, C_c/C_r tends to increase for shallower depth (50-300 m) independently on the considered site.

How can all these parameters be contextualized in NATSUB3D model? First of all, the void ratio and its own variation help to quantify compaction because a soil layer having initial void ratio e_0 and initial thickness s_0 experiences a decrease in e and s due to an increase in effective stress $\Delta\sigma_z$ which follows the dissipation of overpressure p . The mathematical laws describing the variation of e and the compaction η are the following:

$$e(z) = e_0 - C_C \log \sigma_z \quad (4.20)$$

$$\eta = s_0 \frac{\Delta e}{1 + e_0} \quad (4.21)$$

Compaction, or better auto-compaction, in subsiding river deltas is one of the main processes causing land subsidence. The gradual accumulation of sediments leads to an increase in total stress and, according to equation (4.16), to effective stress. It can be expressed also as "compaction ratio" by considering the difference between compacted and uncompact thickness of each layer with respect to its original thickness:

$$\%C = \frac{s - s_0}{s_0} \cdot 100 \quad (4.22)$$

Such parameter is useful, for example, when analysing how the percentage of compaction changes with depth or when comparing the behaviour of soil strata at different time steps in a simulation. The compaction ratio, indeed, proves to have a strong dependence on core depth and lithology. NATSUB3D provides also the "integrated compaction", meaning that it reports where each point inside a soil layer would have been located if compaction had not occurred. This means that, taking into account a soil column, this variable would range from zero on the bottom to a certain value on the top. When compaction takes place in a soil layer, the pore water is forced to escape. When water flow happens "unsufficiently" fast, an overpressure

develops. As will be shown in detail in the discussion of the results, this situation develops within low permeability units in correspondence of the deposition of significant amounts of sandy layers in a short time interval, for example only one year. Then, overpressure gradually dissipates returning to a hydrostatic pressure distribution. Another parameter helps to give a complete portrait of the process: the post depositional lowering, which will be referred to as "pdl". It computes how much a point in the soil column settles after being deposited. This parameter returns values equal to zero on top and bottom of the soil column as in the first case the material has just deposited, whereas in the second case it has placed on the fixed basement. The central part of the soil column experiences the higher values of pdl.

Finally, it is important to mention the sedimentation rate ω which allows to assign the quantity of a given material depositing in a certain period of time. This is the way the considered soil column of Myrtle Grove superstation is reconstructed by the model. The average sedimentation rate ω over a certain time interval Δt is computed as

$$\omega = \frac{\Delta l}{\Delta t} \quad (4.23)$$

where Δl is the sediment thickness deposited during Δt before compaction. A fundamental step to be discussed, at this point, is the one which allows to determine Δl . A decompaction procedure has been followed in order to obtain this value and, consequently, the sedimentation rate ω for each soil layer. To achieve this goal, a 1D decompaction model has been used. It returns as outcome the original thickness of the sedimentary layers composing the soil column together with the corresponding effective stress variation with depth. The main steps of this procedure are summarized as follows:

- Distinction of typology, number and thickness of the litological classes within the soil column in the final time step;

- Assignment of the values of geotechnical properties to the lithological units, i.e.: C_c , C_r , e_0 and γ_s ;
- Launch a pre-processing code which produces a table of the properties varying with depth for each material, e.g., e vs σ_z . These are the inputs for the decompaction model;
- Launch the 1D decompaction model which computes the decompacted thickness Δh of each layer using the evolution of void index e and effective stress σ_z which are linked by equation (4.20). Δl is calculated as

$$\Delta l = (1 - e_0) \int_{z_1}^{z_2} \frac{dz}{1 + e(z)} \quad (4.24)$$

where $z_2 - z_1$ defines the depth interval to which decompaction is applied and corresponding to deposition time $\Delta t = t_2 - t_1$.


- The uncompacted thickness returns the values of Δl for each lithological unit which are used to determine the correspondent sedimentation rate ω .

Chapter 5

Modeling the evolution at the Myrtle Grove Superstation

5.1 Model set-up

After illustrating all parameters and equations involved in NATSUB3D, it is fundamental to understand how the input data are organized. The simulator needs an *input.parm* file in which both the soil parameters and the corresponding sedimentation rates are set for each soil class. Moreover, contains the maximum number of iterations required to reach convergence for the iterative procedure implemented to solve the parameter and geometric nonlinearities in equation (4.1) and the associated tolerance must be provided. The model uses an adaptive mesh with elements changing shape and number according to consolidation and new sediment deposition over time. The initial element thickness is equal to 10 cm and its length along x and y is 20 cm. The base layer contains a total of 24 elements. It must be outlined that NATSUB3D is here used to simulate a 1D problem. The domain is represented by a soil column discretized with a total of 4662 nodes and 12408 elements in its final configuration, with the results shown



	γ_s [g/cm ³]	σ_0 [kPa]	σ_p [kPa]	e_0 [-]	C_c [-]	C_r [-]	K_{z0} [m/yr]
Sand	2.65	0.01	4	1	0.033	0.033	31.5
Silty clay loam	2.65	0.01	4	1.7	0.6	0.009	31.5
Peat	1.14	0.01	4	13	4.72	0.8	3.15
Silty clay	2.65	0.01	4	1.8	0.57	0.0008	0.0315
Silty loam	2.65	0.01	4	1.1	0.23	0.07	3.15
Humic clay	1.90	0.01	4	6.9	2.38	0.42	3.15

Figure 5.1: Lithological classes composing the sedimentary column of the Myrtle Grove Superstation and their parameters as provided by Bridgeman (2017) and Keogh et al. (2021).

for the central column nodes. As anticipated in Chapter 4, the model is set considering the lateral surfaces of the soil column as no-flow (Neumann boundary condition). The basement is assumed as impermeable and a null overpressure (Dirichlet boundary condition) is prescribed on the column top. From a physical point of view this condition states that the land surface approximately grew with the mean sea level during the Holocene. The simulated column derives from a simplification of the detailed lithostratigraphy provided in Bridgeman (2017) (Figure 5.2) and it is composed, in its final configuration, of six lithological classes located at different depth and therefore deposited at different times during the Holocene. The lithologies are sand, silt loam, silty clay loam, silty clay, humic clay and peat and their characteristics are summarized in Figure 5.1. The choice of the values to assign to each parameter was made according to a deep literature research together with observations provided by the Myrtle Grove Superstation. The final set-up of the input parameters includes e_0 , C_c , C_r and K_{z0} taken from Bridgeman (2017) and γ_s according to Keogh et al. (2021). The humic clay characteristics have been determined by averaging the peat and the silty clay parameters.

The adopted simplified representation of the sedimentary column considers the silty clay as a unique homogeneous block whereas the column in Bridgeman’s representation includes also a small sandy layer at about 28 m depth. The same happens for the silty clay loam between 8 m and 10 m depth which, in our case, does not account for the presence of thin layers of

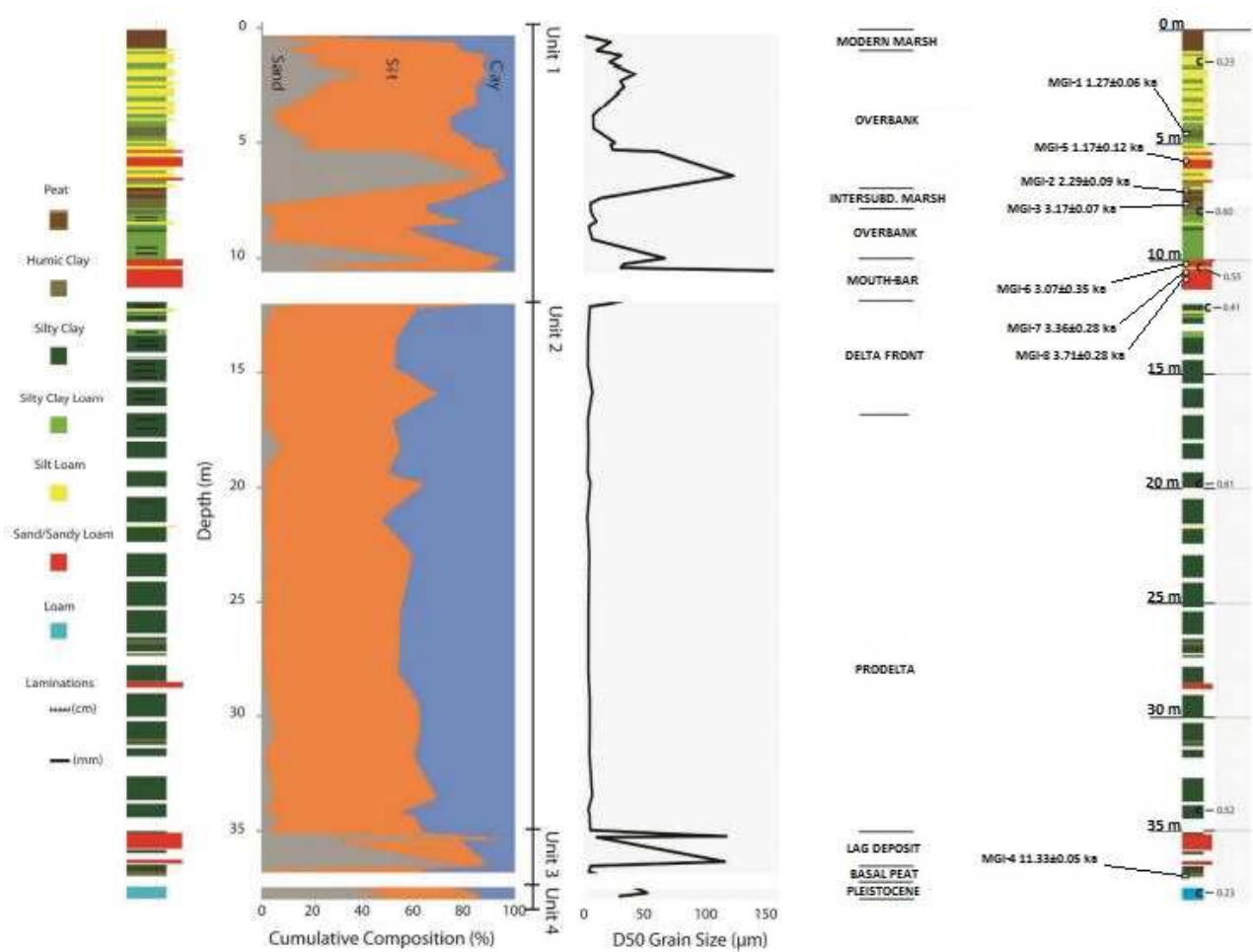


Figure 5.2: Myrtle Grove I representation of the grain size and dating of the lithology after Bridgeman (2017).

silty clay and silty loam. Finally, the overbank sequence of silty loam and silty clay loam is much more regularized in our case than in Bridgeman's column. The simplification performed in our discretization of the soil column was based on the choice to represent layers whose compacted thickness in the final configuration was at least equal to 0.2 m. This explains why some thin laminations have been excluded. The discretization was performed manually through a proportion between the known real depth scale reported in Bridgeman's representation (with a step of 5 m) and the thickness of each soil strata measured on the same column printed on an A3 paper using a ruler.

Then, as a consequence of the assumption of the soil parameters and the discretization as

just discussed, the sedimentation rate of each soil unit has been derived through the decompaction procedure, which returns the original thickness of the layer and the associated stress and allows to determine ω for each age interval. Owing to the fact that Bridgeman (2017) depth-age model is rather uncertain within the overbank, three scenarios for overbank deposition have been developed in agreement with the researchers (prof. Torbjörn Törnqvist) from Tulane University collaborating to the project. They are outlined in paragraph 5.3 and the model has been run accordingly.

5.2 Preliminary analysis

Testing the applicability of a model is an essential step before its use on a real complex case. The preliminary analysis permits to understand the coherence of the model response to a change in the values of the input parameters. In this framework, a set of simulations have been performed for the following simple cases considering a time period of 1000 years:

1. One soil with homogeneous characteristics ($e_0=10$, $C_r=0.1$, $C_c=3$, $K_{z0}=0.0315$ m/yr, $\sigma_0=0.1$ kPa, $\sigma_p=2$ kPa, $\gamma_s=2.70$ g/cm³);
2. The same soil as in the previous step changing its geotechnical parameters one-by-one;
3. Two soils with different characteristics. The soil having the following characteristics has been added to the previous one: $e_0=0.75$, $C_r=0.1$, $C_c=0.8$, $K_{z0}=3.15$ m/yr, $\sigma_0=0.1$ kPa, $\sigma_p=2$ kPa, $\gamma_s=2.90$ g/cm³.

Figure 5.3 shows the temporal evolution of the soil column in case 1. Considering the strain as an example, the model returns the expected increment of such variable over time in the

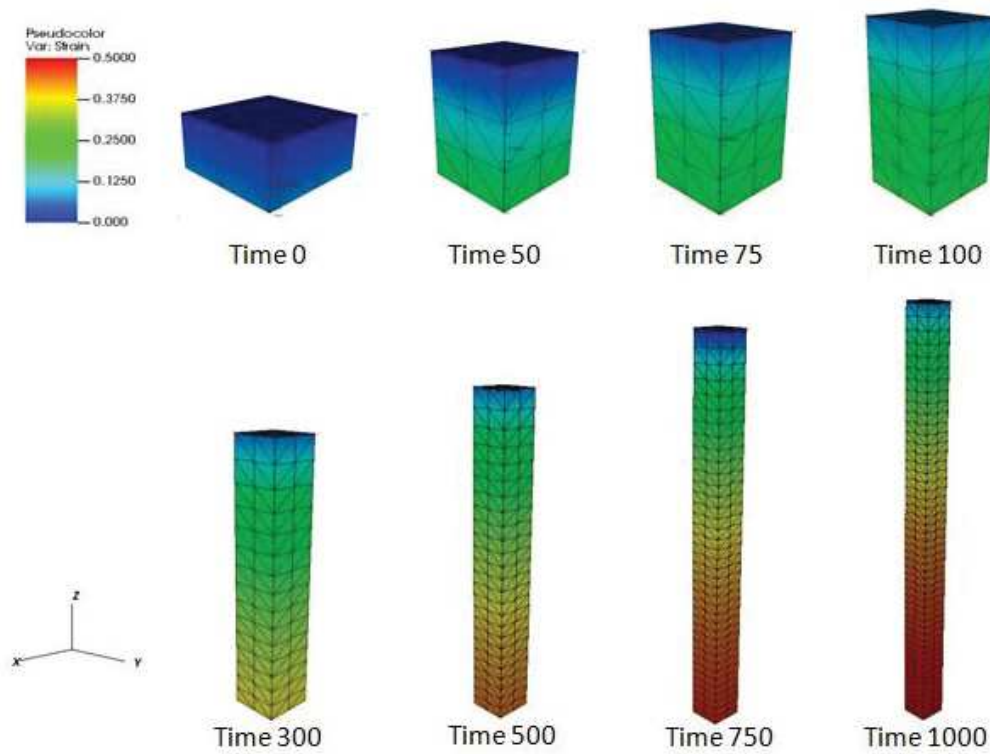


Figure 5.3: Case 1 - Temporal behaviour of the sedimentary column and the soil strain due to autocompaction for the case of a single soil class. Notice that the horizontal and vertical scale change from plot to plot, only colours are consistent for plot comparison.

lower layers as a consequence of the gradual deposition of sediment on the column top (Figure 5.3).

Figure 5.4 shows the strain distribution along the height of the soil column for case 2. The most evident effect is the one given by a change in the compression index C_C . If its value is doubled, the thickness of the soil column reduces significantly compared to the initial case because we are assuming that the material becomes twice more compressible. The opposite happens by doubling the sedimentation rate ω , as this means that much more soil is being deposited and undergoing compaction in the same time period. Less strain together with a larger thickness of the soil column can be noticed by doubling the initial void ratio. This is the consequence of more pore space at the column top and, therefore, a lighter soil that causes a smaller effective stress and a smaller strain.

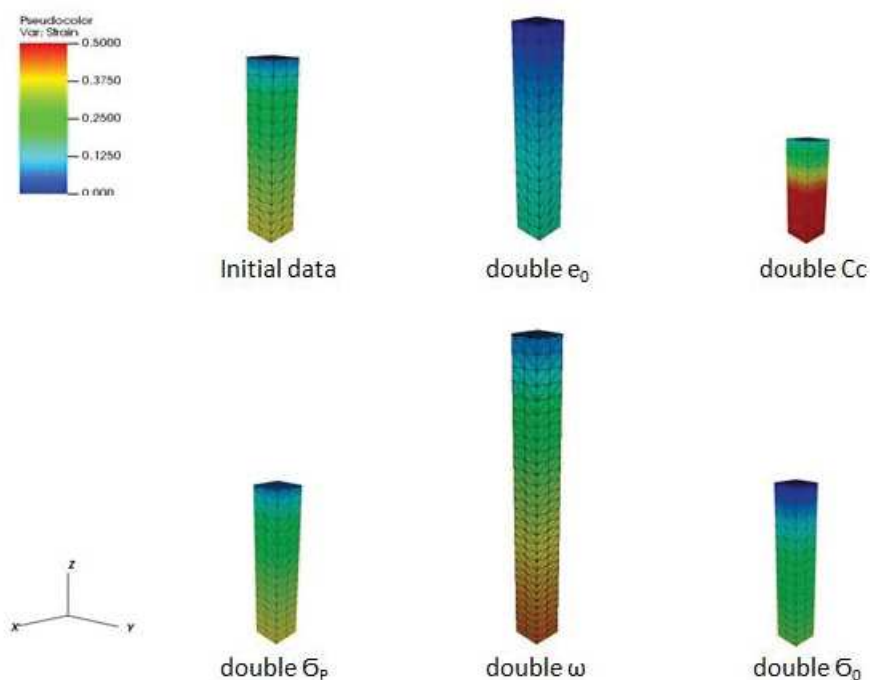


Figure 5.4: Case 2 - Model outputs in terms of column thickness and strain for the various soil parameters considered in the preliminary analysis. The results refer to the simulation time $t=300$ yr. Notice that the horizontal and vertical scale change from plot to plot, only colours are consistent for plot comparison.

To better understand the model behaviour a second layer of material with different characteristics from the previous one has been introduced. The same sedimentation period of 1000 years is simulated. The results over time for a single soil and two soil columns are shown in Figures 5.3 and 5.5. As expected, by considering again the variable strain, the model returns a jump in the strain values, thus pointing out the different behaviour when two soil classes are considered. The base layer undergoes less strain than the lower part of the upper layer. This means that it is less deformable.

5.3 Possible scenarios for the overbank deposition

The Myrtle Grove soil column previously outlined shows that below the top peat deposit a series of silty loam and silty clay loam layers characterise the site down to a first sandy layer.

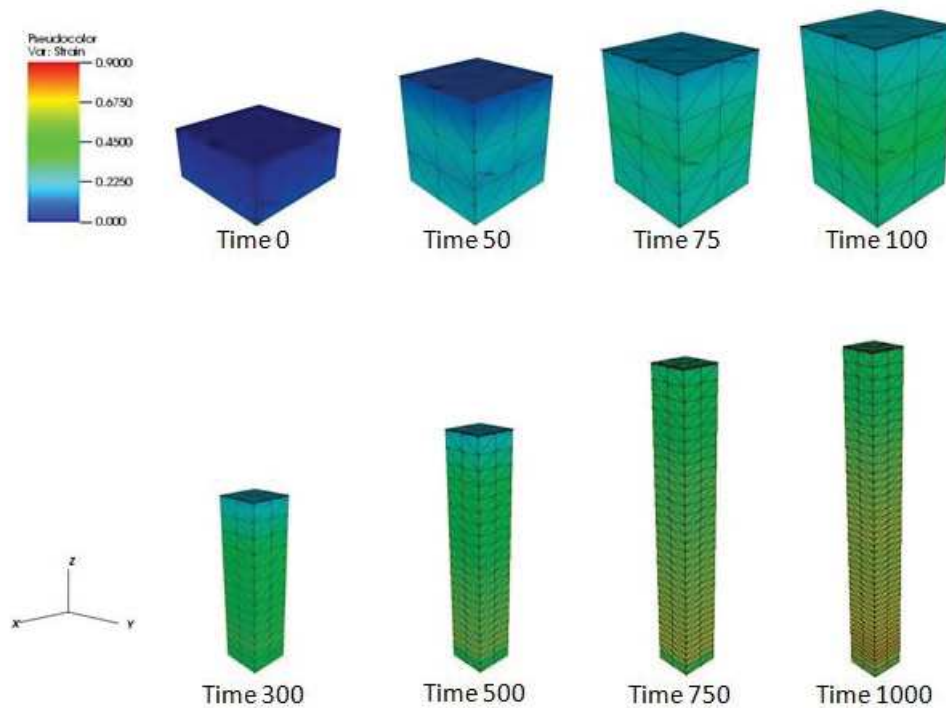


Figure 5.5: Case 3 - Temporal behaviour of the sedimentary column and strain in the case of two soil classes. Notice that the horizontal and vertical scale change from plot to plot, only colours are consistent for plot comparison.

This complex sequence represents an overbank deposition occurred between 80 yr BP and 1300 yr BP. It is generally believed that rates of overbank aggradation in delta plains do not display relevant variations over time and such conclusion has been supported by the observation that very few difference in aggradation occurs comparing less-frequent, large magnitude floods and more frequent, average floods. On the other hand, though, other studies have raised doubts and weakened this outcome (Sambrook Smith et al., 2010). It has been shown that accumulation of overbank strata may happen at exceptionally high rates in large areas as a consequence of a flood event. For this reason and because of the lack of specific datings as explained in paragraph 5.1, three possible scenarios of the overbank deposition have been developed:

- Scenario A: a middle-growth of the overbank equal to 10 mm/yr is assumed;
- Scenario B: a rapid growth of the overbank equal to 20 mm/yr is assumed;

Scenario A			Scenario B			Scenario C		
Stratigraphy	Year of deposit	sed rate [mm/yr]	Stratigraphy	Year of deposit	sed rate [mm/yr]	Stratigraphy	Year of deposit	sed rate [mm/yr]
peat	10920	11.625	peat	10920	11.625	peat	10920	11.625
silty loam	10855	10	silty loam	10888	20	silty loam	10761	4.08
silty clay loam	10823	10	silty clay loam	10872	20	silty clay loam	10682	4.08
silty loam	10777	10	silty loam	10849	20	silty loam	10570	4.08
silty clay loam	10754	10	silty clay loam	10837	20	silty clay loam	10513	4.08
silty loam	10695	10	silty loam	10808	20	silty loam	10369	4.08
silty clay loam	10659	10	silty clay loam	10790	20	silty clay loam	10280	4.08
silty loam	10586	10	silty loam	10753	20	silty loam	10101	4.08
silty clay loam	10114	1.84	silty clay loam	10192	1.55	silty clay loam	9888	4.08
humic clay	9838	1.84	humic clay	9863	1.55	humic clay	9763	4.08
silty clay loam	9702	1.84	silty clay loam	9702	1.55	silty clay loam	9702	4.08
silty loam	9701	675	silty loam	9701	675	silty loam	9701	675
sand	9700	675	sand	9700	675	sand	9700	675
silty loam	9400	3.8	silty loam	9400	3.8	silty loam	9400	3.8
	8700	0		8700	0		8700	0
peat	8342	1.79	peat	8342	1.79	peat	8342	1.79
humic clay	7800	1.79	humic clay	7800	1.79	humic clay	7800	1.79
silty clay loam	7401	6.89	silty clay loam	7401	6.89	silty clay loam	7401	6.89
sand	7400	1820	sand	7400	1820	sand	7400	1820
silty clay	4440	7.09	silty clay	4440	7.09	silty clay	4440	7.09
	1	3.15		1	3.15		1	3.15
sand	0	2160	sand	0	2160	sand	0	2160

Figure 5.6: Sedimentation rates [mm/yr] in the different scenarios for overbank deposition. Notice that the years are indicated in terms of simulation time, not as yr BP.

- Scenario C: a constant rate equal to 4 mm/yr is used and encompasses also the more organic deposits.

The sedimentation rates and years of deposition over the various layers are represented in Figure 5.6. The sedimentation span a total time interval of 11000 years, i.e. from 11000 yr BP to today. Below the overbank, i.e. before 3599 yr BP (simulation time 7401 in 5.6) the sedimentary sequence is composed of a mouth bar sand, formed very rapidly as the delta prograded seaward, over a very thick silty clay layer which marks the first thick part of the Holocene stratigraphy and is classified as a prodelta deposit. It contains both delta-front and bay-floor deposits as silty clay muds are dominant but also very thin laminations of sand or silt are present. Notice that they are not included in our model representation because their thickness was smaller than 0.2 m as already discussed in paragraph 5.1.

The sedimentation hiatus at year 8700 (i.e. 2300 yr BP) derives from the erosion of the peat layer, which had grown more before it got eroded by the crevasse. One of the aims of the task is to understand whether in any of these three scenarios for the evolution of the Myrtle Grove soil column a certain amount of overpressure persists until the ending time step influencing the

possible soil compaction also nowadays.

5.4 Results

The results for the three scenarios are represented in terms of five main variables, i.e. column thickness, stress, strain, pressure, and integrated compaction, that provide a clear overview of the evolution of the soil column. The next paragraphs briefly discuss the temporal behaviour of each variable by comparing the outcome of NATSUB3D with those published by Bridgeman (2017).

Column thickness The three scenarios return a soil column having the same final thickness (Figure 5.7), although resulting clearly from a different evolution over time between 1300 yr BP and 0 yr. The value is coherent with Bridgeman (2017) representation (Figure 5.2). It is interesting to notice that for a short period after time 1300 yr BP, when sand deposition has completed, the thickness of the soil column reduces instead of increasing following accretion (Figure 5.8). This happens as a consequence of the compaction of the soil layers below the sand, which reduce their thickness in response to significant sand weight. Finally, the flat trend displayed from 2300 yr BP to 1600 yr BP corresponds to the hiatus period in which nothing deposited.

Pressure Two main peaks of overpressure have been computed in all scenarios. The first one (20 kPa) at simulation time 7401 yr (i.e. 3599 yr BP) soon after the deposition of a sand layer (Figure 5.9) and the second one (about 13 kPa) at simulation time 9702 (i.e. 1298 yr BP) after the deposit of a third sand layer and of silty loam and silty clay loam (Figure 5.10). Over the last hundreds years, a certain overpressure has been computed in scenario B at

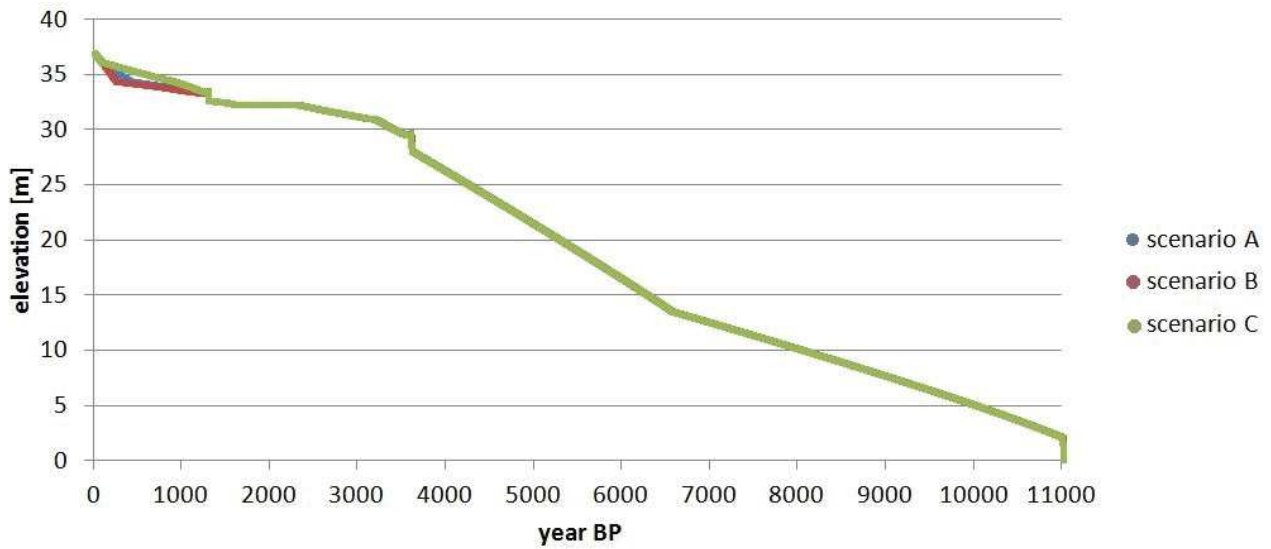


Figure 5.7: Variation over time of the elevation of the soil column computed by NATSUB3D for the three scenarios.

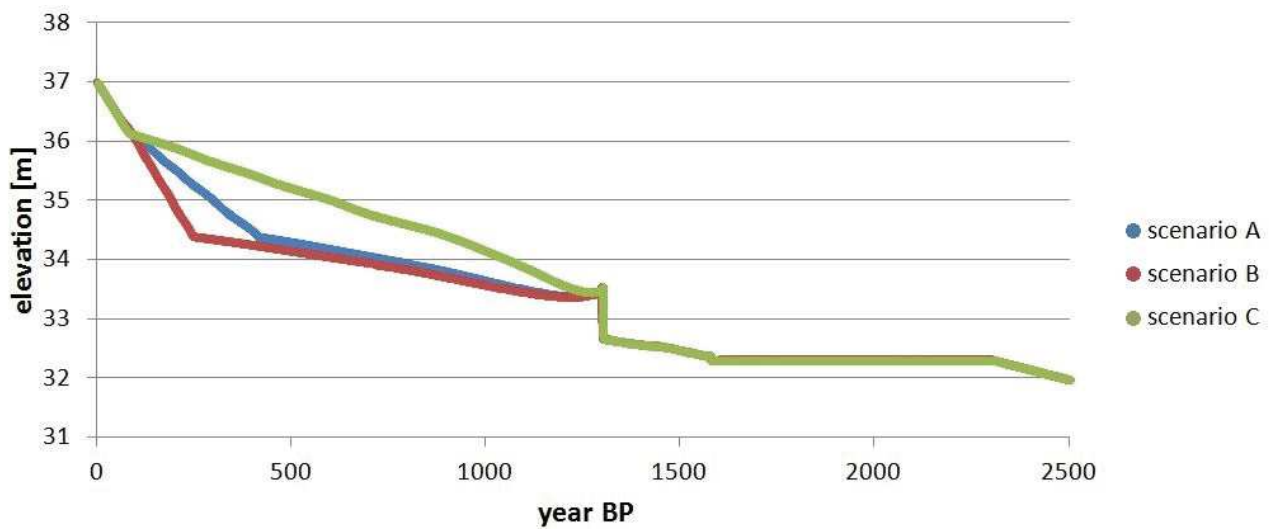


Figure 5.8: Variation over time of the elevation of the soil column computed by NATSUB3D for the three scenarios between 2500 yr BP and 0 yr BP.

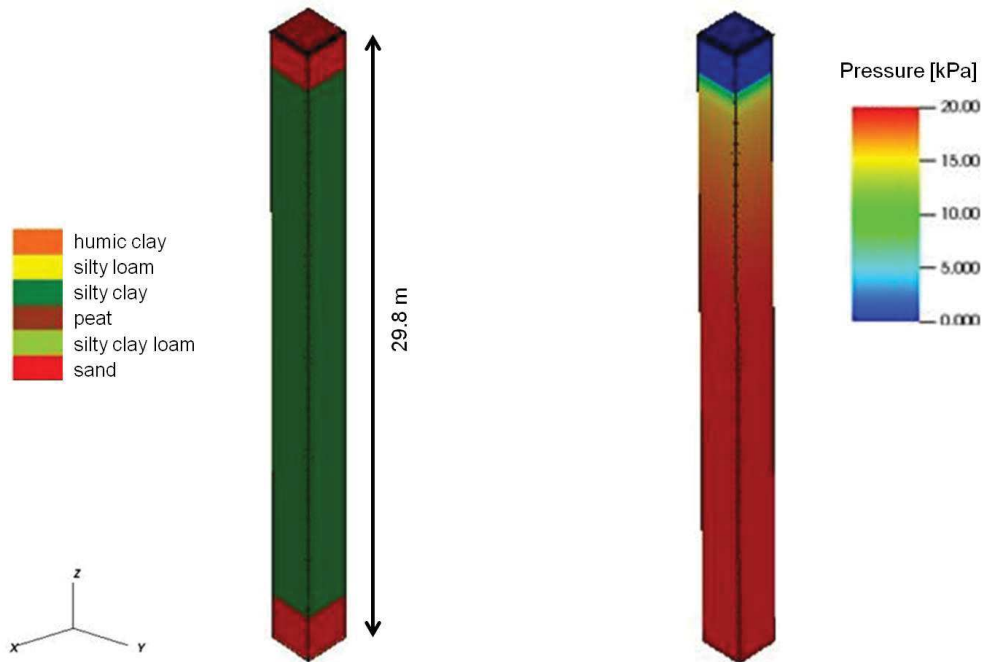


Figure 5.9: Scenario A: sediment classes and overpressure [kPa] at simulation time $t=7401$ yr (i.e. 3599 yr BP).

simulation times 10778 (i.e. 222 yr BP, in Figure 5.11), 10824 (i.e. 176 yr BP, in Figure 5.12) and 10921 (i.e. 79 yr BP, in Figure 5.13) due to the greater sedimentation rate. At these steps the overpressure amounts to about 5 kPa and 9 kPa. In all the three scenarios the situation at present is characterised by a low overpressure in the whole column, proving that all the overpressure peaks developed in the recent past dissipated.

Effective stress The general behaviour shows a gradual increase of the effective stress with the deposition of the different layers and no relevant changes can be observed between the three cases at present since the overpressure is negligible. As expected, the lower part of the soil column shows larger values of stress (up to 309 kPa). It is worth remembering that the behaviour of σ_z is given by the following expression:

$$\sigma_z = \phi\gamma_w z + (1 - \phi)\gamma_s z \quad (5.1)$$

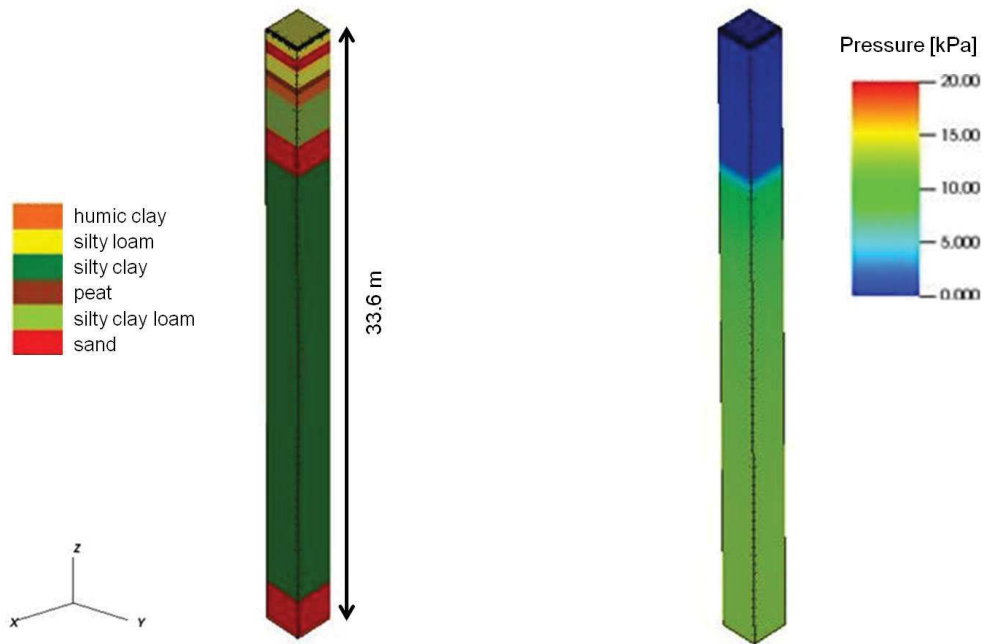


Figure 5.10: Scenario A: sediment classes and overpressure [kPa] at simulation time $t=9702$ yr (i.e. 1298 yr BP).

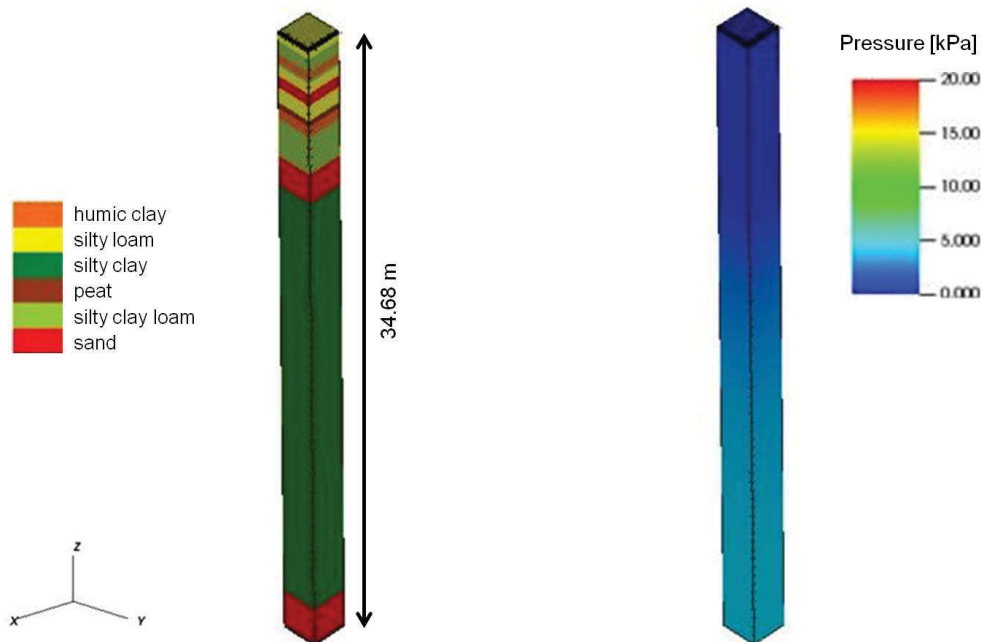


Figure 5.11: Scenario B: sediment classes and overpressure [kPa] at simulation time $t=10778$ yr (i.e. 222 yr BP).

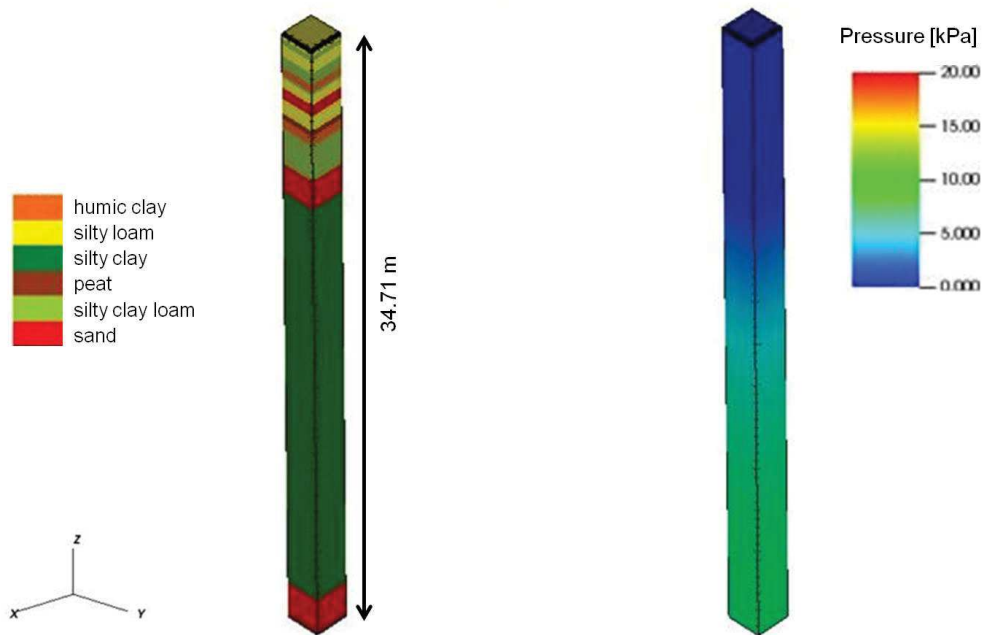


Figure 5.12: Scenario B: sediment classes and overpressure [kPa] at simulation time $t=10824$ yr (i.e. 176 yr BP).

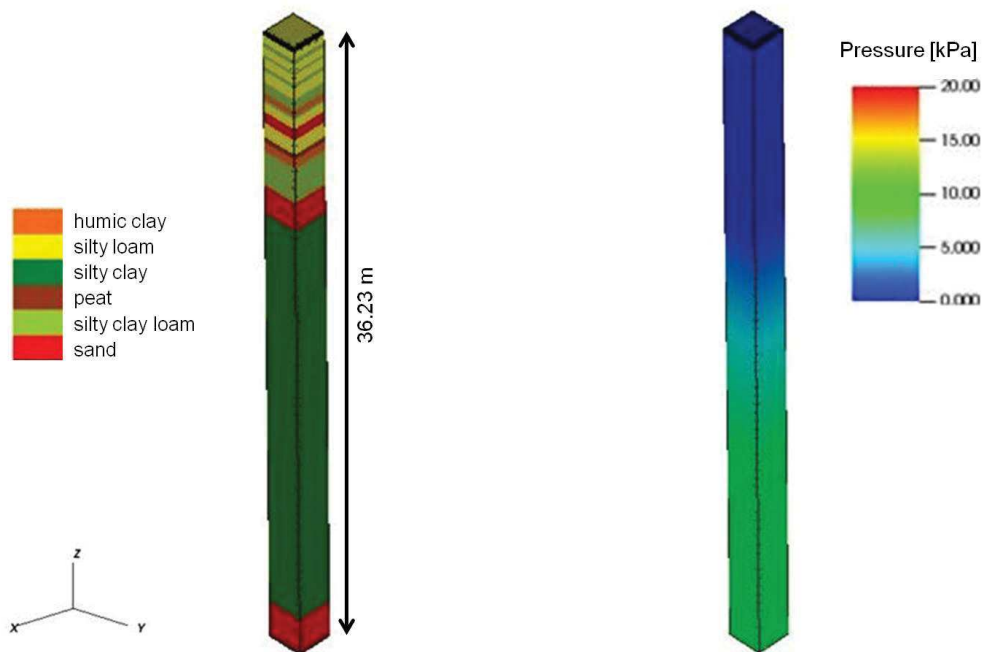


Figure 5.13: Scenario B: sediment classes and overpressure [kPa] at simulation time $t=10921$ yr (i.e. 79 yr BP).

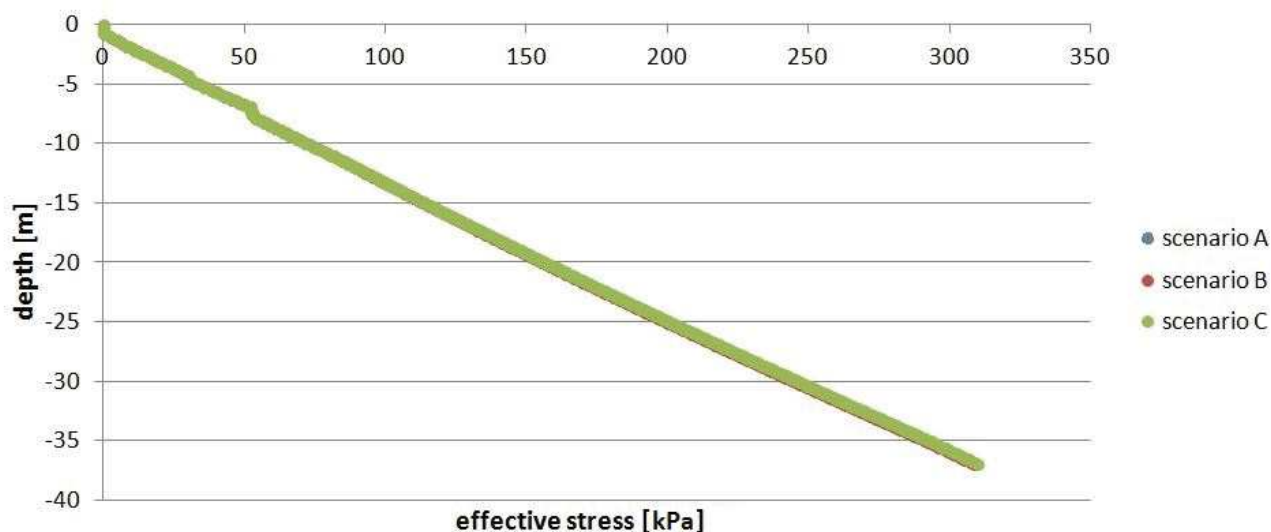


Figure 5.14: Effective stress behaviour versus depth for the three scenarios of overbank deposition.

that is a function of the specific weight of water (γ_w), the specific weight of grains (γ_s), depth (z) and porosity (ϕ). In our case the slope does not change significantly as the same value for the specific weight has been set for sand, silty clay loam, silty clay, and silt loam. Figure 5.14 shows the effective stress behaviour versus depth for the three scenarios. The curves are almost coincident.

Figure 5.15 shows a comparison between the σ_z versus z behaviour computed by NAT-SUB3D and presented by Bridgeman (2017).

The difference is significant, with an overestimation of Bridgeman's values of about 30%. This is due to the value of γ_s used in this work (Figure 5.1) derived from Keogh et al. (2021). The values by Bridgeman (2017) have been evaluated as improper.

Strain As it can be easily understood from Figure 5.16, taken from the final time of the three scenarios, the general behaviour is coherent with the soil characteristics. Indeed, the deformation peak is computed for the deeper peat layer (about 55%), whereas the sandy layers, which are stiffer, display the smallest strain (between 5-10%). As expected for thicker layers,

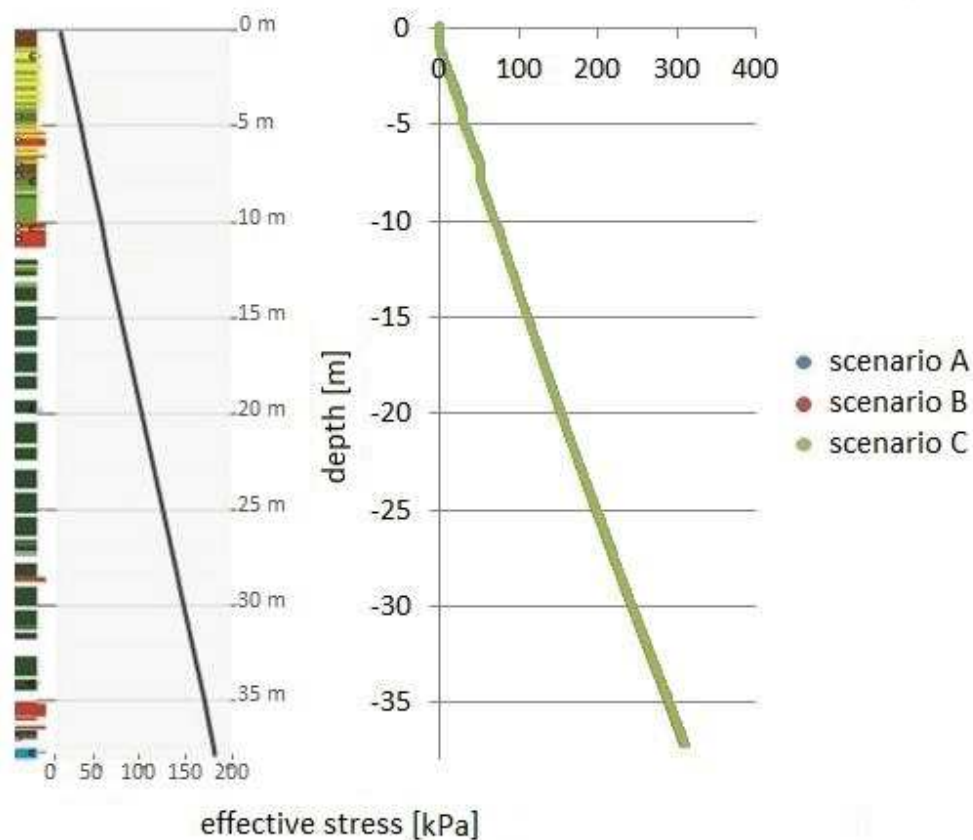


Figure 5.15: Comparison between the effective stress behaviour versus depth provided by Bridgeman (2017) to the left and computed with NATSUB3D to the right.

such as the silty clay, strain gradually increases with depth from the top part to the bottom in response to the load exerted by the upper layers. In agreement with overpressure and strain distribution, no relevant variations can be noticed nowadays among the three scenarios.

Integrated compaction For a better interpretation of the results it is useful to remind that this parameter indicates the loss of elevation of a column point due to the compaction of the underlying deposits. Obviously, the larger values are computed at the column top and, conversely, instead, the integrated compaction is null at the bottom (Figure 5.17). The maximum compaction amounts to about 15 m and, consistently with the other parameters, does not depend on the scenario.

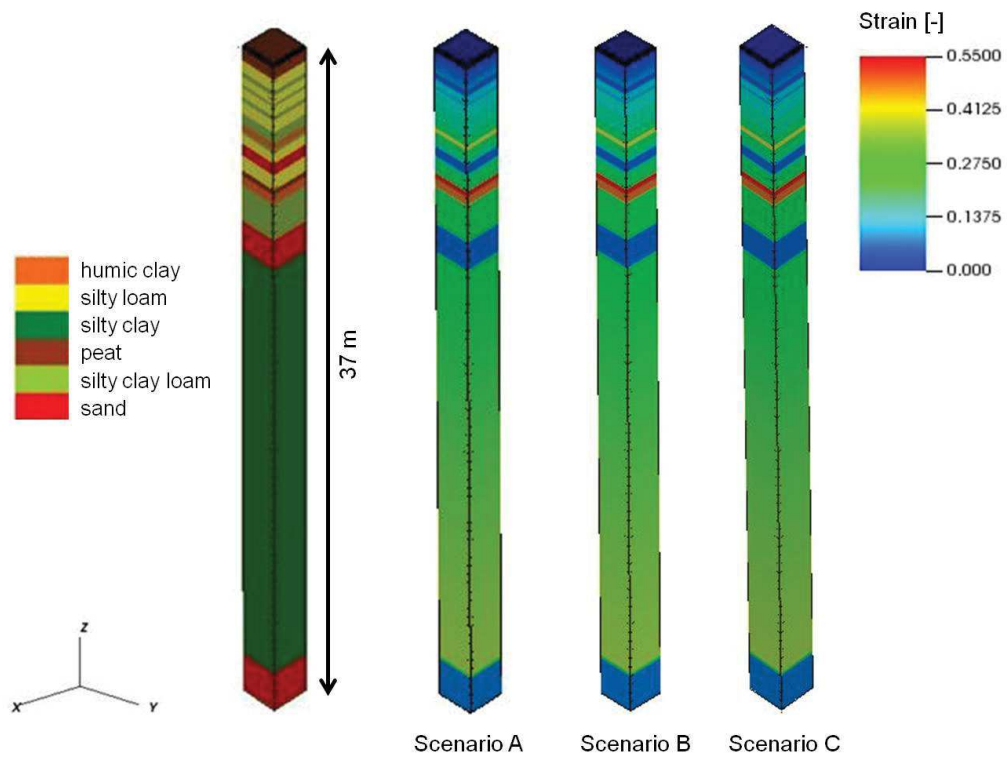


Figure 5.16: Strain distribution computed along the sedimentary column at present (simulation time $t=11000$ yr, i.e. 0 yr BP) in the three scenarios of overbank deposition.

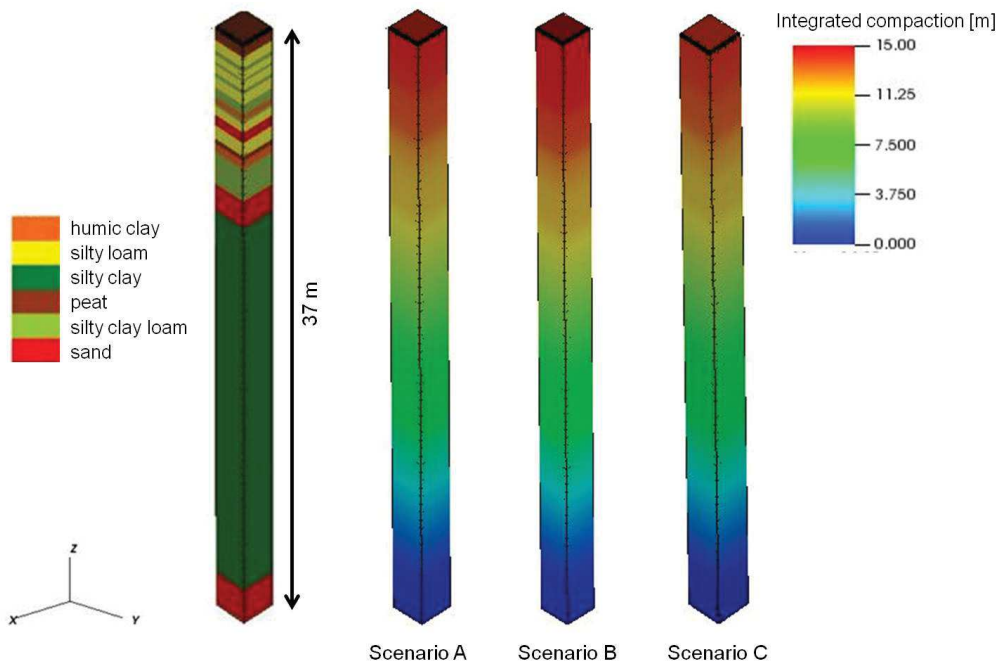


Figure 5.17: Integrated compaction [m] for the three scenarios of overbank deposition at present time (simulation time $t=11000$ yr, i.e. 0 yr BP).

5.5 Model validation

A fundamental step when developing a model is the validation phase, which is aimed at comparing the model outcomes with datasets independent from those used for the model calibration. In the present study the validation phase is based on data provided by Bridgeman (2017) and by the Coastwide Reference Monitoring System (CRMS) of the Louisiana country referred to the Myrtle Grove I core. The validation consists of two phases which are discussed in this chapter in detail:

- Validation in terms of post-depositional lowering (PDL) using deep subsidence rates as provided by Torbjorn Tornqvist (personal communication) and relative sea-level (RSL) rise and relative displacement;
- Validation in terms of surface elevation change (SEC) over the last 12 years. The model outcomes are compared with the data measured by the CRMS of the Louisiana country located in the nearby of the Myrtle Grove Superstation (CRMS 276).

PDL and deeper subsidence validation In his MSc thesis Bridgeman provides Figure 5.18 showing RSL over the Holocene for the Mississippi River Delta obtained from basal peat data (Yu et al., 2012). RSL curve can be approximated by the following equation:

$$y = \frac{(a + cx)}{(1 + bx)} \quad (5.2)$$

where $a = -0.22972607$, $b = -9.604e-05$, $c = -0.00031812$.

The four points highlighted in Figure 5.18 represent samples whose dating is available and that were located at an elevation equal to the mean sea level when sedimented. They correspond to humic clay, sand and peat soils. The upper humic clay has been named “humic clay 2” in

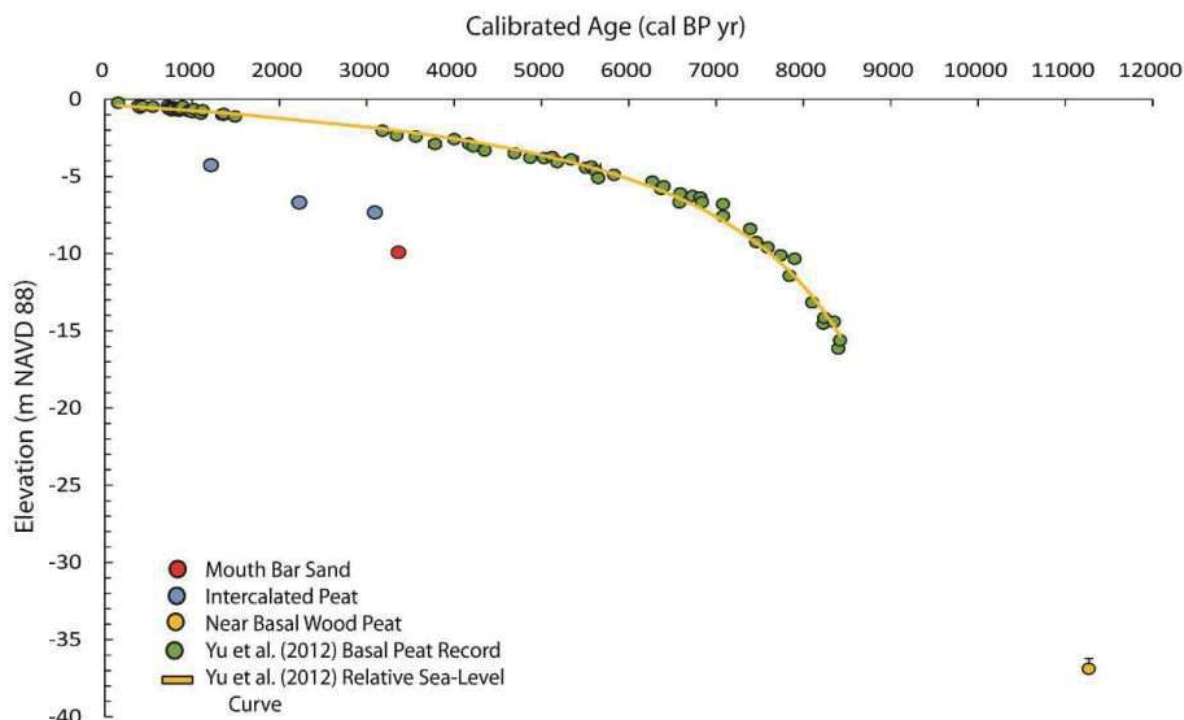


Figure 5.18: RSL curve and present elevation of dated samples of Myrtle Grove station as provided by Bridgeman (2017).

Sample Name	FCER [m]	FE [m]	VD [m]	WMA [ka]	MDR [mm/yr]
Humic clay 2	-4.17 to -4.19	-1.06 +	3.12 +	1.21 to 1.33	2.46 +
Peat	-4.14 to -6.50	-1.56 to -0.54	2.58 to 5.96	2.20 to 2.38	1.12 to 2.60
Humic clay 1	-4.80 to -7.21	-2.09 +	2.71 +	3.10 to 3.24	0.85 +
Sand	-6.64 to -9.80	-2.58 to -1.66	4.06 to 8.04	3.25 to 3.61	1.18 to 2.34

Table 5.1: Elevation and displacement data of humic clay, sand and peat samples dated at Myrtle Grove Superstation. Notice that for the two humic clay samples some parameters report the lower bound only because they are identified as freshwater and therefore they only have minimum formation elevations of mean tide level. The "+" marks the absence of a value for the upper bound.

order to distinguish it from the deeper soil. The relative distance between their elevation and the RSL curve at the same date is representative of the PDL experienced by the soil. This experimental PDL has been compared with the values obtained through NATSUB3D.

We take advantage of the details about these samples provided by Bridgeman (2017). They are summarized in Table 5.1.

The meaning of the parameters listed in Table 5.1 are the following:

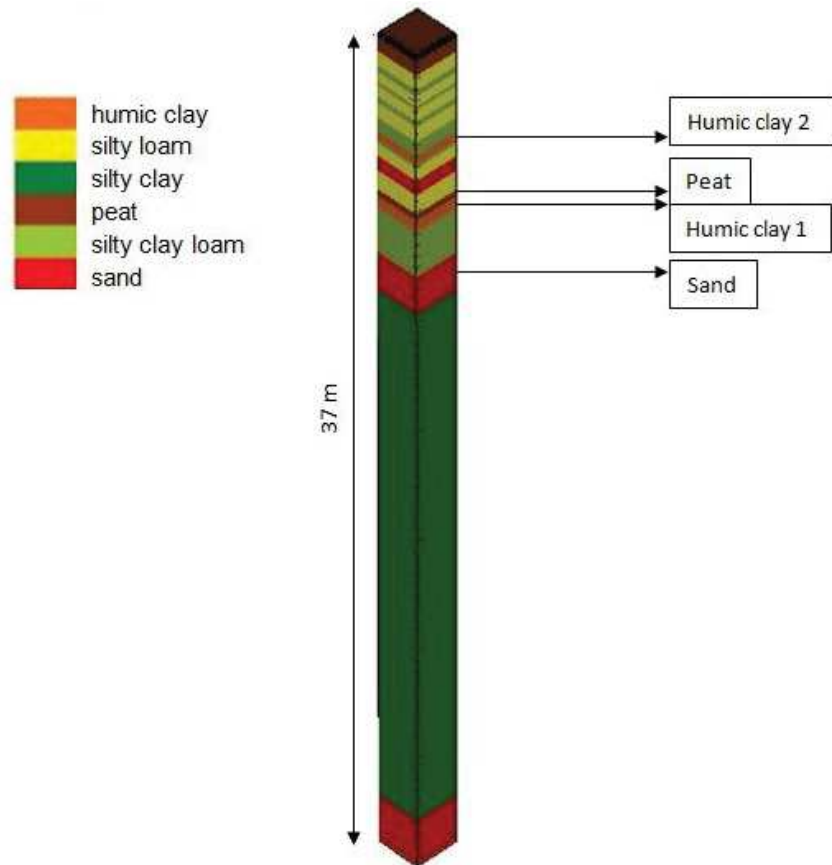


Figure 5.19: Location of the 4 samples involved in the PDL validation phase within the Myrtle Grove sedimentary column.

- FCER (Facies Contact Elevation Range) is the sum of PDL, deep subsidence and sea-level curve;
- FE (Formation Elevation) is the elevation of the four considered samples and it accounts for uncertainties related to non-vertical drilling, sampling and surveying;
- VD (Vertical Displacement) is the sum of PDL and deep subsidence. It is measured through C^{14} dated peat and OSL dated mouth-bar sands;
- WMA (Weighted Mean Age) is the range of the dating for each sample;
- MDR (Mean Displacement Rate) is calculated by dividing the vertical displacement by the time elapsed since formation.

	Yr BP	DS1 [m]	DS2 [m]	DS3 [m]	DS4 [m]
Humic clay 2	1270	1.27	1.91	2.54	3.18
Peat	2290	2.29	3.44	4.58	5.73
Humic clay 1	3170	3.17	4.76	6.34	7.93
Sand	3360	3.36	5.04	6.72	8.41

Table 5.2: Average age and deep subsidence for the four dated samples at Myrtle Grove Superstation.

NATSUB3D gives the PDL as output, but does not include the deep subsidence (DS) due to tectonic, glacial isostatic adjustment (GIA), sediment isostatic adjustment (SIA), and underground fluid production, which need to be assumed. Based on information provided by Torbjorn Tornqvist (personal communication) four possible values have been considered for DS: 1 mm/yr (DS1 in the following), 1.5 mm/yr (DS2 in the following), 2 mm/yr (DS3 in the following), and 2.5 mm/yr (DS4 in the following).

The DS values provided in Table 5.2 have been obtained by multiplying the above subsidence rates by the age of the sample. DS+PDL computed by NATSUB3D can be compared (Tables 5.3-5.7 and Figures 5.20-5.22) with the values provided in Table 5.1. In the following pages a summary of the data and the plots related to each scenario is provided. PDL values refer to the three simulated scenarios A, B and C.

Tables and plots Scenario A

	Mean PDL (from model data)	PDL+DS1 [m]	PDL+DS2 [m]	PDL+DS3 [m]	PDL+DS4 [m]
Humic clay 2	1.28	2.55	3.19	3.82	4.46
Peat	2.29	4.59	5.73	6.88	8.02
Humic clay 1	2.01	5.17	6.76	8.34	9.93
Sand	2.71	6.07	7.75	9.43	11.11

Table 5.3: Computed PDL obtained with scenario A and PDL+DS for the four samples and the four DS values.

	RSL (from Bridgeman)	FCER1 [m]	FCER2 [m]	FCER3 [m]	FCER4 [m]
Humic clay 2	-0.72	-3.27	-3.91	-4.54	-5.18
Peat	-1.23	-5.82	-6.96	-8.11	-9.25
Humic clay 1	-1.78	-6.95	-8.54	-10.12	-11.71
Sand	-1.92	-7.99	-9.67	-11.35	-13.03

Table 5.4: RSL and FCER obtained with scenario A and the four DS values.

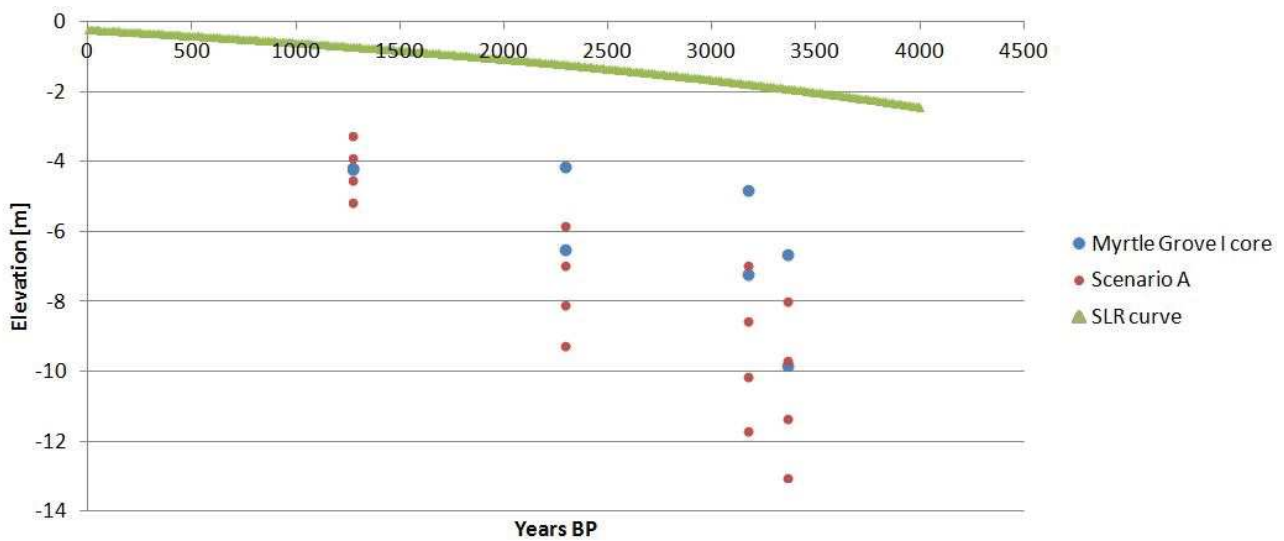


Figure 5.20: Comparison between Bridgeman (2017) data and NATSUB3D outcome for scenario A and the four DS values. Notice that Myrtle Grove data are reported in terms of upper and lower bound. The range for humic clay 2 is so restricted that only one dot is apparently visible in the plot.

Tables and plots Scenario B

	Mean PDL (from model data)	PDL+DS1 [m]	PDL+DS2 [m]	PDL+DS3 [m]	PDL+DS4 [m]
Humic clay 2	1.26	2.53	3.17	3.80	4.44
Peat	2.27	4.56	5.71	6.85	7.99
Humic clay 1	1.99	5.16	6.75	8.33	9.92
Sand	2.71	6.07	7.75	9.43	11.11

Table 5.5: Computed PDL in scenario B and PDL+DS for the four samples and the four DS values.

	RSL (from Bridgeman)	FCER1 [m]	FCER2 [m]	FCER3 [m]	FCER4 [m]
Humic clay 2	-0.72	-3.26	-3.89	-4.53	-5.16
Peat	-1.23	-5.79	-6.94	-8.08	-9.23
Humic clay 1	-1.78	-6.94	-8.53	-10.11	-11.69
Sand	-1.92	-7.98	-9.66	-11.34	-13.02

Table 5.6: RSL and FCER obtained with scenario B and the four DS values.

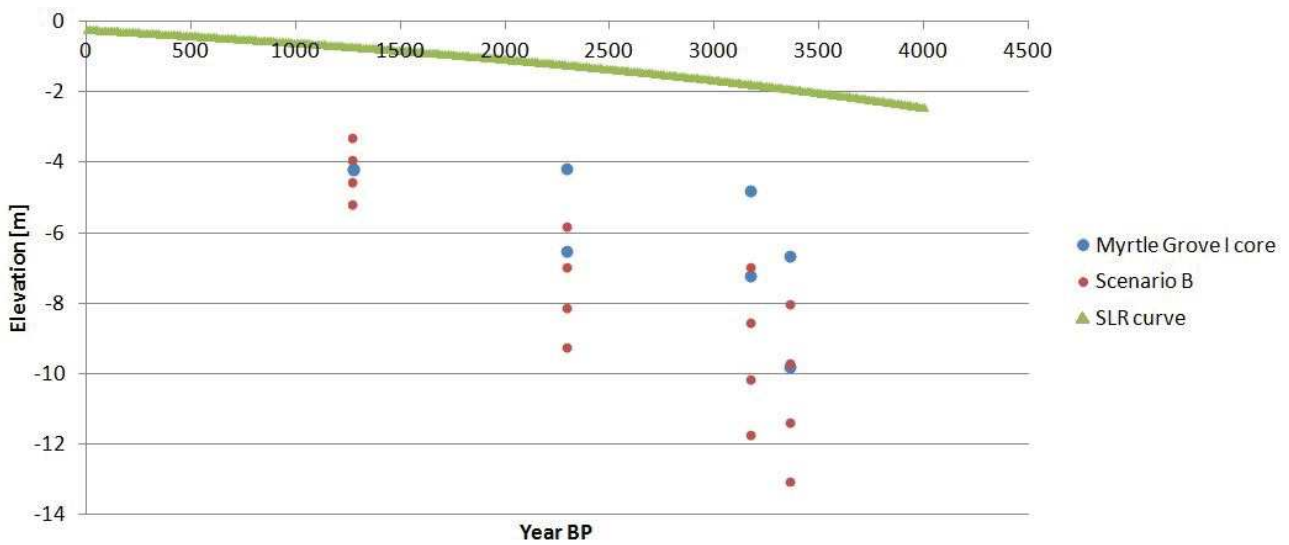


Figure 5.21: Comparison between Bridgeman (2017) data and NATSUB3D outcome for scenario B and the four values for DS. Notice that Myrtle Grove data are reported in terms of upper and lower bound. The range for humic clay 2 is so restricted that only one dot is apparently visible in the plot.

Tables and plots Scenario C

	Mean PDL (from model data)	PDL+DS1 [m]	PDL+DS2 [m]	PDL+DS3 [m]	PDL+DS4 [m]
Humic clay 2	1.29	2.56	3.19	3.83	4.47
Peat	2.29	4.58	5.72	6.87	8.01
Humic clay 1	2.01	5.18	6.76	8.35	9.93
Sand	2.72	6.08	7.76	9.44	11.12

Table 5.7: Computed PDL in scenario c and PDL+DS for the four samples and the four DS values.

	RSL (from Bridgeman)	FCER1 [m]	FCER2 [m]	FCER3 [m]	FCER4 [m]
Humic clay 2	-0.72	-3.29	-3.92	-4.56	-5.19
Peat	-1.23	-5.80	-6.95	-8.09	-9.24
Humic clay 1	-1.78	-6.96	-8.54	-10.13	-11.71
Sand	-1.92	-7.99	-9.68	-11.36	-13.04

Table 5.8: RSL and FCER obtained with scenario C and the four DS values.

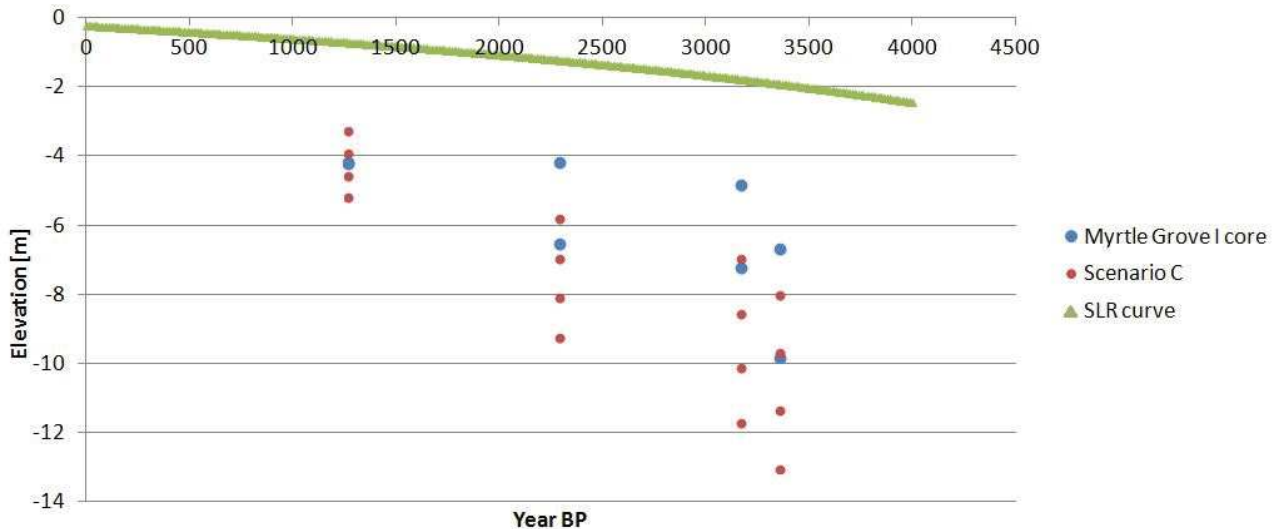


Figure 5.22: Comparison between Bridgeman (2017) data and NATSUB3D outcome for scenario C and the four values for DS. Notice that Myrtle Grove data are reported in terms of upper and lower bound. The range for humic clay 2 is so restricted that only one dot is apparently visible in the plot.

The outcomes show that Bridgeman (2017) data can be captured satisfactorily with a deep subsidence equal to 1.5 mm/yr. On the other hand, no relevant differences can be noticed between scenarios A, B and C due to the fact that the PDL values do not change significantly.

SEC validation For this step of the validation phase, the data provided by the CRMS 276 station have been used. The records are freely available from the CRMS website (<https://www.lacoast.gov/crms/Home.aspx?msclkid=87a5e227bc1511ec87b3a9b90d2578fe>). This system is a direct consequence of the need to monitor land loss crisis occurring in this country and it was promoted in 1990 by the U.S. Congress. Its aim is to monitor the effectiveness of

restoration actions at multiple spatial scales from individual projects to the influence of projects on the entire coastal landscape. The total number of sites which are still benefiting from such initiative is around 390, including the one in the nearby of Myrtle Grove. The CRMS 276 data for study site refer to the SEC measured over the last 12 years i.e. from 2009 to 2021. The definition of this parameter is provided in the website as follows: *The Rod Surface Elevation Table (RSET) method, as implemented within the CRMS network, is used to estimate surface elevation change rates. One RSET benchmark is located at each CRMS site (with the exception of floating marshes and perpetually flooded, flocculent swamps). From the RSET benchmark, surface elevation is measured at nine points in four directions to calculate elevation change at 6-months intervals. Surface elevation change is defined as cumulative elevation change since station establishment. For each sampling event, mean cumulative elevation change is calculated for each of the four directions, and an elevation rate is estimated using linear regression of elevation change against time.* By considering the elevation over time of the column top as reproduced by NATSUB3D it is possible to validate the model outcome against the CRMS data. Figure 5.23 provides the CRMS 276 records and the linear interpolation of the data returning an average accretion equal to 8 mm/yr. The model results obtained for the three scenarios, which do not display significant differences, are shown in Figure 5.24. The computed SEC rate amounts to about 10-11 mm/yr that satisfactorily reproduces the CRMS 276 values.

5.6 Uncertainty quantification and sensitivity analysis

The model has been applied using the deterministic properties of the various soil classes as suggested by the literature. Because these data are characterised by a certain uncertainty (Bridgeman, 2017; Chamberlain et al., 2018; Keogh et al., 2021) a Monte Carlo simulation has

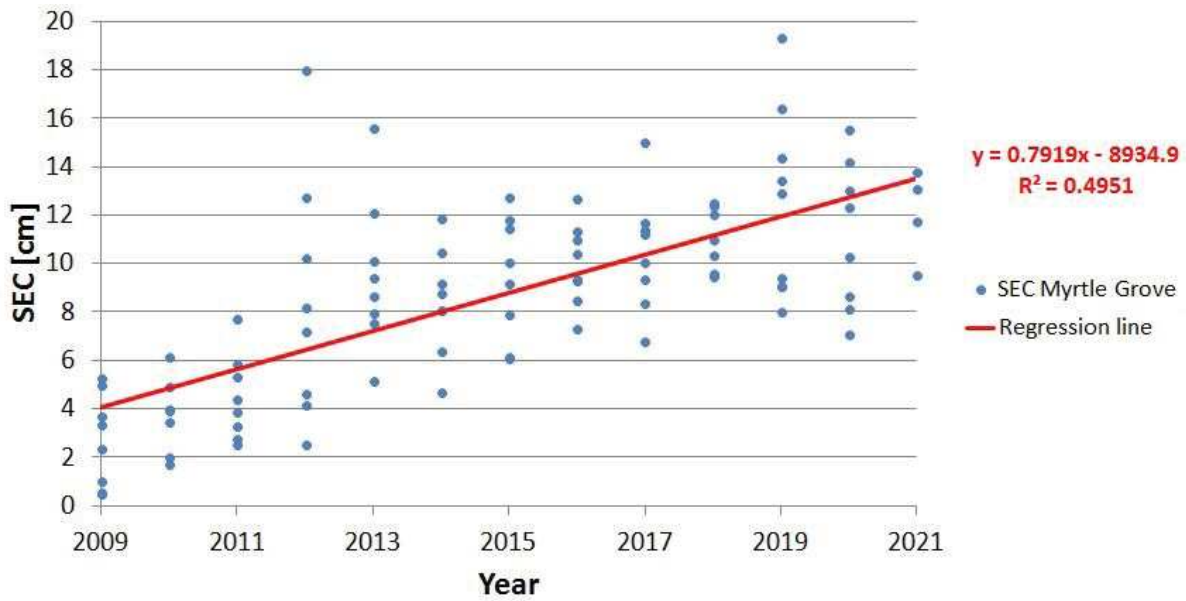


Figure 5.23: Surface Elevation Change (SEC) over the last 12 years at the CRMS 276. The regression line is provided.

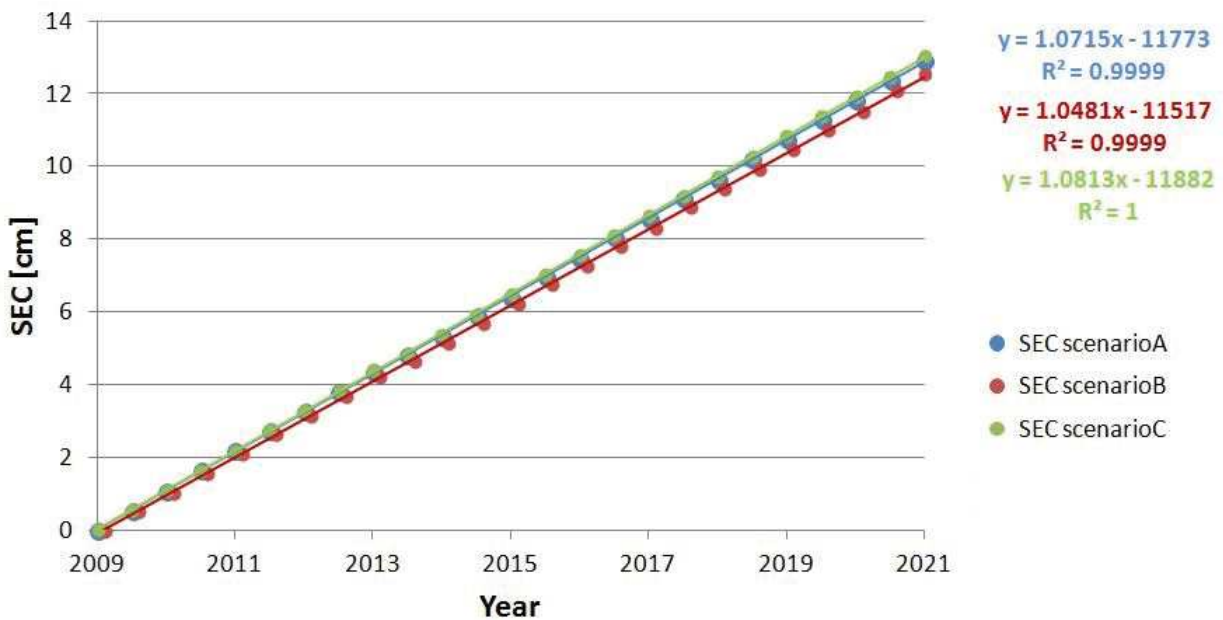


Figure 5.24: Model results in terms of SEC for scenarios A, B and C over the last 12 years at the Myrtle Grove site.

Lithological class	min	σ_p [kPa]	max	min	e_0 [-]	max	min	γ_s [g/cm ³]	max
sand	2.8	4	5.2	0.5	1	1.5	2.52	2.65	2.78
silty clay loam	2.8	4	5.2	0.85	1.7	2.55	2.52	2.65	2.78
peat	2.8	4	5.2	6.5	13	19.5	1.08	1.14	1.19
silty clay	2.8	4	5.2	0.9	1.8	2.7	2.52	2.65	2.78
silty loam	2.8	4	5.2	0.55	1.1	1.65	2.52	2.65	2.78
humic clay	2.8	4	5.2	3.45	6.9	10.35	1.81	1.90	1.99

Table 5.9: Range of soil parameters for the Monte Carlo simulations (part1). The central column for each parameter provides the values used in the deterministic analysis.

Lithological class	min	C_r [-]	max	min	C_c [-]	max	min	K_{z0} (exp) [m/s]	max
sand	0.0231	0.033	0.0429	0.0231	0.033	0.0429	5	6	7
silty clay loam	0.0063	0.009	0.0117	0.42	0.6	0.78	5	6	7
peat	0.56	0.8	1.04	3.304	4.72	6.136	6	7	8
silty clay	0.00056	0.0008	0.00104	0.399	0.57	0.741	8	9	10
silty loam	0.049	0.07	0.091	0.161	0.23	0.299	6	7	8
humic clay	0.294	0.42	0.546	1.666	2.38	3.094	6	7	8

Table 5.10: Range of soil parameters for the Monte Carlo simulations (part2). The central column for each parameter provides the values used in the deterministic analysis.

been implemented to investigate the effect of the parameter uncertainty on the model outcome.

The process for the application of such method includes the following steps:

- Selection of a statistical probability distribution for the various soil parameters. A uniform distribution has been used in this analysis. The minimum and maximum values set for each soil parameter are provided in Tables 5.9 and 5.10.
- A Matlab script is programmed to sample a N_{MC} number of values from the probability distributions. N_{MC} has to be set considering both computational burden and the representativeness of the analysis. N_{MC} has been fixed equal to 1000 in the present analysis. A number of Monte Carlo simulations have been performed to understand in more detail the effect of the parameters uncertainty on the model outcome. Initially (a) all the parameters have been considered uncertain. Then, (b) in each analysis a group of pa-

rameters, namely (1) σ_p , C_r , C_c , (2) γ_s , e_0 and (3) $K_{z,0}$ have been assumed stochastically distributed and the others are considered as fixed. This has allowed to verify the model uncertainty in relation to density, geomechanical, and hydraulic parameters, respectively.

- A shell script selects the input parameter values for each soil type and automatically runs NATSUB3D N_{MC} times extracting the output of interest, i.e. the behaviour vs depth and time of effective stress (σ_z), strain (ϵ), pressure, integrated compaction, compressibility (c_b), porosity, and post depositional lowering (PDL).
- The Monte Carlo outputs are post processed to derive the mean and associated standard deviation of each quantity versus depth, FE layer and lithological unit.

The Monte Carlo analysis has been carried out with scenario A in relation to overbank depth-age model. Figures 5.25 – 5.31 show the Monte Carlo outcomes in terms of effective stress, strain, integrated compaction, PDL, porosity, bulk density, and compressibility with respect to the thickness/depth of the soil column for case (a) in which all soil parameters have been considered uncertain. It can be noticed that the variability in terms of thickness covers a wide range close to 10 m (from about 34 m to about 44 m). Therefore, the column may result as composed of a very stiff or weak stratigraphy and also by intermediate configurations resulting from the random sampling. Also the effective stress range is consequently wide, from a minimum of about 220 kPa to a maximum of nearly 440 kPa at the bottom. Consequently, this leads to a significantly variability in soil compaction all over the column. This, together with the strong variability shown in the other plots, proves the significant influence of the soil parameters on the outcomes. A zoom of the parameter behavior within the shallow overbank portion is provided in Figure 5.32. Notice the variability related to the alternation between silty loam and silty clay loam deposits.

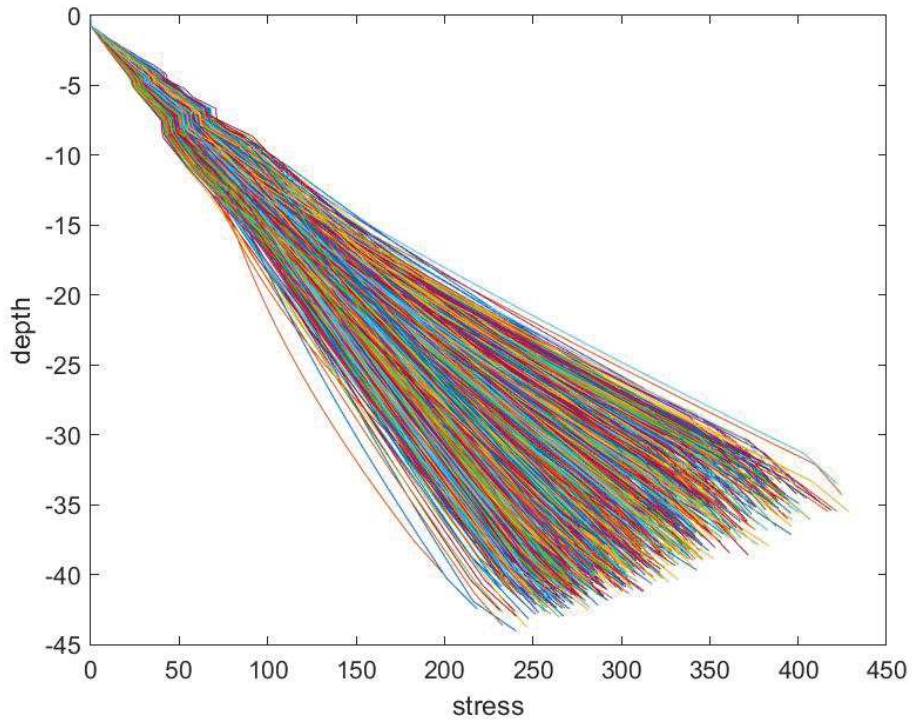


Figure 5.25: Monte Carlo outcomes in terms of effective stress [kPa] with respect to depth considering all soil parameters as uncertain.

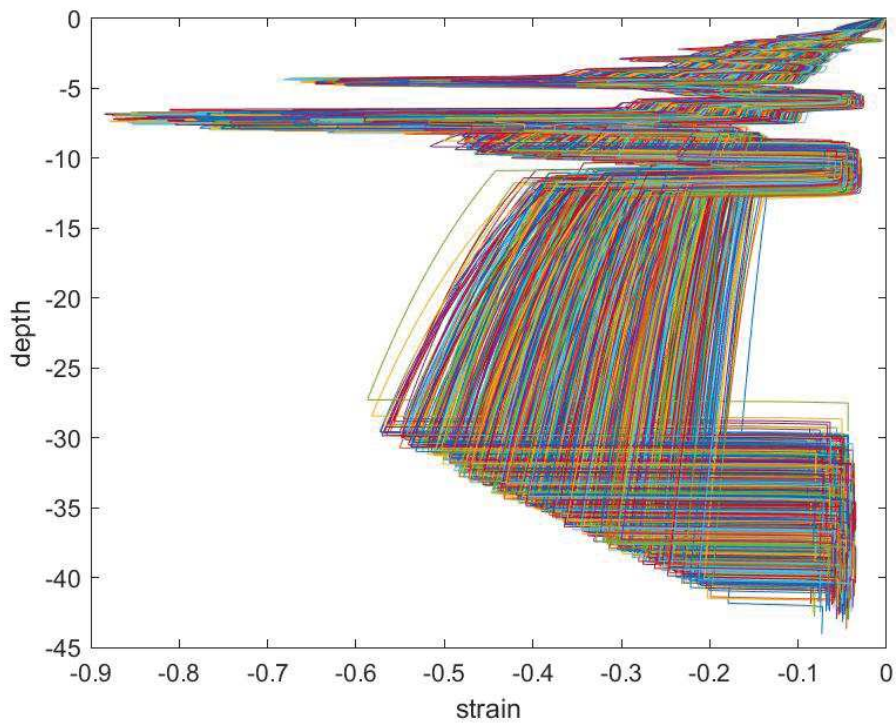


Figure 5.26: Monte Carlo outcomes in terms of strain [-] with respect to depth considering all soil parameters as uncertain.

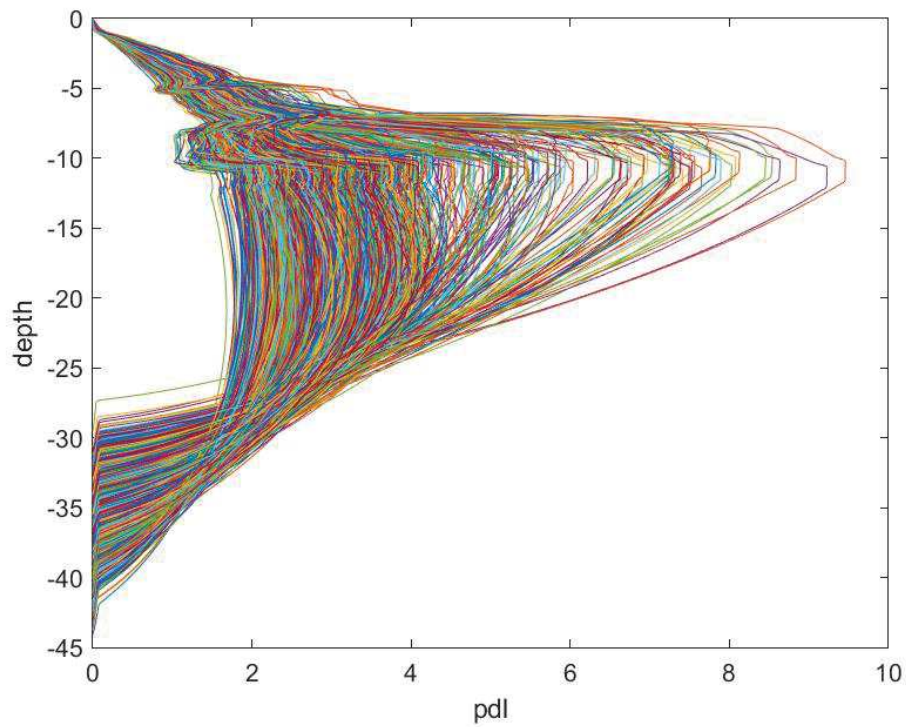


Figure 5.27: Monte Carlo outcomes in terms of PDL [m] with respect to depth considering all soil parameters as uncertain.

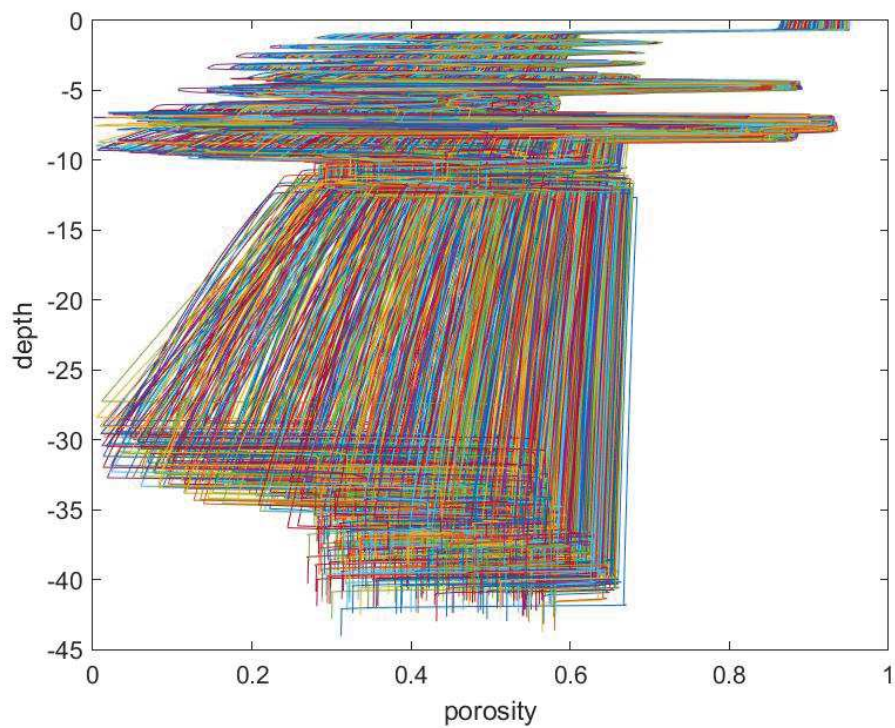


Figure 5.28: Monte Carlo outcomes in terms of porosity [-] with respect to depth considering all soil parameters as uncertain.

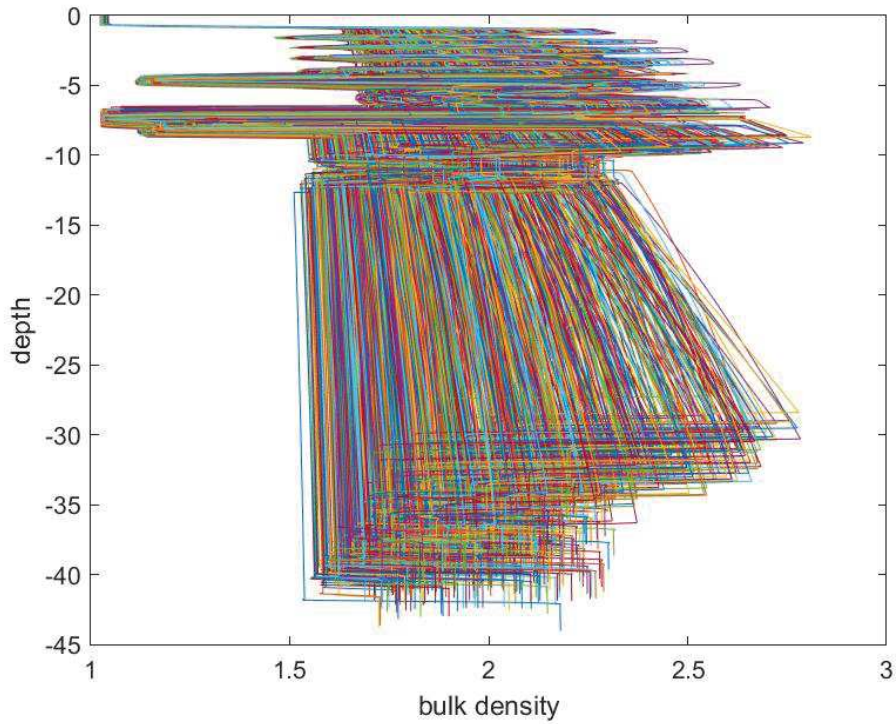


Figure 5.29: Monte Carlo outcomes in terms of bulk density [g/cm^3] with respect to depth considering all soil parameters as uncertain.

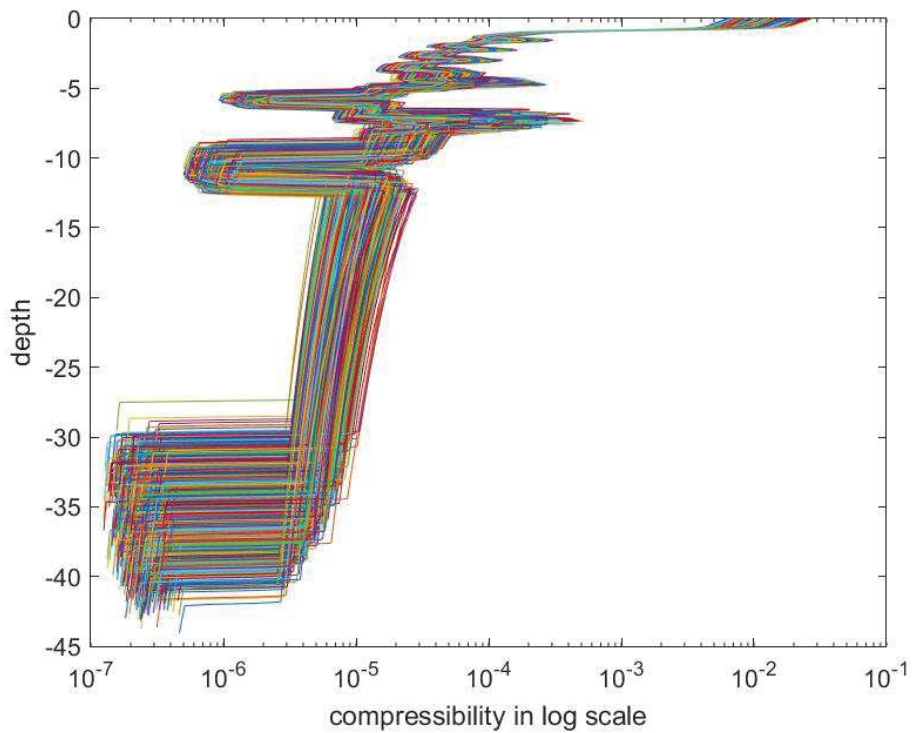


Figure 5.30: Monte Carlo outcomes in terms of compressibility [kPa^{-1}] with respect to depth considering all soil parameters as uncertain.

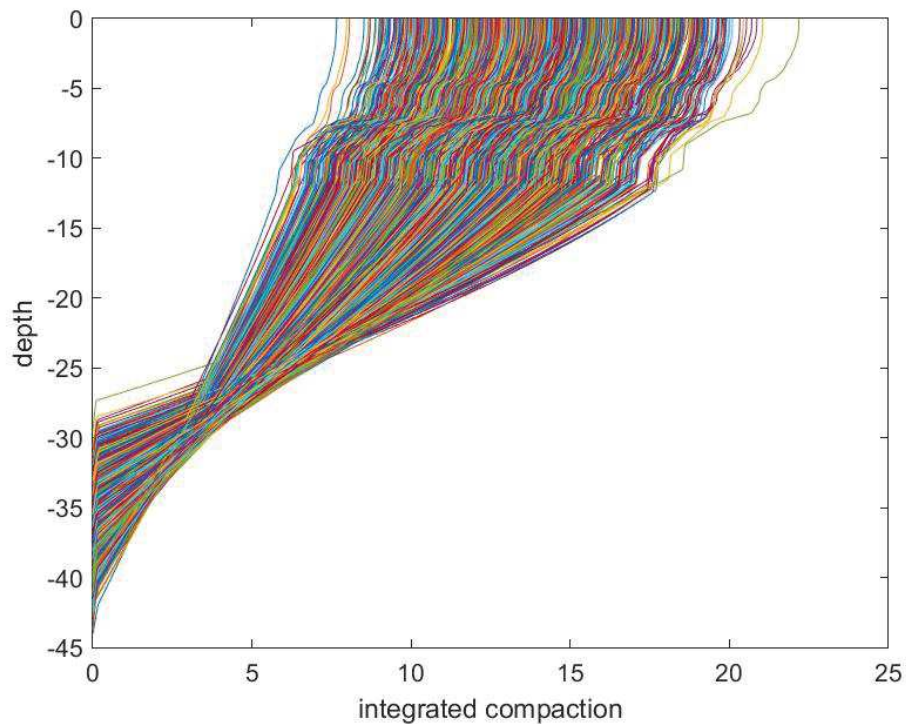


Figure 5.31: Monte Carlo outcomes in terms of integrated compaction [m] with respect to depth considering all soil parameters as uncertain.

Then, the dependency of the model outcome on restricted groups of parameters (that are, as mentioned above (1) σ_p , C_r , C_c , (2) γ_s , e_0 and (3) $K_{z,0}$) has been investigated to understand more in depth how geomechanical, density, and hydraulic features of the soil control the column compaction. In these so-called case (b) The results are visualized at the end of the simulated time interval for the same variables discussed in case (a) using two representations:

- each variable is plotted versus the model layer number (totalling 518 as reported above) for each Monte Carlo run together with the mean value and the 2.5, 25, 50, 75, 97.5% quantiles obtained by statistically post-processing of the model ensemble. For some variables a zoom on the shallower part of the soil column (from 0 m to about -12 m) is provided in order to better understand the behaviour within the overbank deposit;
- a second group of plots has been obtained using the so-called “pcolor” Matlab function

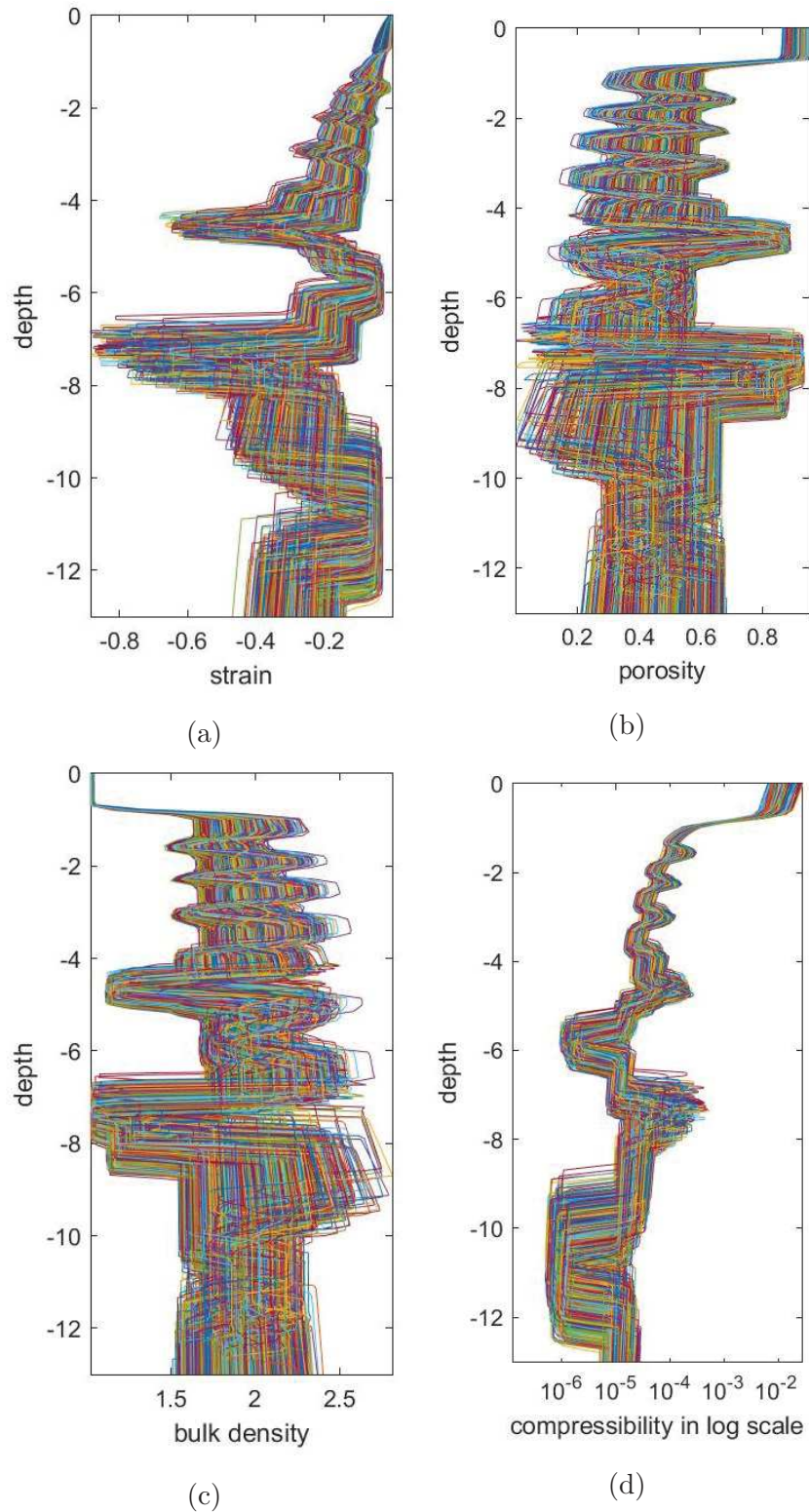


Figure 5.32: Monte Carlo outcomes in terms of strain [-], porosity [-], bulk density [g/cm³] and compressibility [kPa⁻¹] with respect to depth considering all soil parameters as uncertain. These four pictures provide a focus on the upper overbank portion.

and allows representing the variable of interest versus the model layer number and simultaneously versus depth using different colors. Indeed, it must be remembered that the number of layers composing the mesh is constant in all simulations. The layers may be more or less deformed according to compaction in response to a change in soil characteristics, but their number does not change between different simulations. What changes, clearly, is the thickness of the soil column, which may be more or less reduced due to compaction. Therefore, the same layer could be associated to different values of depth depending on the simulation.

The results which are presented and discussed in the following paragraphs for the various variables provided by the simulator.

Effective stress Figure 5.33 shows the behaviour of effective stress versus column layer numbers obtained with the Monte Carlo simulations. From Figure 5.33a, it is clear that stress increases from top to bottom of the column with mean values corresponding to those obtained in the scenario A simulation. From the group Monte Carlo analysis (Figure 5.33b,c,d) it is evident that the main contribution to stress variability is given by e_0 and γ_s (Figure 5.33d). Indeed, the effective stress depends only on the deposited soil density if overpressure is totally dissipated. The effect of overpressure (thus K_{z0}) to effective stress is shown in Figure 5.33b. Decreasing the value of K_{z0} , the overpressure (gently) increases and the effective stress (gently) decreases with respect to the mean value. Figure 5.34 shows that, considering a fixed layer, the stress variability is reflected by a different column depth/thickness with a general trend in which larger stresses correspond to smaller depths/thicknesses at a fixed layer. This means that for larger soil densities, the column weight increases thus producing larger compaction and decreasing the column thickness (or depth in this case).

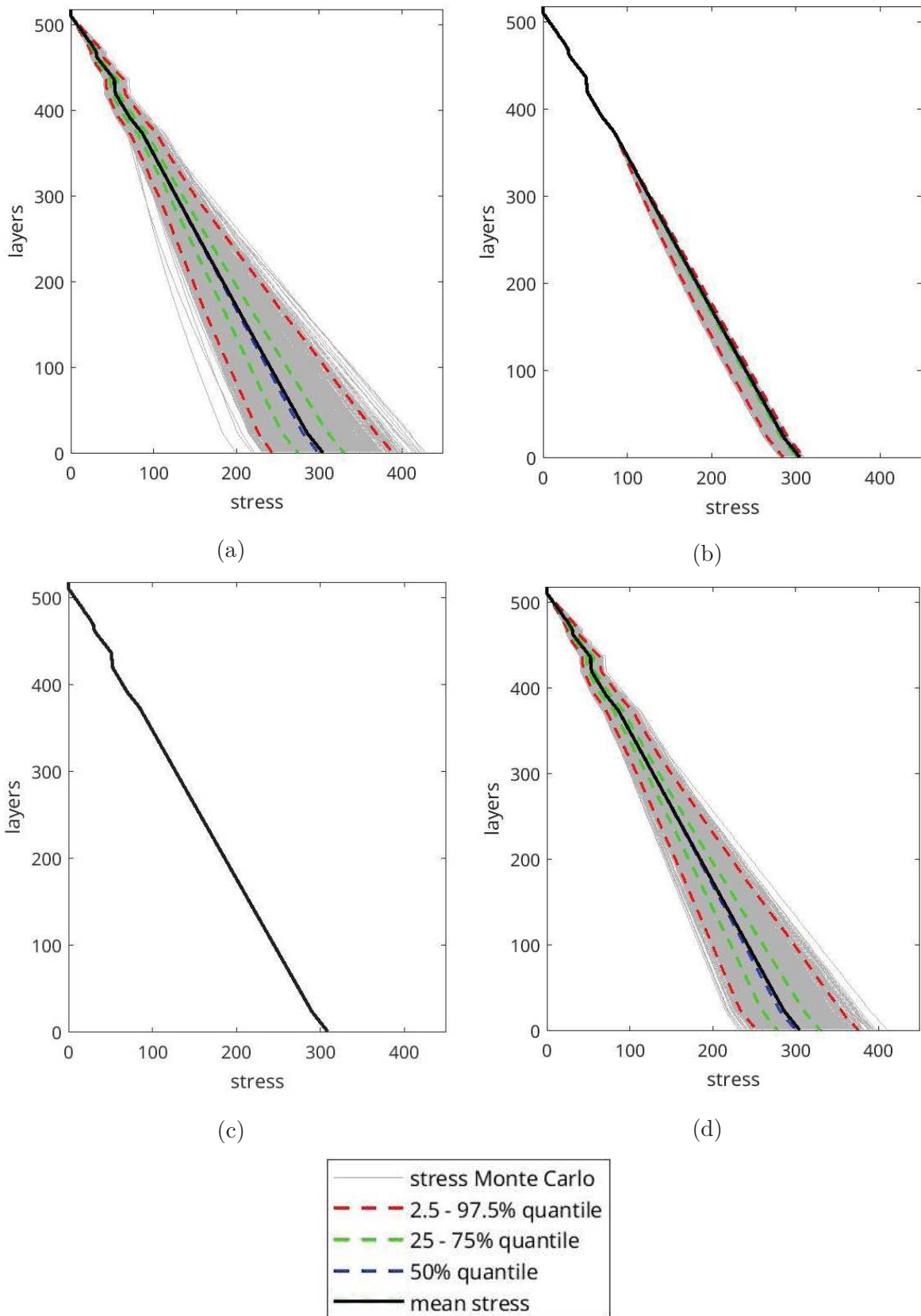


Figure 5.33: Monte Carlo outcomes and related statistics in terms of effective stress [kPa] versus model layer number for the four analyses developed in the study assuming as uncertain (a) all the parameters and (b) the hydraulic, (c) the geomechanical, and (d) the density parameters only.

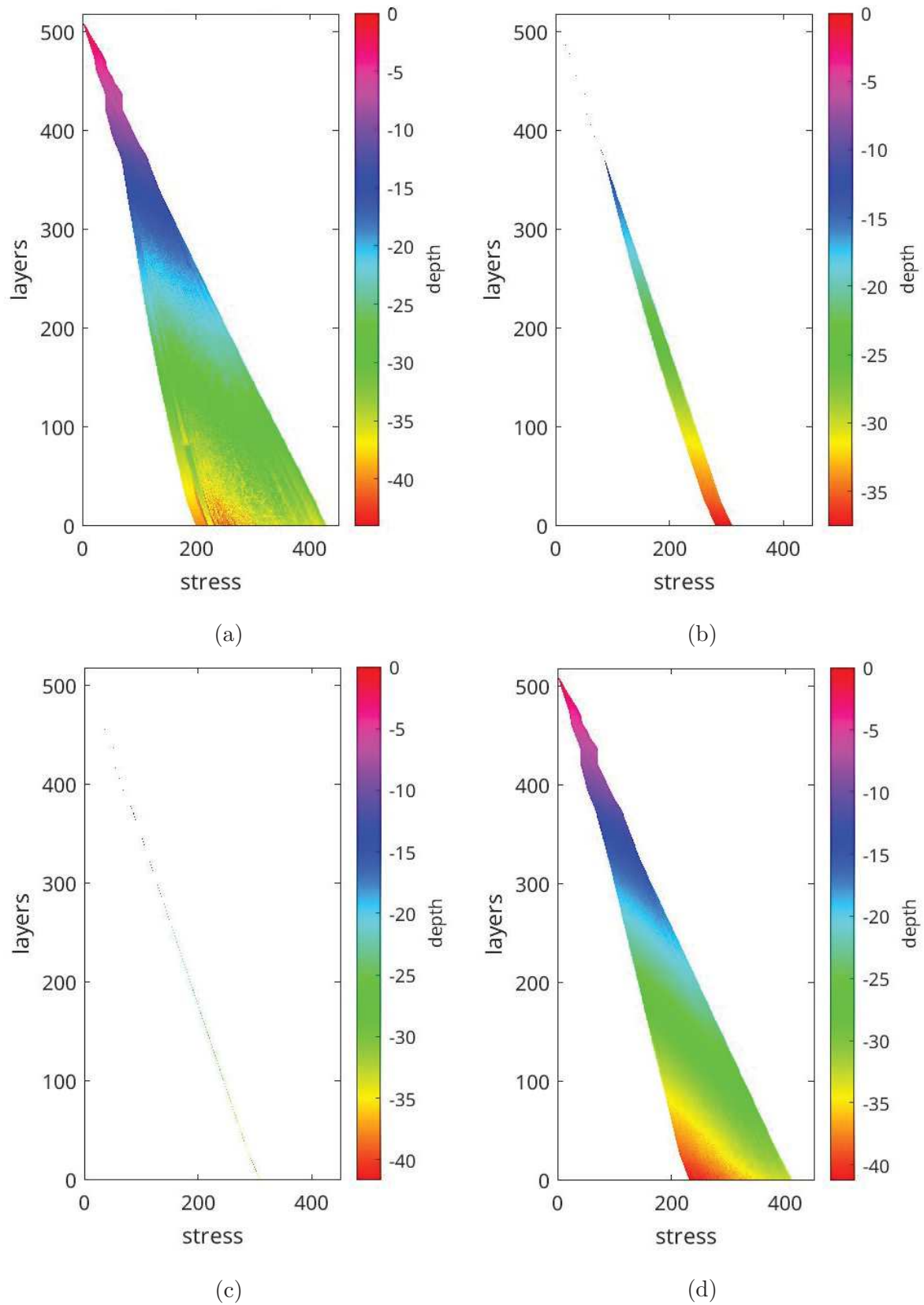


Figure 5.34: Monte Carlo outcomes in terms of effective stress [kPa] versus model layer number and depth/thickness [m] for the four analyses developed in the study assuming as uncertain (a) all the parameters and (b) the hydraulic, (c) the geomechanical, and (d) the density parameters only.

Strain Figure 5.35 shows the variation of strain with column layer number captured by the Monte Carlo simulations. The sub-panels display the mean behaviour corresponding to the behavior obtained by scenario A (Figure 5.16). Coherently with the characteristics of the various classes, strain very close to zero is computed for the sandy soils independently on depth (layers 1-25, 375-391, and 447-453). The strain increases from the top to the bottom of the thick silty clay unit located between layers 26 and 374 and it peaks in correspondence of the peat soil between layers 429 and 435 (Figure 5.36). Clearly, soil recently deposited experienced a low value due to the small load on its top (layers 480-518). The strain variation, as shown in Figures 5.35c and 5.35d, depends on geomechanical properties and soil densities that make a given soil more or less prone to compaction and more or less heavy (i.e., more or less able to cause compaction of the overlying units). A variation of K_{z_0} , as shown in Figure 5.35b, is almost not felt because overpressure at the end of the simulation is almost totally dissipated. Figure 5.37 shows that, for a given model layer, a smaller value of strain corresponds to a larger depth/thickness. This happens because for larger soil densities, the column weight increases and, as a result, the column compacts significantly.

PDL Figure 5.38 shows the behaviour of PDL versus column layer numbers obtained with the Monte Carlo simulations. The PDL represents the settlement of a soil layer after its deposition. The behavior in Figures 5.38a,b,c,d displays values close to zero at the extremes of the soil column in correspondence of layers that have just been deposited and just above the column basement, with the maximum in the middle of the profile as usually occurs. The peak is much more pronounced in Figure 5.38b, proving that K_{z_0} has a significant impact on the PDL. This happens as K_{z_0} governs the evolution over time of the overpressure resulting from the gradual deposit of soils: a small K_{z_0} causes a layer to be deposited on a column

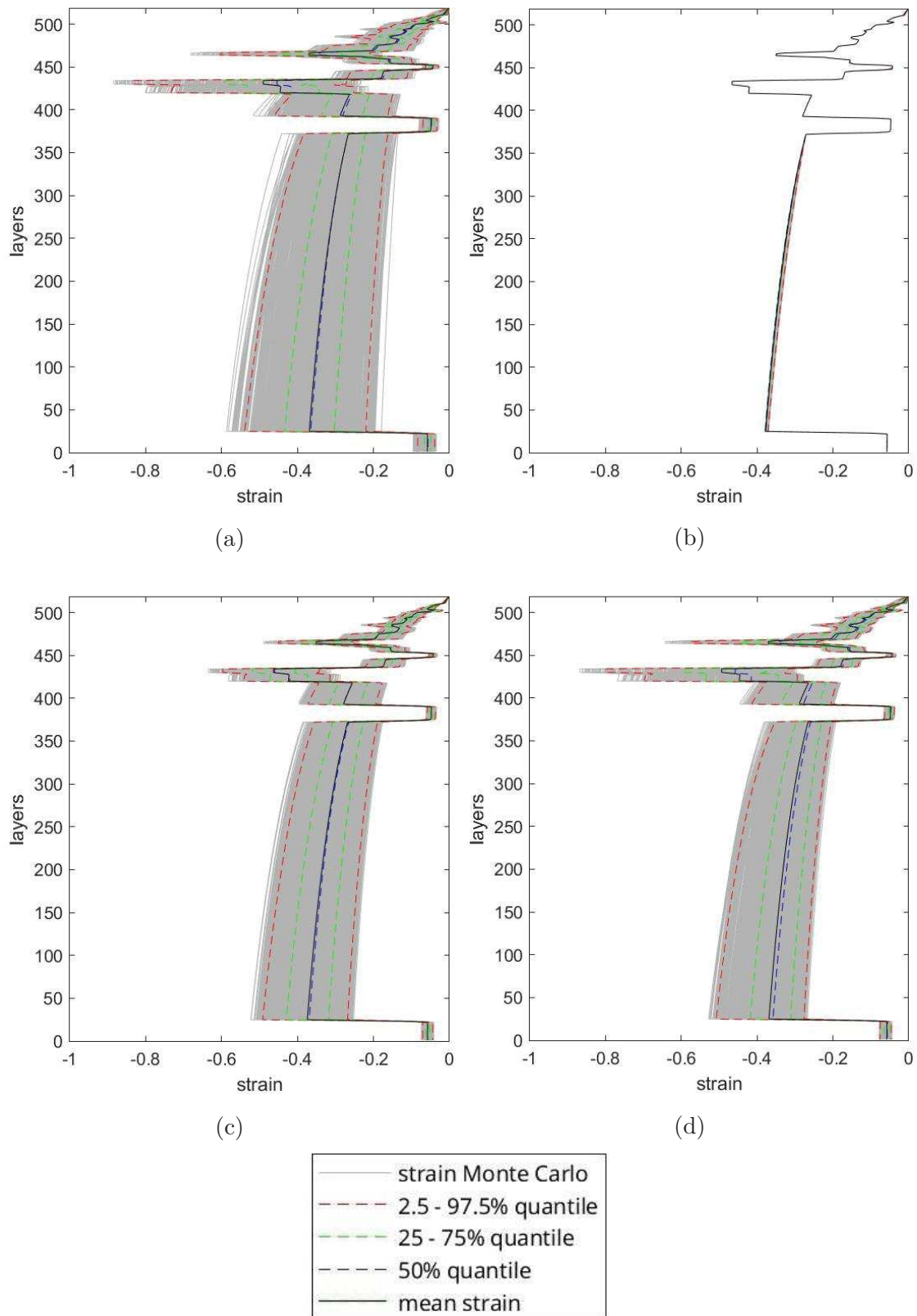


Figure 5.35: Monte Carlo outcomes and related statistics in terms of strain [-] versus model layer number for the four analyses developed in the study assuming as uncertain (a) all the parameters and (b) the hydraulic, (c) the geomechanical, and (d) the density parameters only.

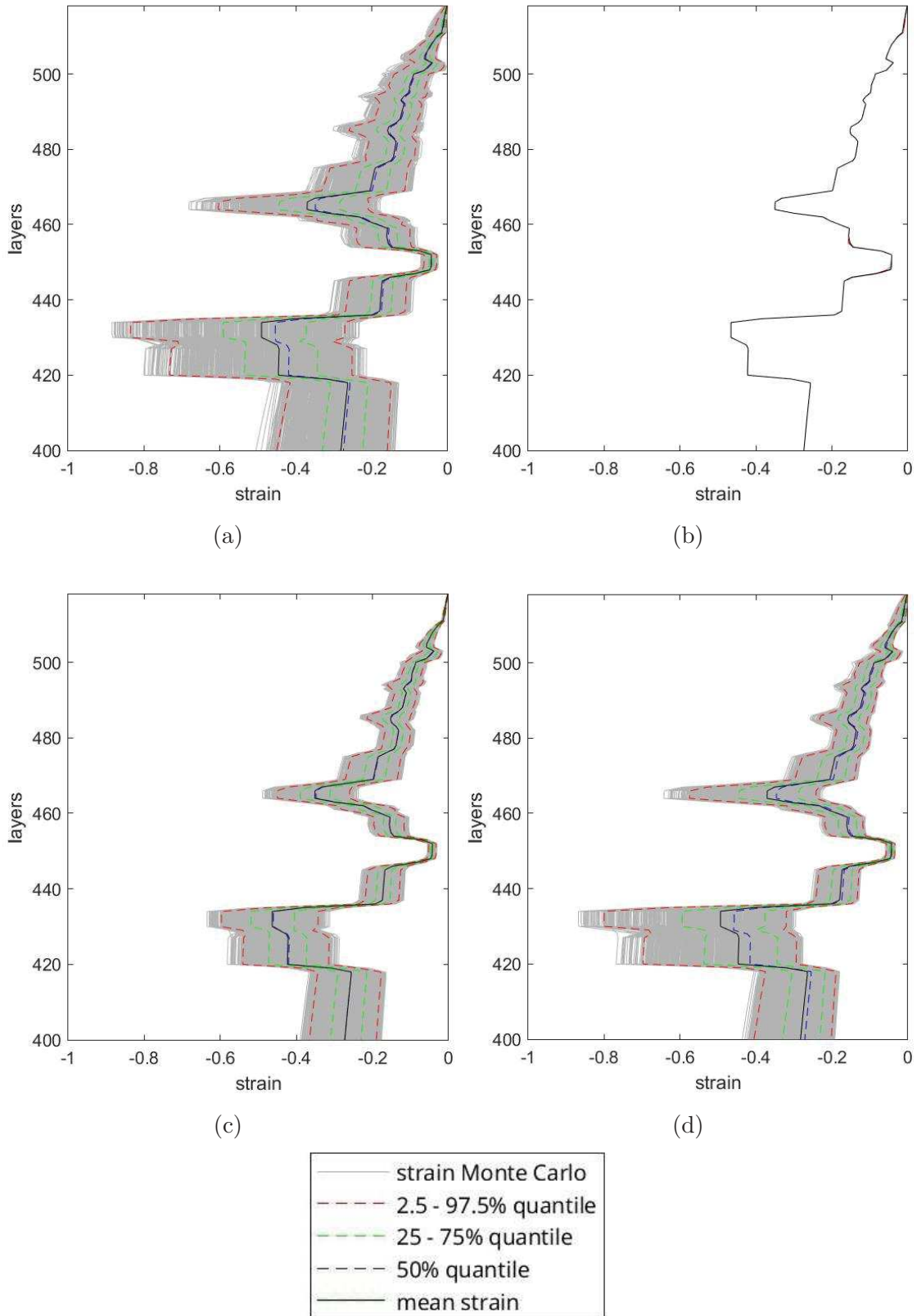


Figure 5.36: Zoom of Figure 5.35 for the shallower overbank units (corresponding to the layer numbers between 400 and 518, i.e. approximately the upper 12 m of the soil column) where a high lithological variability is observed.

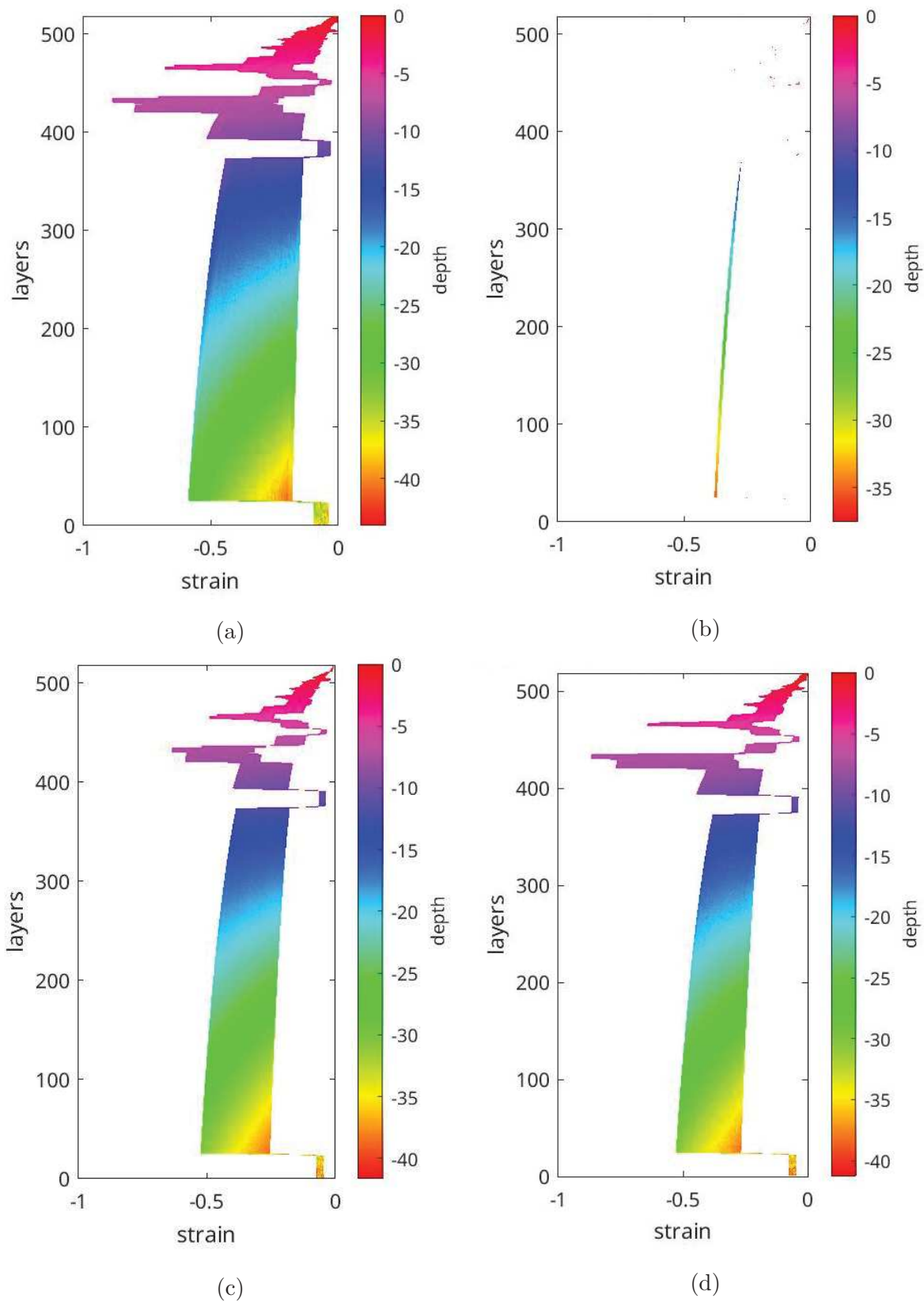


Figure 5.37: Monte Carlo outcomes in terms of strain [-] versus model layer number and depth/thickness [m] for the four analyses developed in the study assuming as uncertain (a) all the parameters and (b) the hydraulic, (c) the geomechanical, and (d) the density parameters only.

Lithological class	reference K_{z0} [m/yr]	$K_{z0,2}$ [m/yr]	$K_{z0,6}$ [m/yr]
sand	31.50	18.68	35.71
silty clay loam	31.50	54.75	117.36
silty clay	0.0135	0.3151	0.0032
peat	3.15	0.34	5.93
silty loam	3.15	0.34	1.91
humic clay	3.15	0.87	0.76

Table 5.11: Values of the hydraulic conductivity for the various lithological classes used in the reference simulation and the two simulations $K_{z0,2}$ and $K_{z0,6}$ providing the minimum and maximum PDL, respectively.

with large overpressure and consequently still underconsolidated. Consequently, this layer will settle more over time than in the case of soil characterized by large K_{z0} when consolidation has been already occurred. Figure 5.39 shows the variation of PDL both with depth/thickness and number of layers. It is possible to notice, coherently with the definition of this variable, that a smaller PDL is verified with a larger depth/thickness if a fixed layer is considered.

The effect of K_{z0} on PDL and, consequently, on the evolution versus time of the column thickness has been investigated in detail for the two simulations that provides the minimum (2 m) and maximum (6 m) PDL values in Figure 5.38b. For the sake of simplicity, the cases are referred to as $K_{z0,2}$ and $K_{z0,6}$, respectively. The input parameters for these two simulations are summarised in Table 5.11.

Figures 5.40 and 5.41 show the evolution over time of the elevation/thickness of the soil column and the overpressure at the column bottom for these two cases. The layer which plays a crucial role is the silty clay. Its hydraulic conductivity value is dramatically different. In the $K_{z0,2}$ case it is one order of magnitude larger than the reference value, thus revealing a more permeable behaviour. The $K_{z0,6}$ case is exactly the opposite: K_{z0} plummets to even two orders of magnitude with respect to $K_{z0,2}$. Consequently, in this last situation a more distributed peak in pressure over time is obtained and the post depositional lowering is larger following the

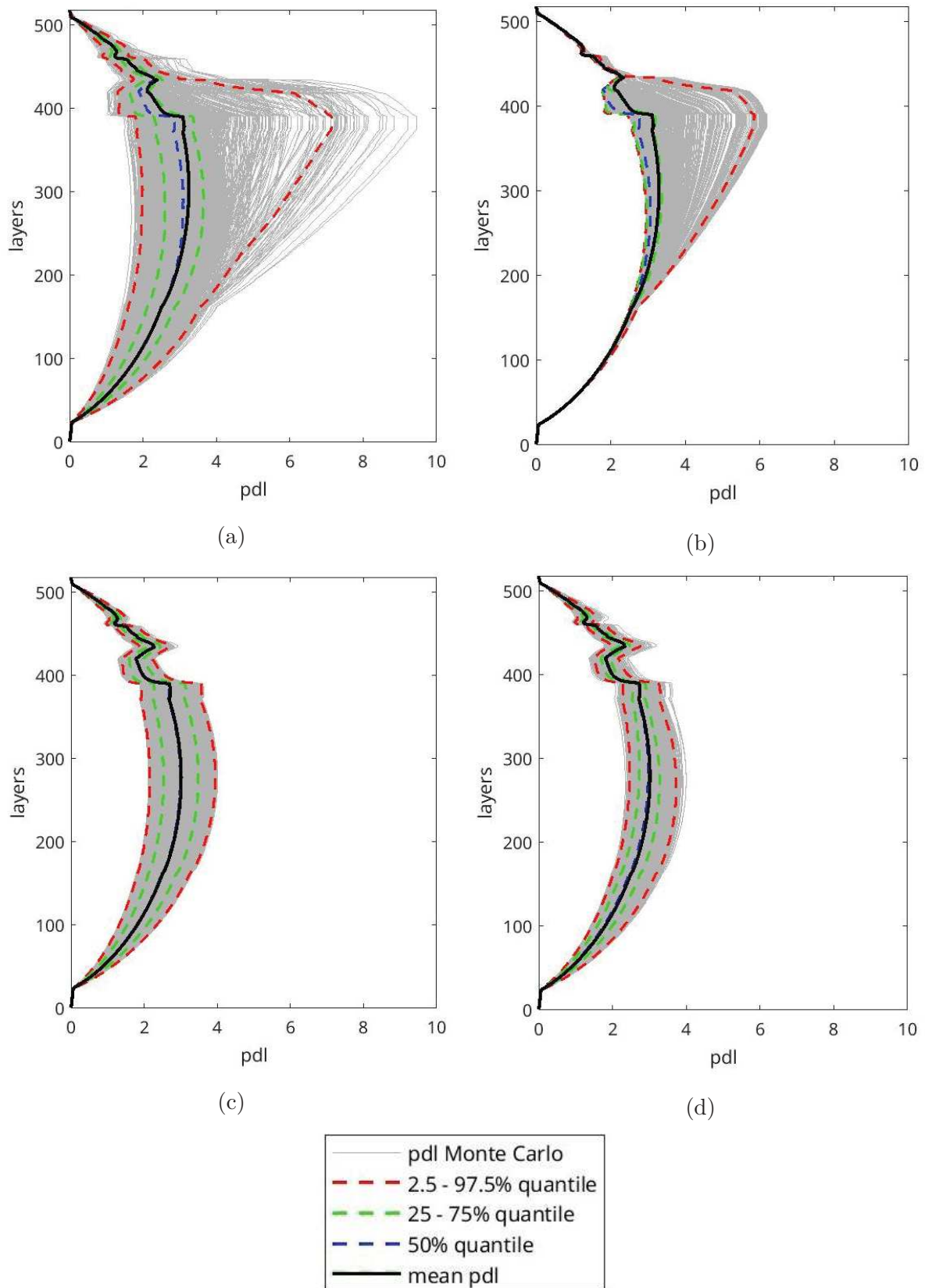


Figure 5.38: Monte Carlo outcomes and related statistics in terms of PDL [m] versus model layer number for the four analyses developed in the study assuming as uncertain (a) all the parameters and (b) the hydraulic, (c) the geomechanical, and (d) the density parameters only.

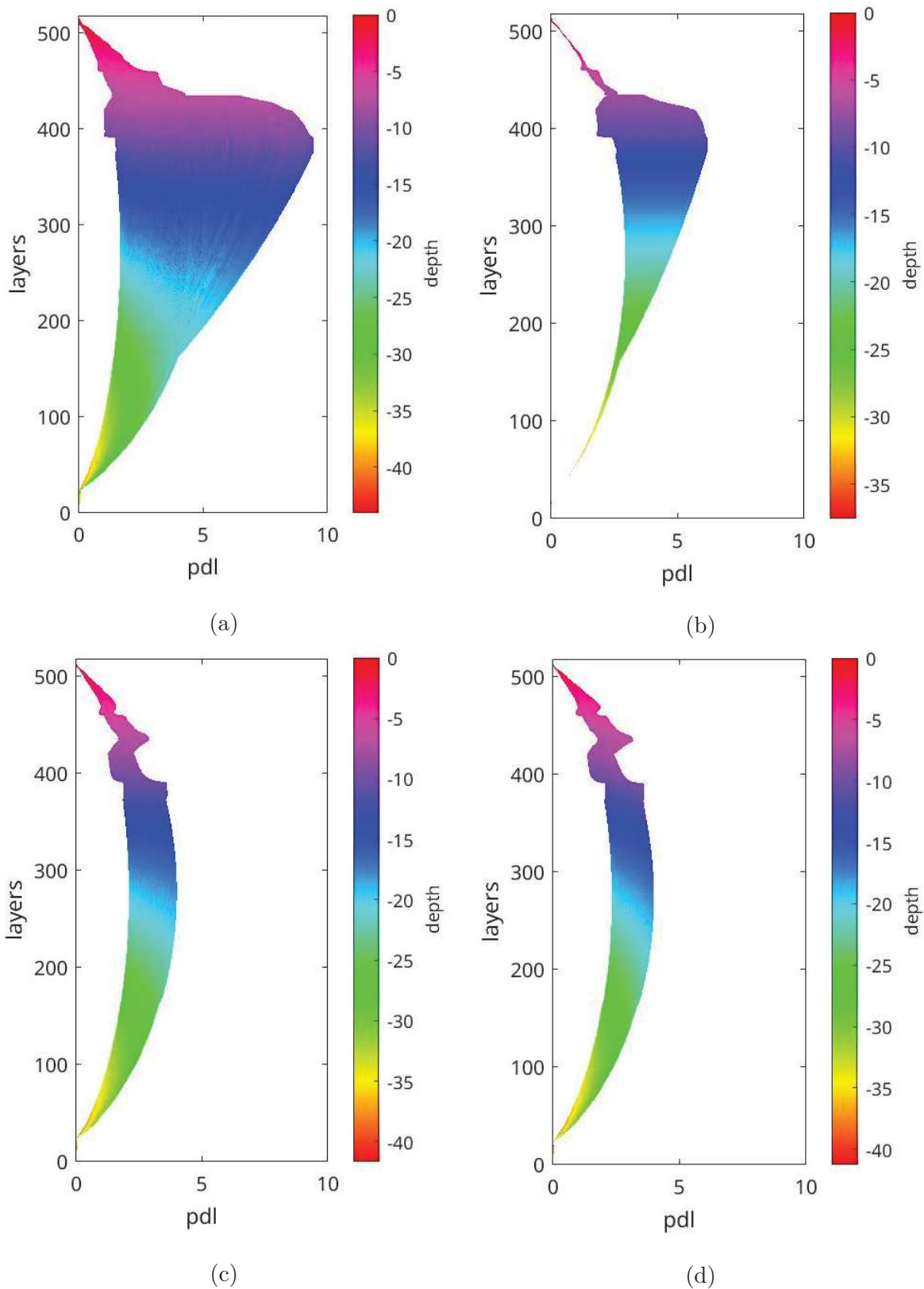


Figure 5.39: Monte Carlo outcomes in terms of PDL [m] versus model layer number and depth/thickness [m] for the four analyses developed in the study assuming as uncertain (a) all the parameters and (b) the hydraulic, (c) the geomechanical, and (d) the density parameters only.

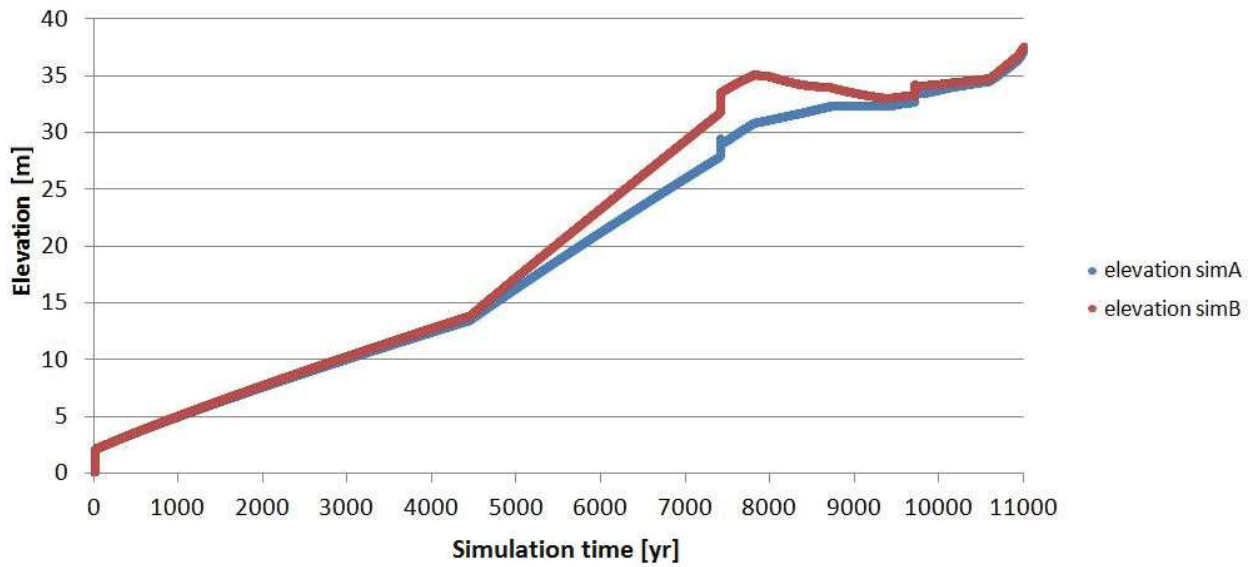


Figure 5.40: Comparison of simulations $K_{z0,2}$ and $K_{z0,6}$ in terms of elevation [m] of the soil column.

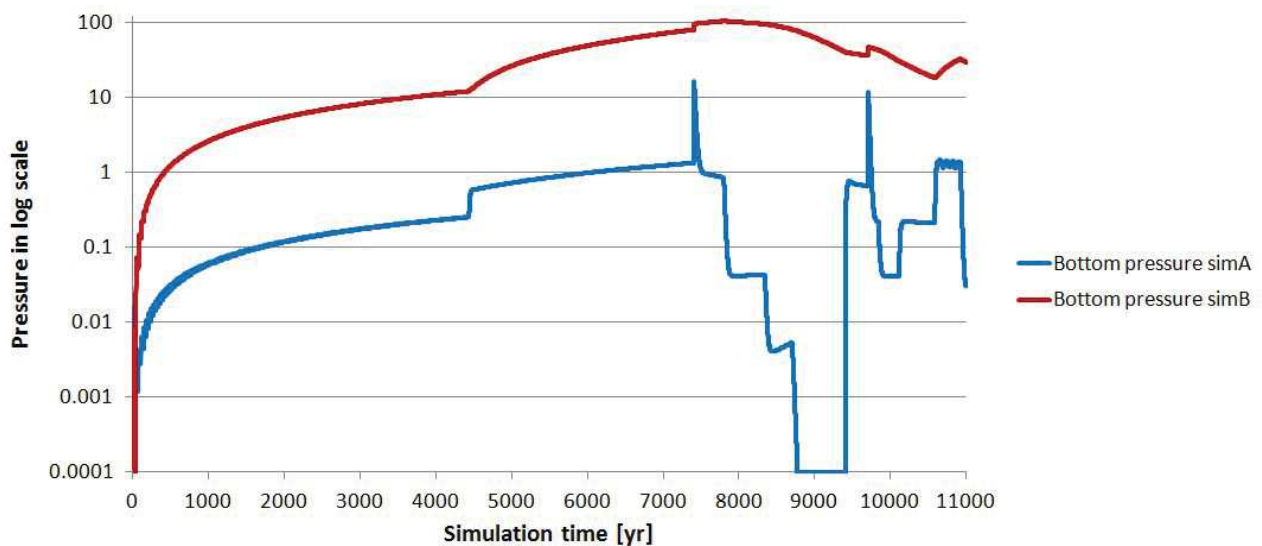


Figure 5.41: Comparison of simulations $K_{z0,2}$ and $K_{z0,6}$ in terms of pressure [kPa] of the bottom of the soil column.

more time needed for overpressure dissipation. In the $K_{z0,2}$ case, on the other hand, a larger permeability leads to a smaller pressure on average during the whole time scale, with local peaks in correspondence to the deposition of heavy material, such as sand.

Porosity Figure 5.42 displays the porosity behavior versus the column layer number as captured by the Monte Carlo simulations. Comparison of Figures 5.42b,c,d shows that the main

contribution to porosity variability is given by e_0 and γ_s . Indeed, the initial value of the void index is a good indicator of the possible trend that porosity may undergo during soil deposition. Starting from a very porous initial state, a given soil is very likely to undergo a fast and significant compaction at least initially. Then, of course, also the variability in specific weight plays an important role because it makes a soil class acting more or less heavily in terms of weight with respect to the other soils in the given column. Conversely, K_{z_0} plays a negligible role (Figure 5.42b). Figure 5.43 represents a zoom on the upper part of the soil column where a high variability in the lithology is observed. Figure 5.44 shows that, considering a fixed layer, the porosity variability is reflected by a different column depth with a general trend in which larger porosity correspond to larger depth/thickness for a fixed layer. This observation is consistent with the fact that a thinner column means more compaction and, consequently, a smaller porosity.

Bulk density It is useful to remind that this parameter depends on the specific weight of grains and bulk porosity. Clearly, it is expected to increase from low values at the surface to larger values at depth. This is what Figure 5.45 confirms, especially within the thick silty clay soil ranging from layer 26 to layer 374. Sudden jumps in bulk density can be observed in the top part of the soil column (Figure 5.46) suggesting that initial burial plays a significant role in terms of shallow sediment compaction as already pointed out in Keogh and Törnqvist (2019). Moreover, light peat layers are located in the shallower part of the profile. As already pointed out for the porosity, also the bulk density variability is mostly influenced by e_0 and γ_s (Figure 5.45d), whereas the influence of K_{z_0} is almost negligible (Figure 5.45b). Figure 5.47 represents the variation of bulk density with both layers and depth/thickness. If a fixed layer is considered, it can be observed that smaller bulk densities correspond to larger depths/thicknesses. In fact,

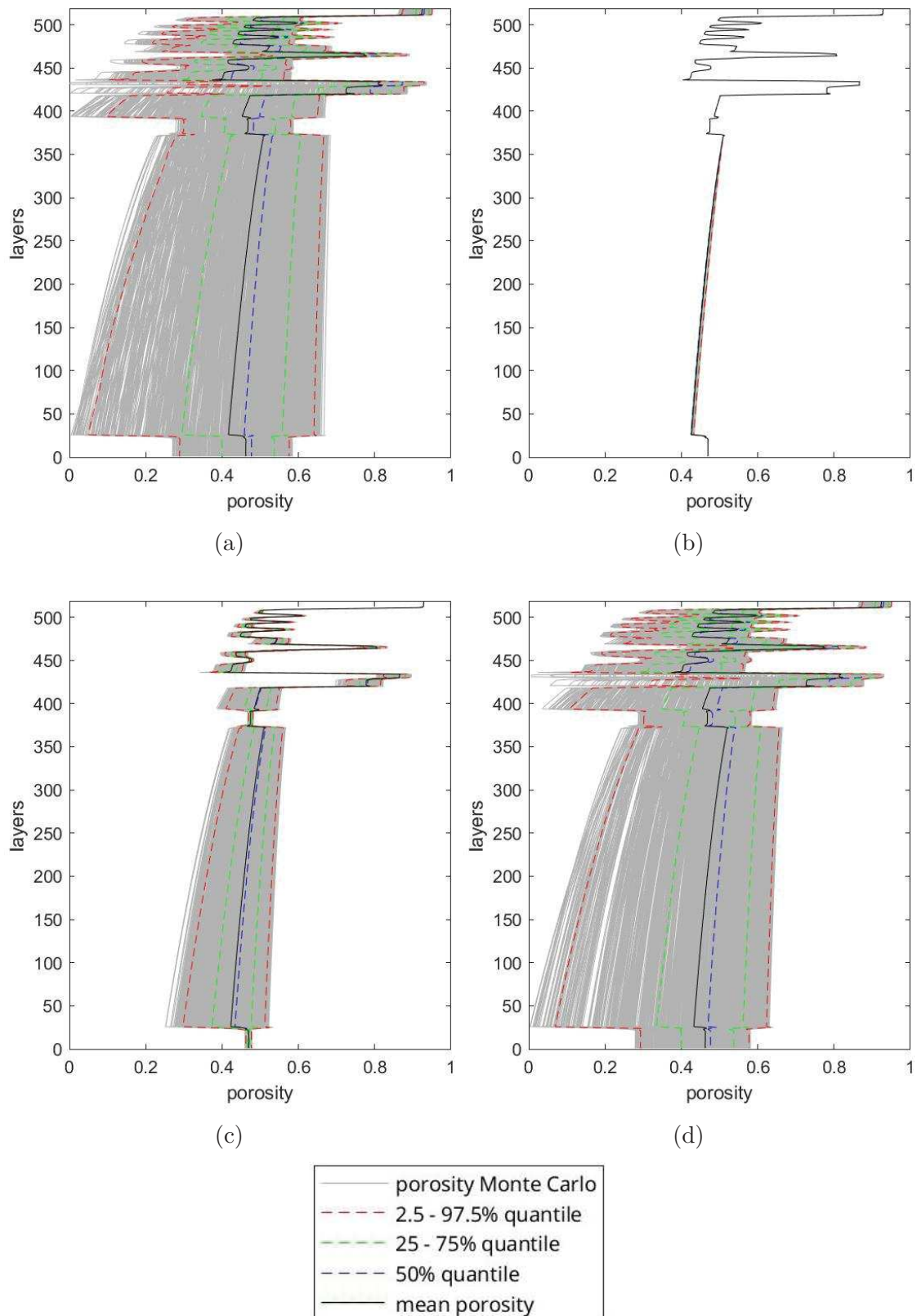


Figure 5.42: Monte Carlo outcomes and related statistics in terms of porosity [-] versus model layer number for the four analyses developed in the study assuming as uncertain (a) all the parameters and (b) the hydraulic, (c) the geomechanical, and (d) the density parameters only.

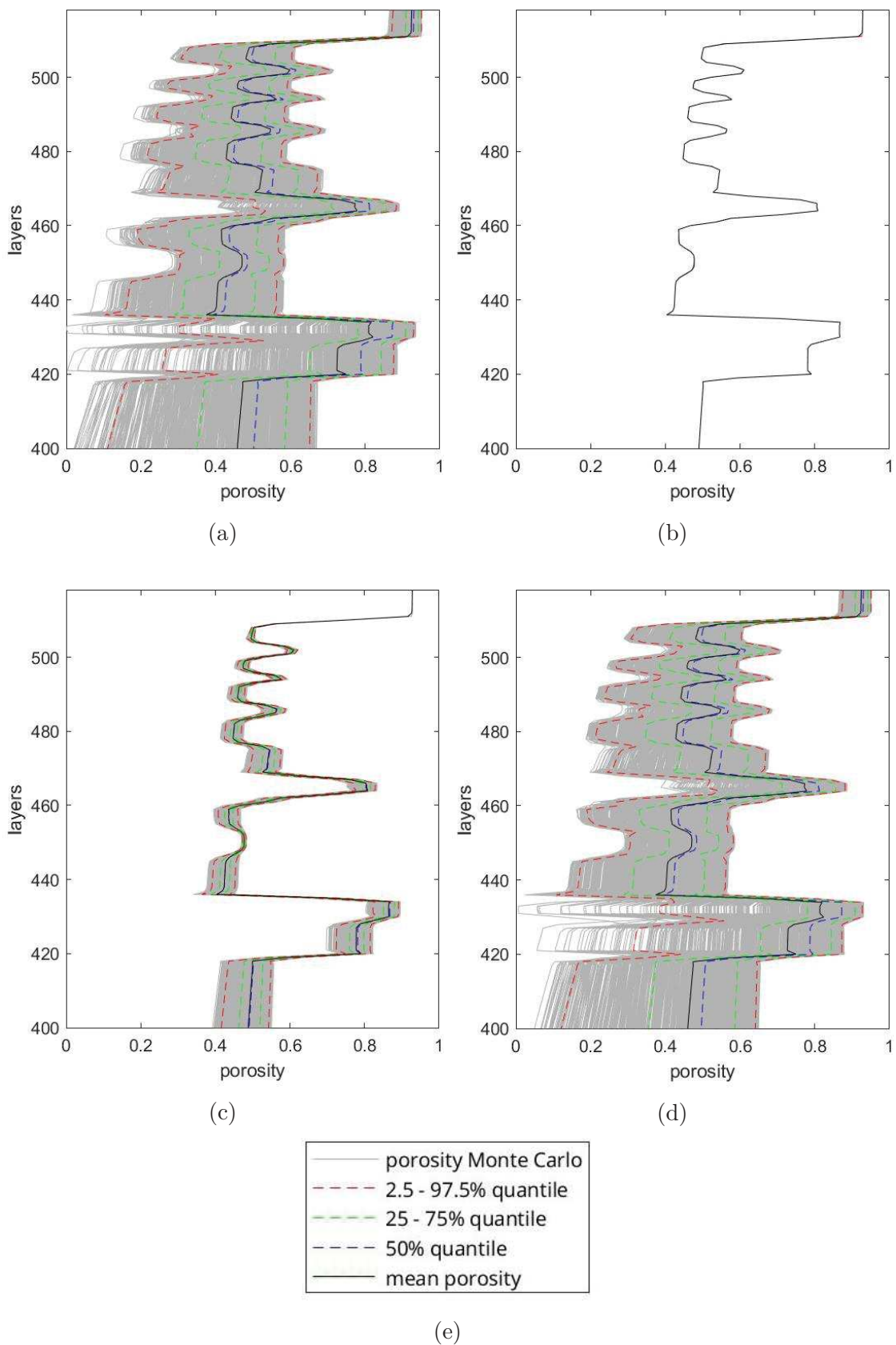


Figure 5.43: Zoom of Figure 5.42 for the shallower overbank units (corresponding to the layer numbers between 400 and 518, i.e. approximately the upper 12 m of the soil column) where a high lithological variability is observed.

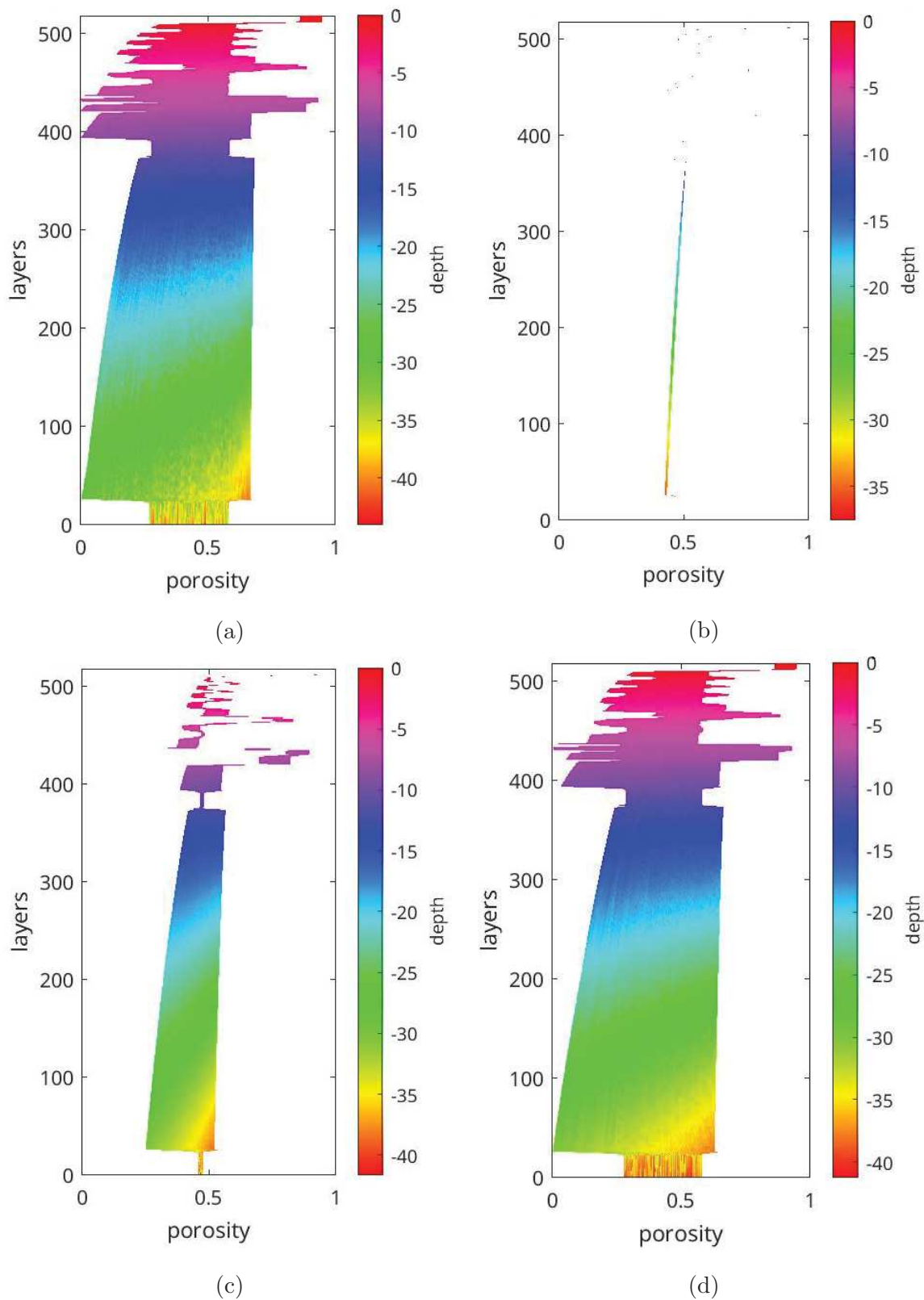


Figure 5.44: Monte Carlo outcomes in terms of porosity [-] versus model layer number and depth/thickness [m] for the four analyses developed in the study assuming as uncertain (a) all the parameters and (b) the hydraulic, (c) the geomechanical, and (d) the density parameters only.

a lighter column compact less.

Compressibility Figure 5.48 shows the behaviour of compressibility versus column layer number as obtained with the Monte Carlo simulations. From Figure 5.48a it is clear that the general trend of compressibility is to decrease of a few orders of magnitude from the column top to bottom, with some localized variations dependent on soil characteristics. For example, the sandy layers located between layers 0-26, 375-391 and 447-453 coherently display smaller compressibility values with respect to the other lithotypes. The upper layers, deposited relatively recently, are characterized by a larger compressibility because compaction in this portion of the soil column reflects a smaller load (Figure 5.49). Figures 5.48c,d show that the geomechanical parameters and, secondarily, density are the parameters influencing more significantly the variability of compressibility. Figure 5.50 helps analysing the variability of compressibility both with layers and depth/thickness. By keeping fixed a generic layer, the plots prove that, coherently with the behavior of porosity and bulk density, a smaller compressibility is associated with larger depth/thickness, i.e. a less compacted column.

Integrated compaction The interpretation of Figures 5.51 and 5.52 is straightforward once the definition of integrated compaction is clear. This variable indicates how much higher a point in the stratigraphic column would be if no compaction took place. This value increases from zero at the column bottom to the maximum at the top. In our case it is, on average according to scenario A, equal to 14 m. Therefore, the Myrtle Grove soil column, whose compacted thickness is 37 m, would be $37+14=51$ m thick in its uncompacted configuration. Figure 5.51 shows the behaviour of integrated compaction versus column layer number returned by the Monte Carlo simulations. The variability of the integrated compaction is mostly influenced by geomechanical

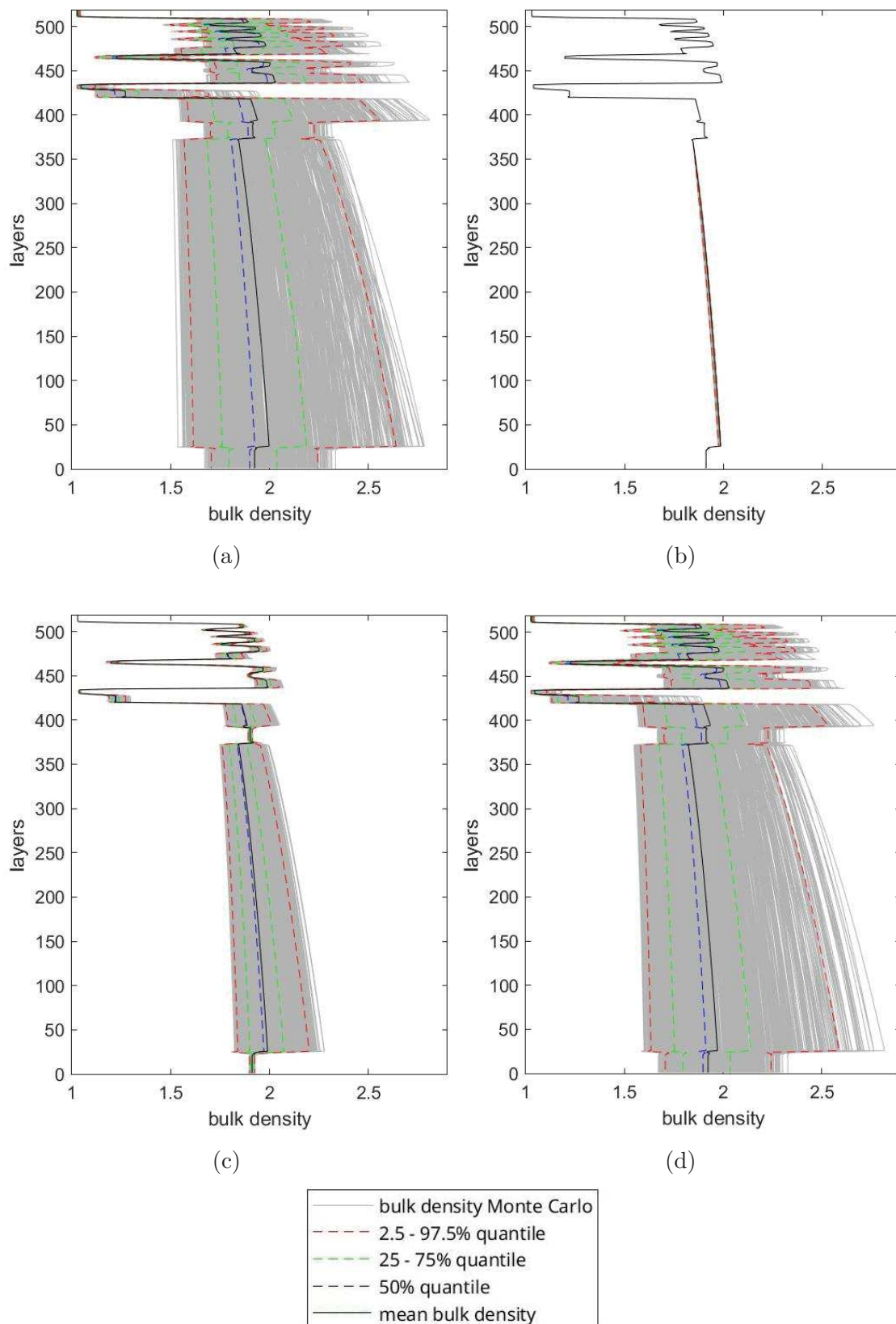


Figure 5.45: Monte Carlo outcomes and related statistics in terms of bulk density [g/cm^3] versus model layer number for the four analyses developed in the study assuming as uncertain (a) all the parameters and (b) the hydraulic, (c) the geomechanical, and (d) the density parameters only.

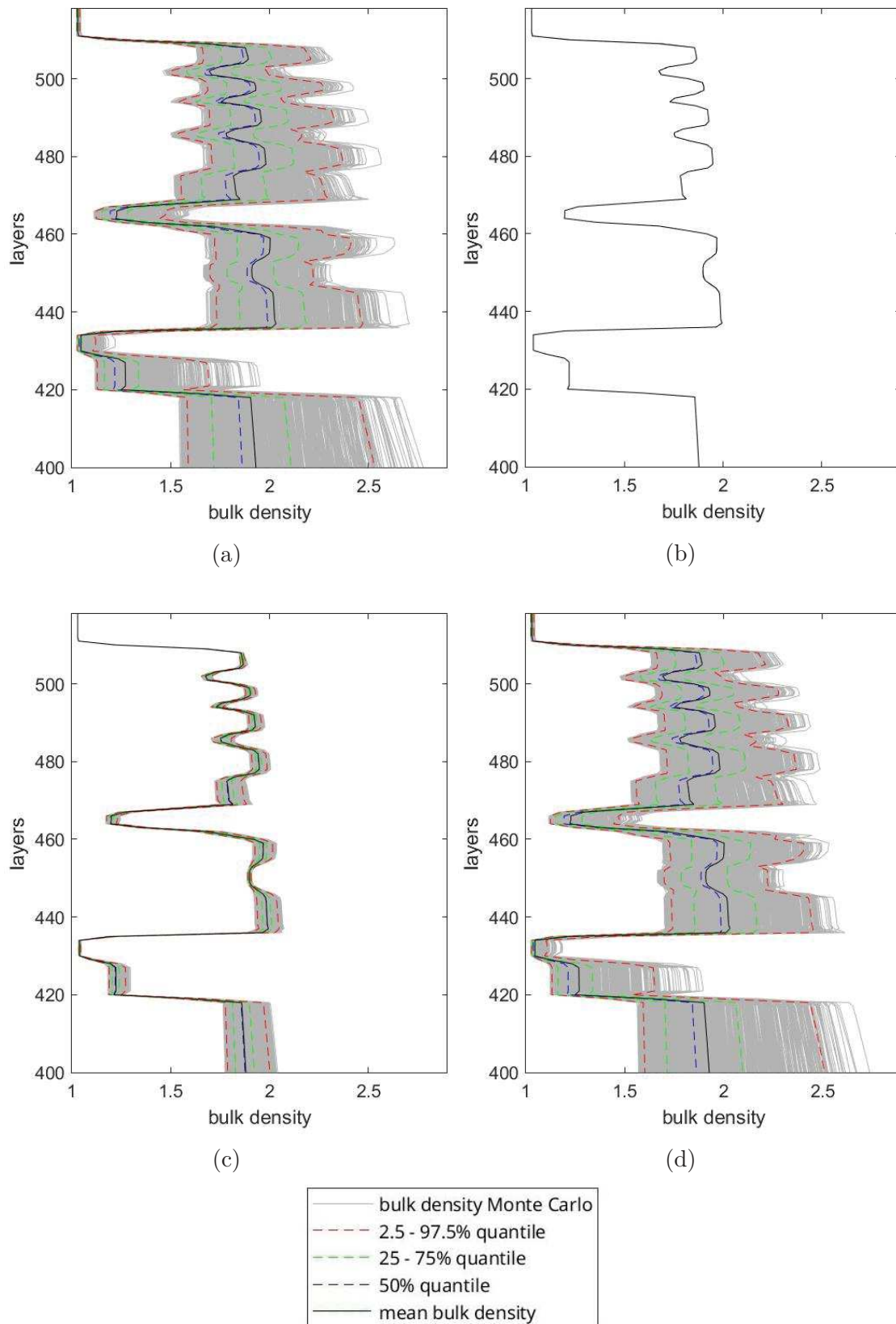


Figure 5.46: Zoom of Figure 5.45 for the shallower overbank units (corresponding to the layer numbers between 400 and 518, i.e. approximately the upper 12 m of the soil column) where a high lithological variability is observed.

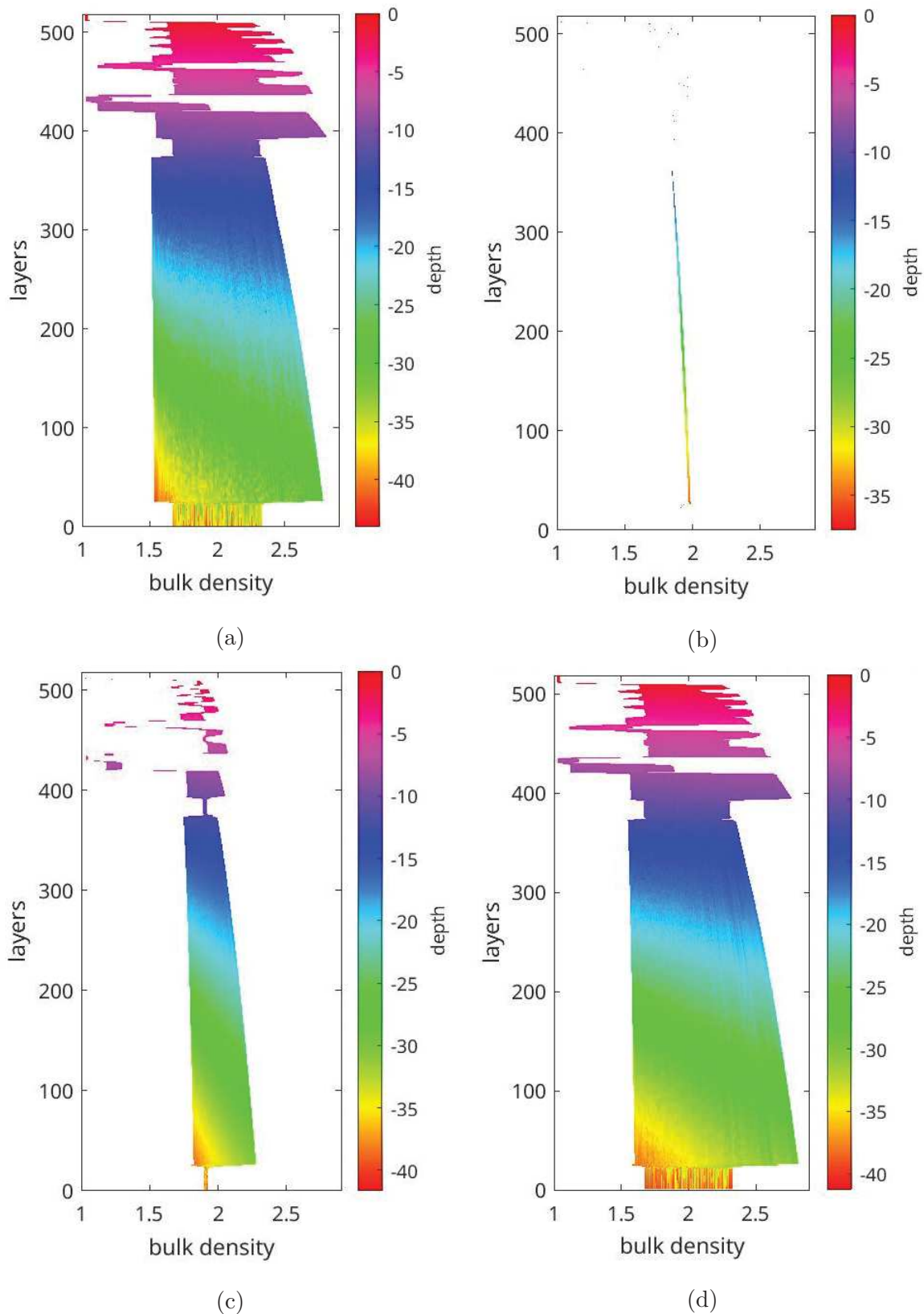


Figure 5.47: Monte Carlo outcomes in terms of bulk density [g/cm^3] versus model layer number and depth/thickness [m] for the four analyses developed in the study assuming as uncertain (a) all the parameters and (b) the hydraulic, (c) the geomechanical, and (d) the density parameters only.

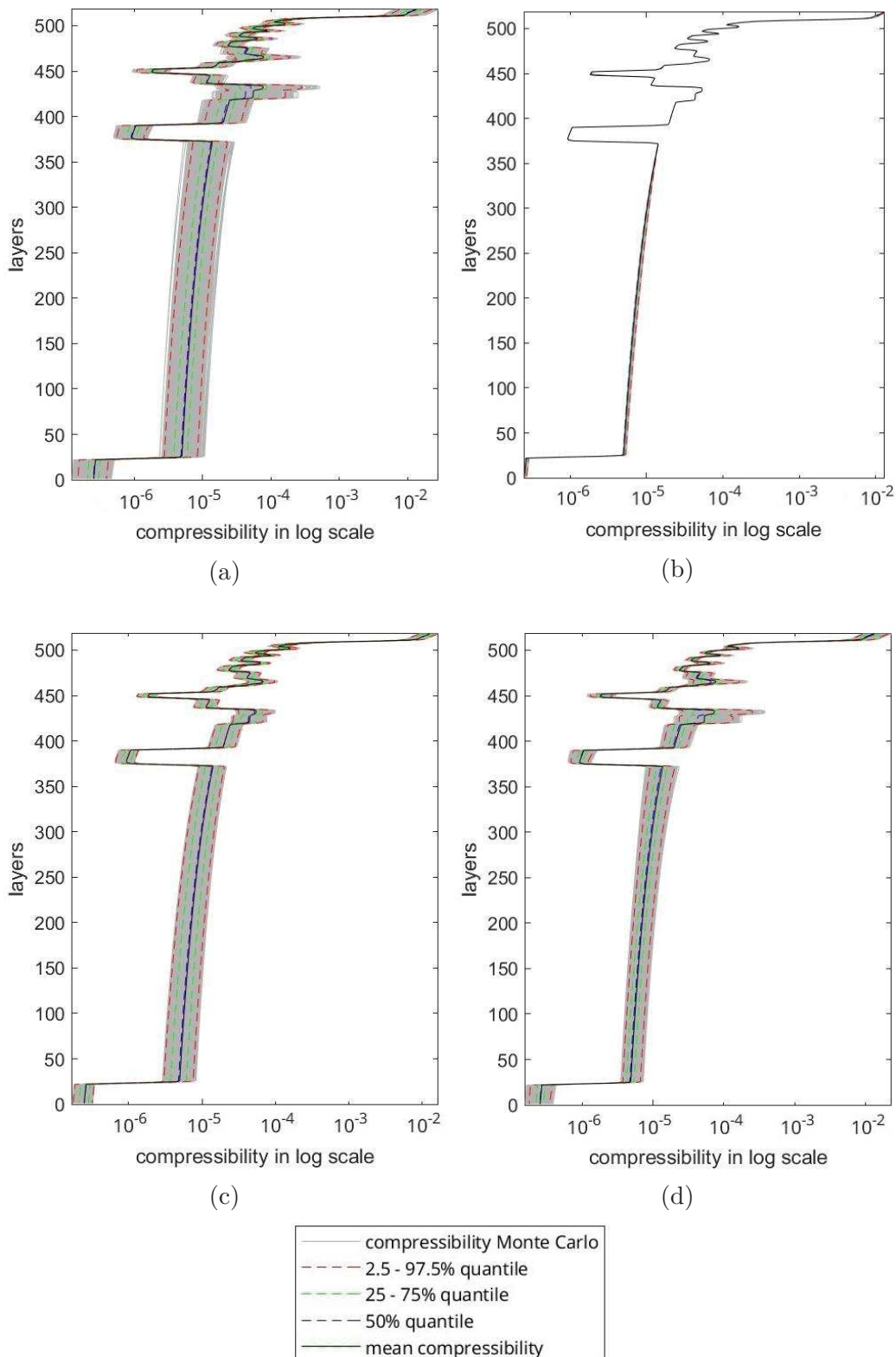


Figure 5.48: Monte Carlo outcomes and related statistics in terms of compressibility [kPa⁻¹] versus model layer number for the four analyses developed in the study assuming as uncertain (a) all the parameters and (b) the hydraulic, (c) the geomechanical, and (d) the density parameters only.

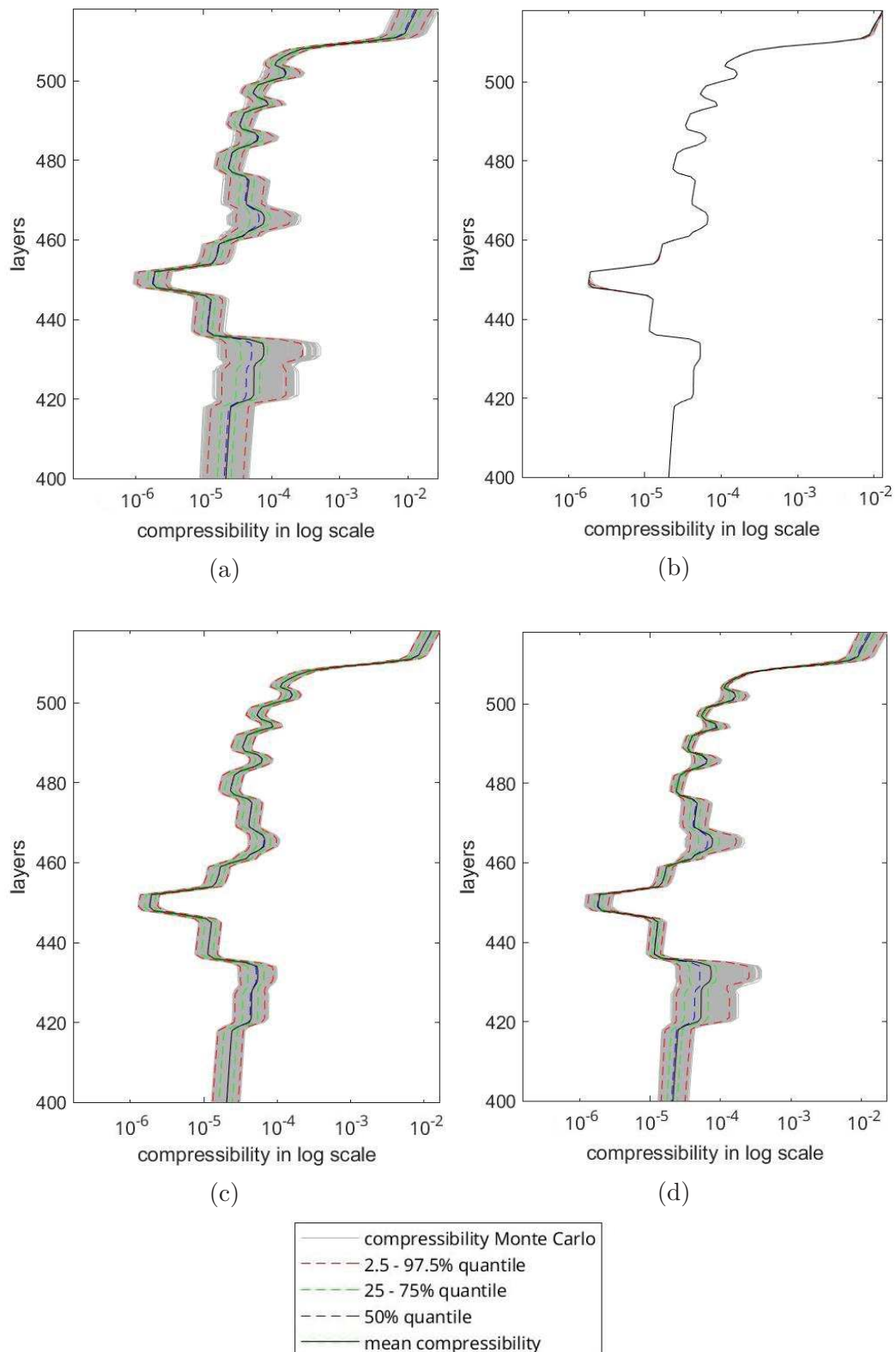


Figure 5.49: Zoom of Figure 5.48 for the shallower overbank units (corresponding to the layer numbers between 400 and 518, i.e. approximately the upper 12 m of the soil column) where a high lithological variability is observed.

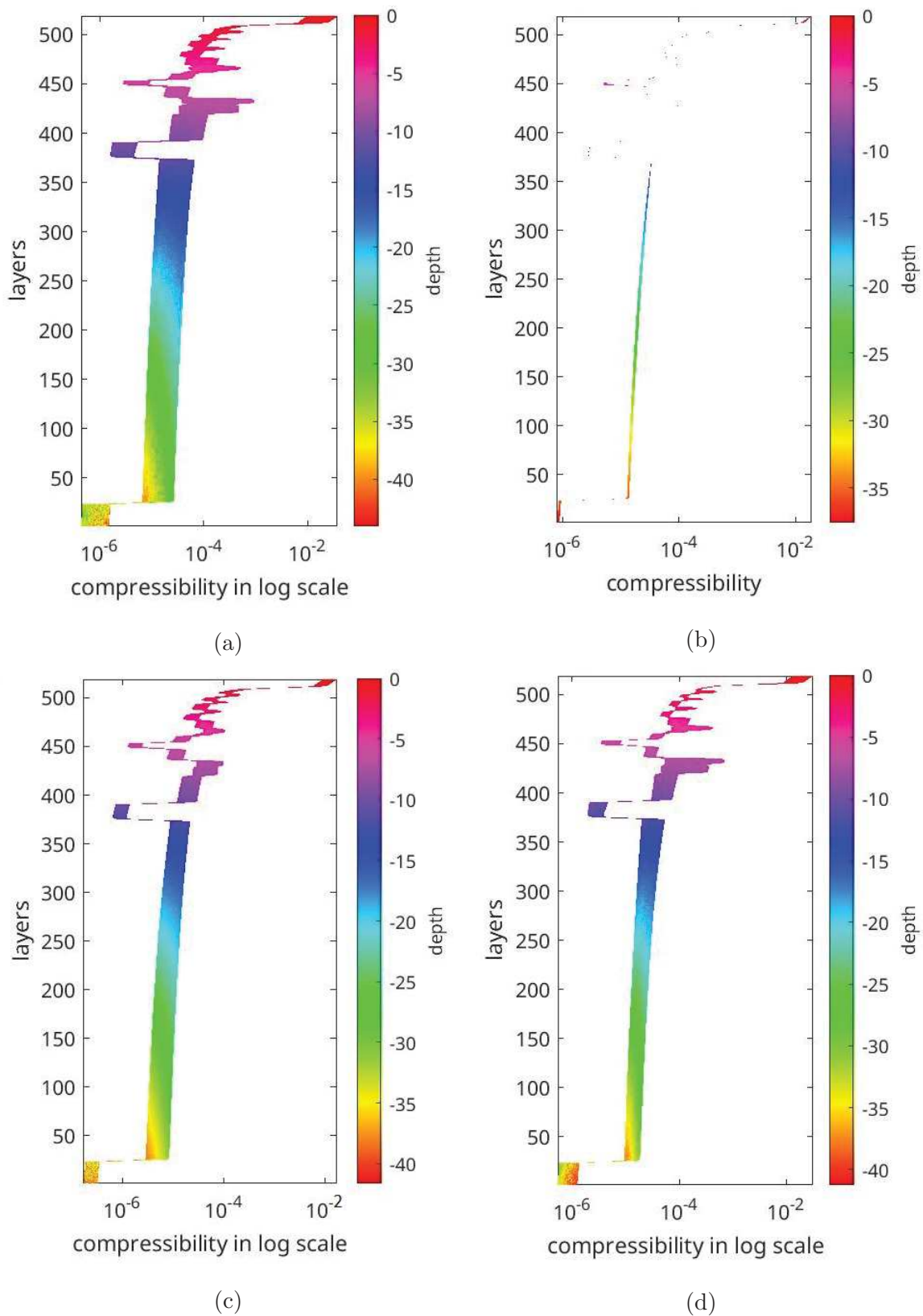


Figure 5.50: Monte Carlo outcomes in terms of compressibility [kPa^{-1}] versus model layer number and depth/thickness [m] for the four analyses developed in the study assuming as uncertain (a) all the parameters and (b) the hydraulic, (c) the geomechanical, and (d) the density parameters only.

and density parameters as shown in Figures 5.51c,d. In fact these are the parameters causing the soil to be stiff or weak and therefore more or less prone to undergo compaction. Figure 5.52 shows that, considering a certain model layer, the integrated compaction is larger for smaller depth/thickness, coherently with the definition previously mentioned.

Average unit compaction A final outcome is represented by the average compaction that each geologic unit detected at the Myrtle Grove Supersite has experienced during the 11'000 year evolution addressed by the simulations. The behavior of this variable (mean and associated standard deviation computed from the Monte Carlo analyses) are shown in Figures Figure 5.53, Figure 5.54, Figure 5.55 and Figure 5.56. By comparing these representations, the first aspect which arises is the very low variability related to K_{z0} coherently with the previous quantities reported above. It is a consequence of its weak influence on compaction compared to all other soil parameters. What links all plots, on the other hand, is the remarkable compaction of the peat layer (larger than 60%) just below the overbank.

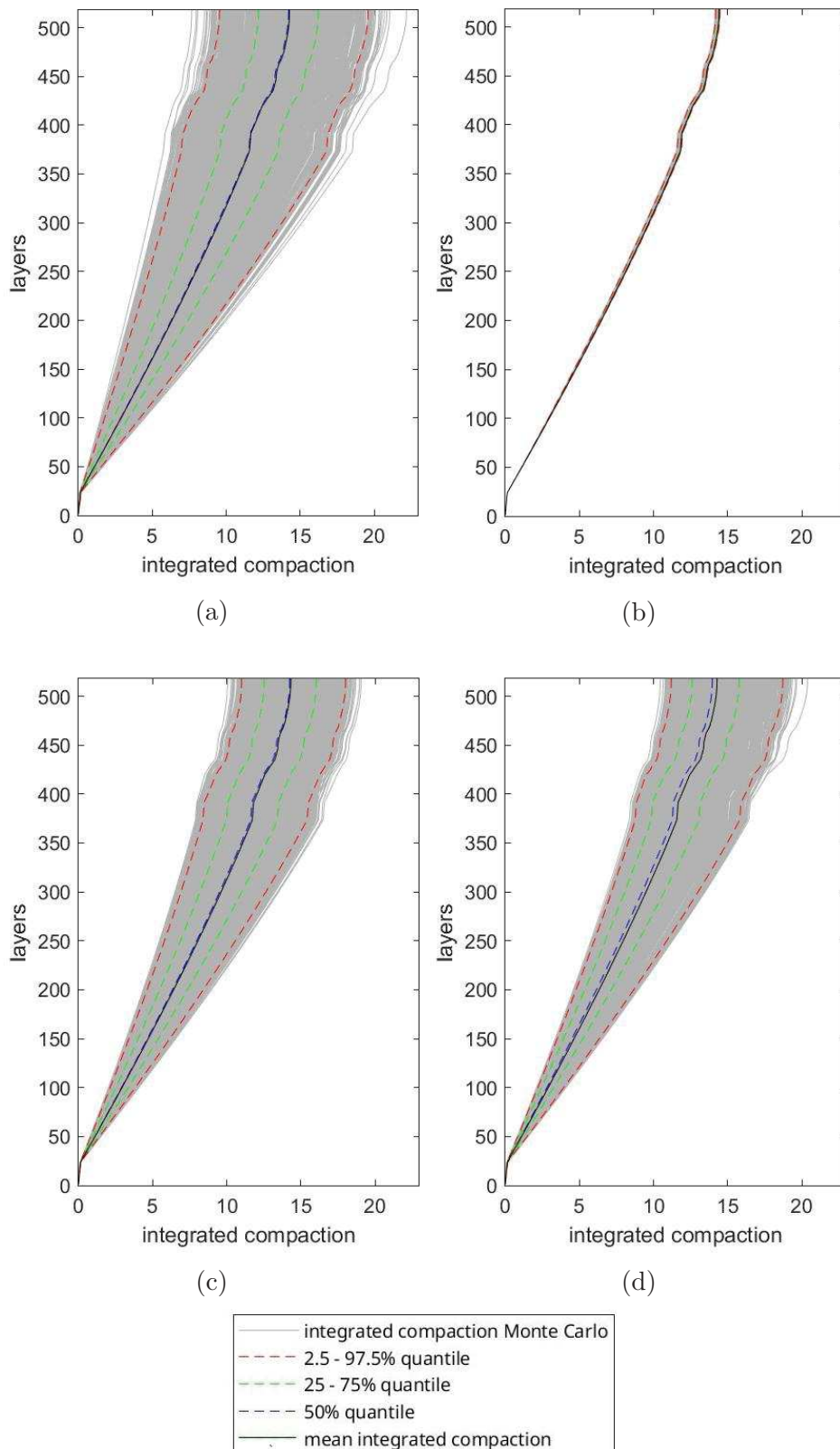


Figure 5.51: Monte Carlo outcomes and related statistics in terms of integrated compaction [m] versus model layer number for the four analyses developed in the study assuming as uncertain (a) all the parameters and (b) the hydraulic, (c) the geomechanical, and (d) the density parameters only.

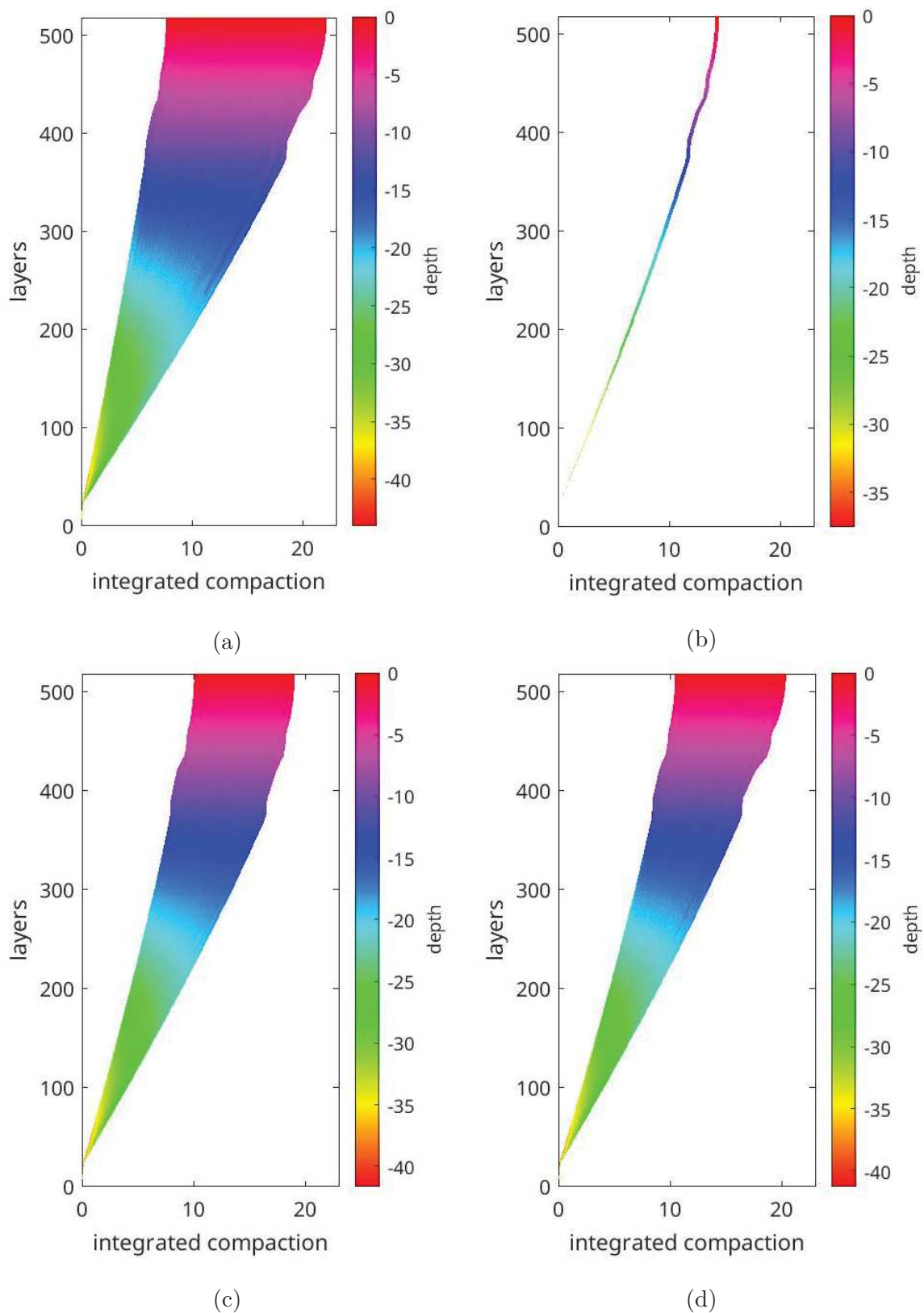


Figure 5.52: Monte Carlo outcomes in terms of integrated compaction [m] versus model layer number and depth/thickness [m] for the four analyses developed in the study assuming as uncertain (a) all the parameters and (b) the hydraulic, (c) the geomechanical, and (d) the density parameters only.

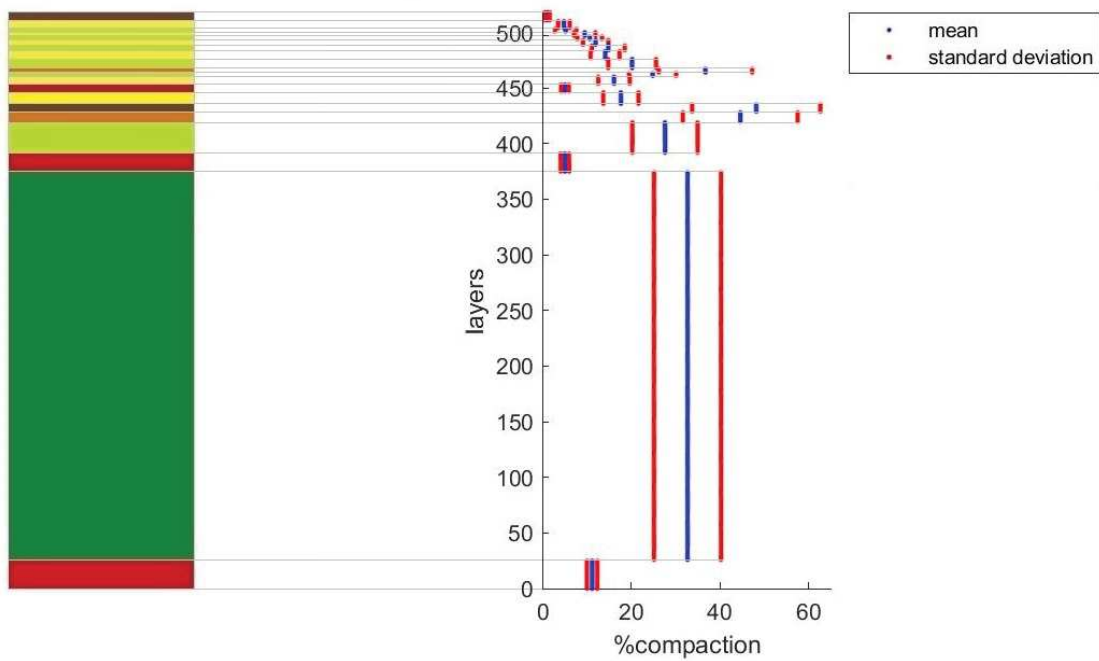


Figure 5.53: Average compaction of the geologic unit used to represent the Myrtle Grove sedimentary sequence. Mean and standard deviation are computed from the Monte Carlo simulation with all parameters assumed uncertain.

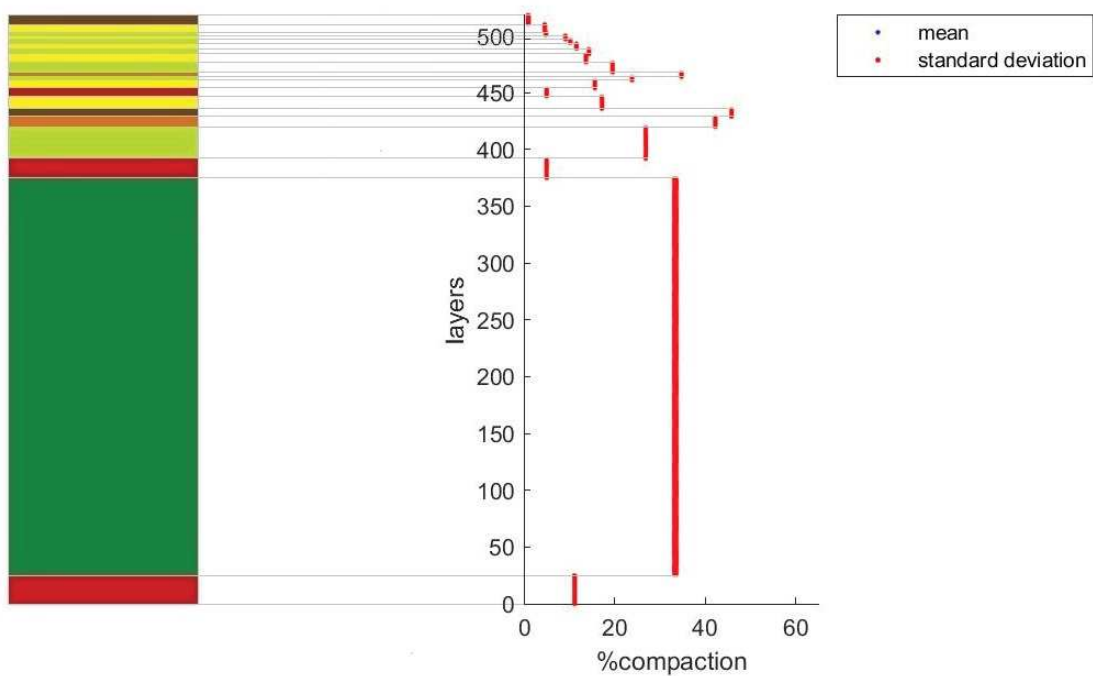


Figure 5.54: Average compaction of the geologic unit used to represent the Myrtle Grove sedimentary sequence. Mean and standard deviation are computed from the Monte Carlo simulation with only K_{z0} assumed uncertain.

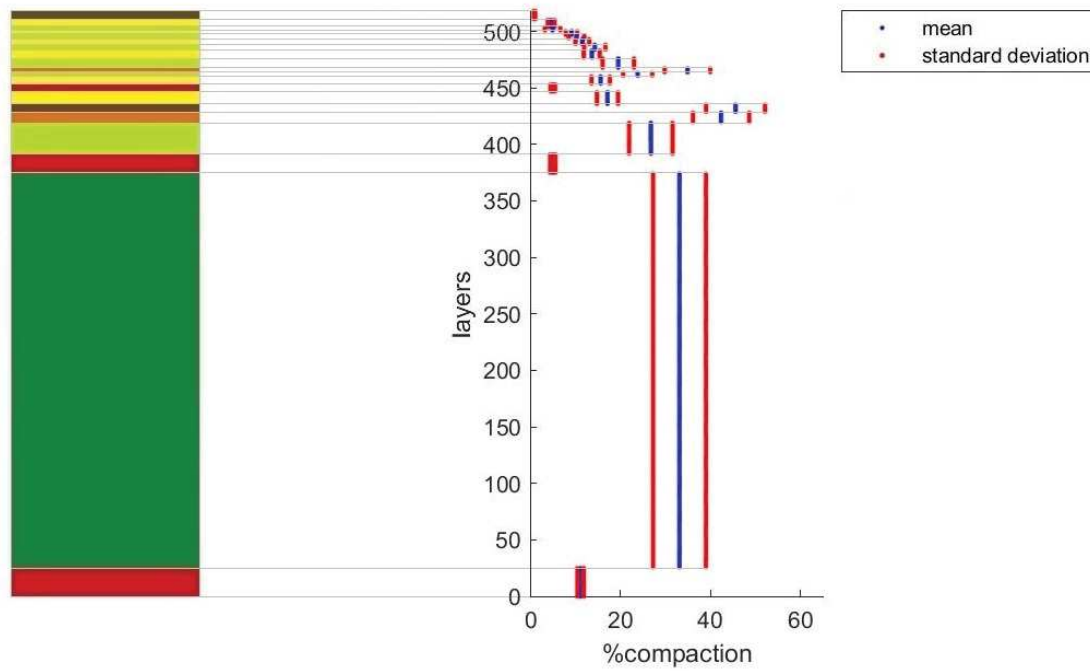


Figure 5.55: Average compaction of the geologic unit used to represent the Myrtle Grove sedimentary sequence. Mean and standard deviation are computed from the Monte Carlo simulation with only C_c , C_r and σ_p assumed uncertain.

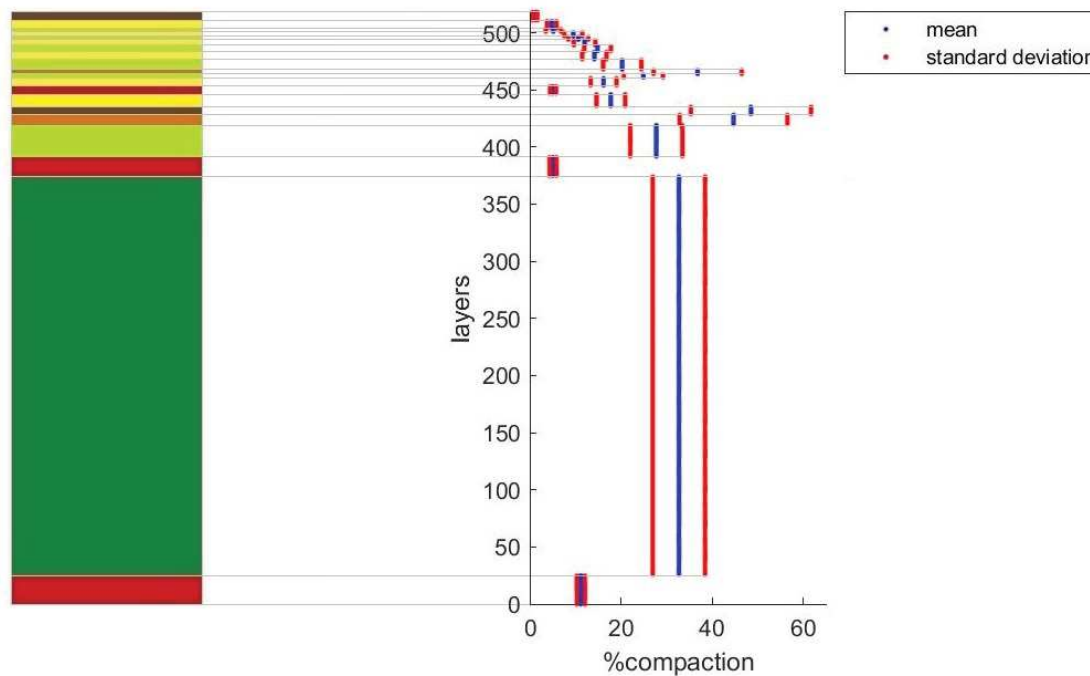


Figure 5.56: Average compaction of the geologic unit used to represent the Myrtle Grove sedimentary sequence. Mean and standard deviation are computed from the Monte Carlo simulation with only e_0 and γ_s assumed uncertain.

Chapter 6

Predicting the effects of artificial nourishment

This chapter presents a last set of simulations aimed at investigating the effectiveness of possible scenarios of artificial nourishment in terms of surface elevation change planned in the Myrtle Grove station. Indeed, this operation is developed to enhance the natural supply of sediment so as to withstand relative sea-level rise. It is a fundamental step because, as already discussed in the introduction, sea-level rise together with subsidence and lack of sediment supply is becoming quite an alarming issue in the Mississippi area and thus a deep investigation of such conditions in the future is required. The nourishment sediment is that transported seaward by the river. In accordance with Keogh et al. (2021) the sediment to use for nourishment operation has been identified with silty clay loam with similar characteristics of those used in the reproduction of the 11000-year deposition of the Myrtle Grove soil column (Table 6.1).

The simulation used as initial condition the final outcome of scenario A already discussed in Chapter 5 and adding this layer of silty clay loam on top. Two scenarios have been investigated:

Lithological class	e_0 [-]	C_r [-]	C_c [-]	K_{z0} [m/yr]	σ_P [kPa]	γ_s [g/cm ³]
silty clay loam	1.7	0.009	0.6	31.5	4	2.65

Table 6.1: Characteristics of silty clay loam used for the additional 50-year nourishment operations.

- 50-year deposit of silty clay loam with a sedimentation rate ω equal to 10 mm/yr, i.e. 0.5 m of additional deposits;
- 50-year deposit of silty clay loam with a sedimentation rate ω equal to 50 mm/yr, i.e. 2.5 m of additional deposits.

The model returns the total thickness of the sedimentary column; therefore, by simply subtracting the value at time 11000 before silty clay loam deposit from the one at time 11050 after its deposition, the SEC value has been obtained. Moreover, also the compaction ratio has been quantified in order to understand how the thickness of the nourishment soil layer changes due to autocompaction as well as the integrated compaction of the whole column and all other parameters previously used to describe the behaviour of the soil. The NATSUB3D results are compared with those by Keogh et al. (2021). However, it has to be pointed out that the characteristics of the silty clay loam assumed in this paper differ from those considered in this thesis (Figure 6.1). Indeed, in Keogh et al. (2021) a distinction is made between "weak" and "stiff" stratigraphy, taking into account different values for the soil layer parameters accordingly.

Moreover, also the lithology of the Myrtle Grove soil column represented in Keogh et al. (2021) differs from that shown in Figure 5.6 with no distinction in the overbank between the small alternate layers of silty loam and silty clay loam, the lack of humic clay and peat in the central part of the soil column and of a third thin sandy layer immediately below the overbank.

Figures 6.2 and 6.3 show the results of the Keogh et al. (2021) and NATSUB3D models respectively in terms of additional compaction caused by the planned nourishment. The com-

Depth (m)	Lithology ^a	Unit weight above phreatic surface (kN m ⁻³)	Unit weight below phreatic surface (kN m ⁻³)	Vertical permeability (m s ⁻¹)	OCR	Weak stratigraphy			Stiff stratigraphy		
						RR	CR	C α	RR	CR	C α
0–1	Peat	11.00	10.50	5.00E-06	2.00	0.1533	0.4600	0.0230	0.1022	0.3067	0.0153
1–7	Silt loam	20.00	19.00	7.00E-06	1.25	0.0110	0.0329	0.0013	0.0077	0.0230	0.0009
7–10	Silty clay loam	20.00	19.00	1.03E-07	1.50	0.0307	0.0920	0.0037	0.0170	0.0511	0.0020
10–11.5	Sand	22.00	20.00	7.00E-06	1.00	0.0038	0.0115	0.0000	0.0019	0.0058	0.0000
11.5–35	Silty clay	19.00	18.00	7.00E-07	1.75	0.0383	0.1150	0.0046	0.0205	0.0614	0.0025
35–36.5	Sand	22.00	20.00	7.00E-06	1.00	0.0038	0.0115	0.0000	0.0019	0.0058	0.0000

Note. Geotechnical parameter values are from the Netherlands Standardization Institute (2006). Details are provided in Table S3 in Supporting Information S1.
^aUS Department of Agriculture sediment texture categories.

Figure 6.1: Soil parameters data used in the simulations by Keogh et al. (2021).

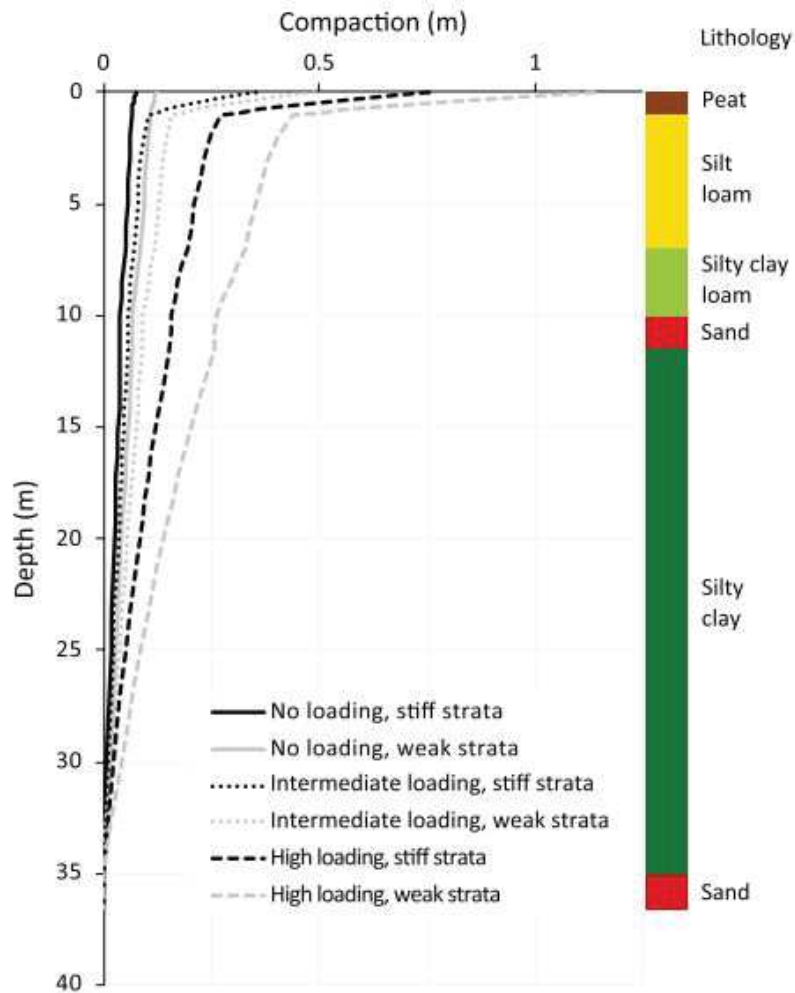


Figure 6.2: Additional compaction [m] along the Myrtle Grove column after the additional 50 years of nourishment operations as computed by Keogh et al. (2021) for the three scenarios.

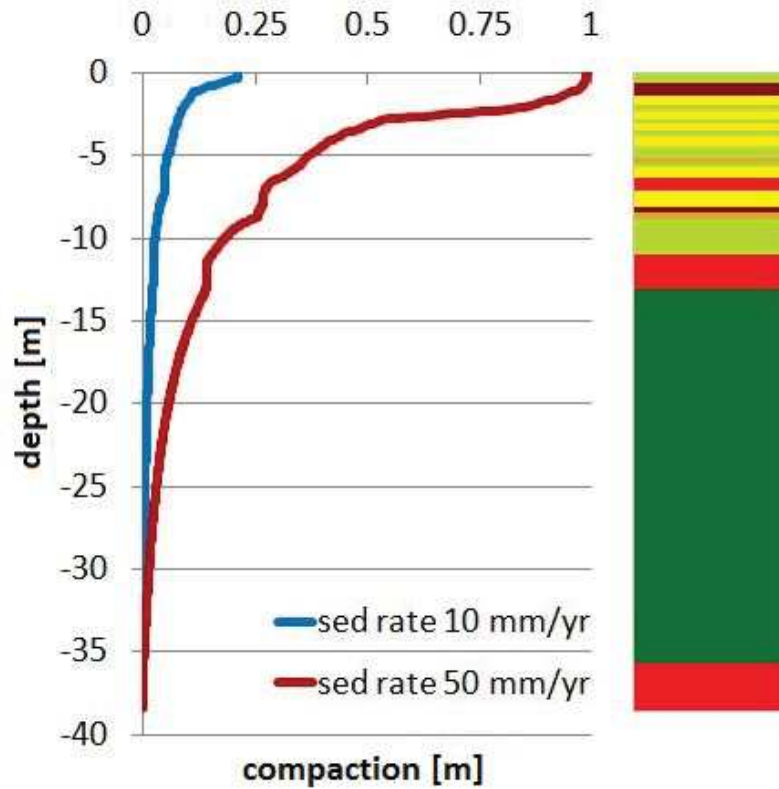


Figure 6.3: Additional compaction [m] along the Myrtle Grove column after the additional 50 years of nourishment operations as computed by NATSUB3D.

parisons between the two solutions points out how the compaction between 10 m and 37 m depth is comparable because the soil classes involved are the same, with little different characteristics depending on the values of the soil parameters. In particular, at -10 m depth both configurations report a value of about 0.1 m compaction for the nourishment with 10 mm/yr sedimentation rate and about 0.2 m compaction for the nourishment with 50 mm/yr sedimentation rate. A certain difference can be observed in the shallower part, although the maximum compaction at the column surface is similar. Another important aspect to be considered is the gain in surface elevation change compared to the accretion rate and the amount of shallow subsidence. Indeed, a nourishment operation performed with very weak soil would be useless as it would undergo significant shallow subsidence soon after depositing and would make its impact against sea-level rise ineffective. The equation to consider for these considerations is

Height of upper nodes of the soil column after nourishment	37.2901	[m]
Height of upper nodes of the soil column before nourishment	37	[m]
SEC (Surface Elevation Change)	0.2901	[m]
AC (Accretion)	0.5	[m]
SS (Shallow Subsidence)	0.2099	[m]

Table 6.2: Accretion data after silty clay loam nourishment with 10 mm/yr sedimentation rate.

Height of upper nodes of the soil column after nourishment	38.5155	[m]
Height of upper nodes of the soil column before nourishment	37	[m]
SEC (Surface Elevation Change)	1.5155	[m]
AC (Accretion)	2.5	[m]
SS (Shallow Subsidence)	0.9845	[m]

Table 6.3: Accretion data after silty clay loam nourishment with 10 mm/yr sedimentation rate.

the following:

$$SEC = AC - SS \quad (6.1)$$

here:

- SEC is the surface elevation change computed as the difference between the ending height of the upper nodes of the mesh reproducing the soil column at time 11000 before silty clay loam deposit and the one at time 11050 after its deposition;
- AC is the accretion rate obtained multiplying the sedimentation rate by the number of years of nourishment operations;
- SS is the shallow subsidence.

Table 6.2 and Table 6.3 report the results obtained by NATSUB3D model for the two nourishment scenarios, whereas Table 6.4 summarizes those obtained in Keogh et al. (2021).

Considering the differences previously mentioned between Keogh et al. (2021) and the configuration data of this thesis work, it is possible to state that the results are comparable. Both of them highlight that sediment compaction is an issue when planning a nourishment operation which cannot be treated with a superficial approach. The gain in surface elevation change

	Shallow subsidence [m]	Accretion [m]	Surface elevation change [m]
1 cm/yr sed. rate and weak strata	0.49	0.5	0.01
1 cm/yr sed. rate and stiff strata	0.35	0.5	0.15
5 cm/yr sed. rate and weak strata	1.14	2.5	1.36
5 cm/yr sed. rate and stiff strata	0.75	2.5	1.75

Table 6.4: Accretion data of silty clay loam nourishment by Keogh et al. (2021).

	Effective stress (bottom) [kPa]	Pressure (bottom) [kPa]
10 mm/yr sed. rate	309.97	2.581
50 mm/yr sed. rate	313.01	11.65
Before nourishment	309.18	0.856

Table 6.5: Comparison of stress and pressure at the bottom of the soil column before and after the nourishment operation.

clearly depends on the amount of sedimentation rate which is assumed, because it goes without saying that more loading leads to more net surface elevation change, but suitability in terms of compaction has to be taken into serious consideration in order to avoid making the nourishment operation ineffective. Finally, to give a complete picture of the ending time step after nourishment, Table 6.5 reports the range of values assumed by effective stress and pressure respect to the situation before nourishment.

Chapter 7

Conclusions

The investigation carried out in this thesis has allowed to effectively reproduce the evolution of the Myrtle Grove site in the Mississippi River Delta over the Holocene (last 11000 years) using an advanced numerical model (NATSUB3D) that accounted for both sedimentation and consolidation. A significant dataset has been collected over the last decade on this site by means of a "subsidence superstation" equipped with various instrumentation (GNSS stations, SET) and deeply characterized from the depositional point of view.

NATSUB3D has allowed to acquire a complete picture of the evolution of the Mississippi sedimentary sequence over time and depth in terms of geomechanical and hydraulic parameters, thickness of the sedimentary column, stress, pressure, and strain fields. The modelling application has addressed the various steps generally required for a proper application of a numerical model to a real system. The calibration phase has allowed to satisfactorily reproduce the present thickness of the Holocene column at the study site although a certain effective stress overestimation has been obtained with respect to previous analyses. The validation step has assessed the reliability of the model outcomes on independent datasets represented, in this case, by a CRMS site and relative sea level behavior provided by independent research. The

model response to parameter uncertainty has been evaluated through a Monte Carlo approach. Undoubtedly, the Monte Carlo simulation has been a computationally expensive phase because it has involved the response of the model to the variation of all the hydro-geomechanical parameters (initial void ratio, soil specific weight, preconsolidation stress, compression and recompression indices, hydraulic conductivity) describing the various soil layers considered in the model discretization. Therefore, the number of data to be post-processed has been huge and the computational time required has been significant.

The final results prove that the various parameters contribute significantly to the variability of the model response. The effective stress distribution is mainly affected by void ratio and soil specific weight, strain by the same parameters as well as by the preconsolidation stress and the compression index, PDL by the hydraulic conductivity, porosity and bulk density by void ratio and grain specific weight, and, finally, bulk compressibility by preconsolidation stress and void ratio. This leads to the conclusion that the correct description of a certain soil is a fundamental step when dealing with a complex system as the one analysed in this thesis.

The long-term simulation (encompassing the whole Holocene) is fundamental to properly define the present (i.e., initial) condition of the sedimentary sequence in relation to future strategies under planning aimed at increasing the possibility of the delta survival under the expected relative sea level rise. One of these scenarios tests the possibility of river diversions to increase artificial nourishment of salt-marshes in the nearby of the Myrtle Grove Superstation. In this thesis two nourishment operations with different sedimentation rate (i.e., 10 and 50 mm/yr over 50 years) have been considered to compensate the lack of natural sedimentation. The model outcomes have shown that, although characterized by the presence of a few metric-thick high-compressible peat layers, the Holocene column will be able to sustain the additional clastic sediments composing the nourishment with the surface elevation change greater than

the elevation lost to compaction. Priority must be given to the accurate evaluation of this last term when addressing a nourishment operation because it must lead to a gain in surface elevation change. Indeed, if the influence of compaction is so high that the shallow subsidence exceeds the surface elevation change, then the nourishment operation returns to be useless. The elevation gain will be about 50% of the initial nourishment thickness.

To conclude, the work developed in this thesis has to be considered as a complete description of the evolution of a given site in the Mississippi River Delta and provides an accurate example of how a numerical model can be tested on a real case study following all steps required: calibration, validation, uncertainty quantification and prediction. Further improvements may include a more accurate representation of the sedimentary sequence, which lacks the presence of very thin strata within thicker soil layers. Moreover, the wideness of the information related to soil parameters of the Myrtle Grove site in scientific papers was quite limited and such aspect would require further detail especially regarding the humic clay, which was assumed having intermediate characteristics between sand and peat. Finally, it must be stated that the depth-age model is an aspect that is currently being updated by the research group of the Tulane University with whose collaboration the thesis has been developed. Therefore, additional information related to this issue may help improve the accuracy in the description of the site evolution in the near future.

References

- Bentley, S. J., Freeman, A. M., Willson, C. S., Cable, J. E., & Giosan, L. (2014). Using what we have: Optimizing sediment management in Mississippi River Delta restoration to improve the economic viability of the nation. *Perspectives on the restoration of the mississippi delta* (pp. 85–97). Springer.
- Bentley Sr, S., Blum, M., Maloney, J., Pond, L., & Paulsell, R. (2016). The Mississippi River source-to-sink system: Perspectives on tectonic, climatic, and anthropogenic influences, Miocene to Anthropocene. *Earth-Science Reviews*, *153*, 139–174.
- Blomqvist, S. (1991). Quantitative sampling of soft-bottom sediments: Problems and solutions. *Marine Ecology Progress Series*, *72*(3), 295–304.
- Bridgeman, J. (2017). *Understanding Mississippi delta subsidence through stratigraphic and geotechnical analysis of a continuous Holocene core at a subsidence superstation* (Master's thesis). Tulane University, School of Science & Engineering. New Orleans, Louisiana.
- Chamberlain, E. L., Törnqvist, T. E., Shen, Z., Mauz, B., & Wallinga, J. (2018). Anatomy of Mississippi Delta growth and its implications for coastal restoration. *Science Advances*, *4*(4), eaar4740.
- Fisk, H. N. (1961). Bar-finger sands of Mississippi delta. *Geometry of sandstone bodies*. American Association of Petroleum Geologists. <https://doi.org/10.1306/SV22354C3>

- Gambolati, G. (1973). Equation for one-dimensional vertical flow of groundwater. 1. The rigorous theory. *9*(4), 1022–1028.
- Gambolati, G., Giunta, G., & Teatini, P. (1998). Numerical modeling of natural land subsidence over sedimentary basins undergoing large compaction. *Cenas* (pp. 77–102). Springer.
- Jankowski, K. L., Törnqvist, T. E., & Fernandes, A. M. (2017). Vulnerability of Louisiana’s coastal wetlands to present-day rates of relative sea-level rise. *Nature Communications*, *8*(1), 1–7.
- Keogh, M. E., & Törnqvist, T. E. (2019). Measuring rates of present-day relative sea-level rise in low-elevation coastal zones: A critical evaluation. *Ocean Science*, *15*(1), 61–73.
- Keogh, M. E., Törnqvist, T. E., Kolker, A. S., Erkens, G., & Bridgeman, J. G. (2021). Organic matter accretion, shallow subsidence, and river delta sustainability. *Journal of Geophysical Research: Earth Surface*, *126*(12), e2021JF006231.
- Kesel, R. H., Yodis, E. G., & McCraw, D. J. (1992). An approximation of the sediment budget of the lower Mississippi River prior to major human modification. *Earth Surface Processes and Landforms*, *17*(7), 711–722.
- Morton, R. A., Bernier, J. C., Barras, J. A., Ferina, N. F., et al. (2005). *Rapid subsidence and historical wetland loss in the Mississippi delta plain: Likely causes and future implications* (tech. rep.). U. S. Geological Survey.
- Mudroch, A., & MacKnight, S. D. (1994). *Handbook of techniques for aquatic sediments sampling*. CRC press.
- Roberts, H. H. (1997). Dynamic changes of the Holocene Mississippi River delta plain: The delta cycle. *Journal of Coastal Research*, 605–627.

- Sambrook Smith, G. H., Best, J. L., Ashworth, P. J., Lane, S. N., Parker, N. O., Lunt, I. A., Thomas, R. E., & Simpson, C. J. (2010). Can we distinguish flood frequency and magnitude in the sedimentological record of rivers? *Geology*, *38*(7), 579–582.
- Syvitski, J. P., & Milliman, J. D. (2007). Geology, geography, and humans battle for dominance over the delivery of fluvial sediment to the coastal ocean. *The Journal of Geology*, *115*(1), 1–19.
- Teatini, P., Gambolati, G., Ferronato, M., Settari, A. T., & Walters, D. (2011). Land uplift due to subsurface fluid injection. *Journal of Geodynamics*, *51*(1), 1–16.
- Törnqvist, T. E., Wallace, D. J., Storms, J. E., Wallinga, J., Van Dam, R. L., Blaauw, M., Derksen, M. S., Klerks, C. J., Meijneken, C., & Snijders, E. (2008). Mississippi Delta subsidence primarily caused by compaction of Holocene strata. *Nature Geoscience*, *1*(3), 173–176.
- Wright Jr, H. (1993). Core compression. *Limnology and Oceanography*, *38*(3), 699–701.
- Yu, S.-Y., Törnqvist, T. E., & Hu, P. (2012). Quantifying Holocene lithospheric subsidence rates underneath the Mississippi Delta. *Earth and Planetary Science Letters*, *331*, 21–30.
- Zoccarato, C., & Teatini, P. (2017). Numerical simulations of Holocene salt-marsh dynamics under the hypothesis of large soil deformations. *Advances in Water Resources*, *110*, 107–119.
- Zoccarato, C., Minderhoud, P. S., & Teatini, P. (2018). The role of sedimentation and natural compaction in a prograding delta: Insights from the mega Mekong delta, Vietnam. *Scientific Reports*, *8*(1), 1–12.